The Role of Rab19 as a Regulator of the Nuclear Envelope-Associated Endosomal Pathway

Poonam Shah

Thesis submitted for the degree of Doctor of Philosophy

Warwick Medical School

University of Warwick

January 2022

Table of Contents

List of Figures:

List of Tables:

List of Abbreviations:

ADP – Adenosine diphosphate

AP – Adaptor Protein

APPL – Adaptor protein, Phosphotyrosine interacting with PH domain and Leucine zipper 1

BCA – Bicinhoninic acid Assay

BSA – Bovine Serum Albumin

CCV – Clathrin Coated Vesicle

CDR – Complementarity Determining Regions

CPP – Cell Penetrating Peptides

DAPI – 4',6-diamidino-2-phenylindole

DMEM – Dulbecco Modified Eagle Medium

DMSO – Dimethyl Sulfoxide

DNA – Deoxyribonucleic Acid

DSCR3 – Down syndrome critical region gene 3

ECL – Enhanced Chemiluminescence

EDTA – Ethylenediaminetetraacetic Acid

EEA1 – Early Endosome Antigen 1

EF2 – Elongation Factor 2

EGF – Epidermal Growth Factor

EGFR – Epidermal Growth Factor Receptor

ELISA – Enzyme-linked Immunosorbent Assay

EphA2 – Ephrin type-A receptor 2

ER – Endoplasmic Reticulum

ERAD – ER-associated protein degradation

ERC – Endocytic Recycling Compartment

FBS – Fetal Bovine Serum

FDA – Food and Drug Administration

FGF – Fibroblast Growth Factor

FGFR – Fibroblast Growth Factor Receptor

FKBP – FK506-binding protein

FR – Framework Regions

FRB – FKBP and rapamycin-binding

GAP – GTPase Activating Protein

GAPDH – Glyceraldehyde-3-phosphate Dehydrogenase

GDI – GDP Dissociation Inhibitor

GDP – Guanosine Diphosphate

GEF – Guanine nucleotide exchange factor

GFP – Green Fluorescent Protein

GPCR – G-Protein Coupled Receptor

GST – Glutathione Sepharose Transferase

GTP – Guanosine-5'-triphosphate

HB–EGF – Heparin-Binding EGF-like growth factor

HGF – Hepatocyte Growth Factor

HIV – Human Immunodeficiency Virus

HRP – Horseradish peroxidase

HTT – Huntingtin

INFS – Integrative Nuclear FGFR-1 Signalling

INM – Inner Nuclear Membrane

INTERNET – INtegral Trafficking from the ER to the Nuclear Envelope Transport

IPTG – Isopropyl ß-D-1-thiogalactopyranoside

KASH – Klarsicht, ANC-1, Syne Homology

KIF16B – Kinesin Family Member 16B

LAMP – Lysosome-Associated Membrane glycoprotein

LB – Lysogeny Broth

LINC – Linker of Nucleoskeleton and Cytoskeleton

LRP1 – Low–density lipoprotein receptor-related protein 1

MAX – myc-associated factor X

MVB – Multivesicular Body

MWCO – Molecular Weight Cut-Off

NAE – Nuclear Envelope-Associated Endosomes

NES – Nuclear Export Signal

NTA – Nitriloacetic acid

NLS – Nuclear Localisation Signal

NPC – Nuclear Pore Complex

NT – Non-Targeting

OD – Optical Density

ONM – Outer Nuclear Membrane

PAR – Protease-Activated Receptor

PBS – Phosphate-Buffered Saline

PCR – Polymerase Chain Reaction

PE – Pseudomonas Exotoxin A

PEG – Polyethylene Glycol

PFA – Paraformaldehyde

PDGFR-b – Platelet–Derived Growth Factor Receptor Beta

PI3K – Phosphatidylinositol-3-OH kinases

PLK – Polo–Like Kinase

PMSF – Phenylmethylsulfonyl Fluoride

PNDD1 – Peptide Nuclear Delivery Device 1

Rab – Ras-related protein

RIPA – Radioimmunoprecipitation assay buffer

RNA – Ribonucleic Acid

RNAi – RNA interference

ROI – Region of Interest

RPM – Revolutions per minute

RT – Room Temperature

RTK – Receptor Tyrosine Kinase

ScFv – Single Chain Variable Fragment

siRNA – Small interfering RNA

SNARE – SNAP Receptor

SNX – Sorting Nexin

SUN1/2 – Sad1 And UNC84 Domain Containing 1/2

TAT – Trans-Activator of Transcription

TBS – Tris-Buffered Saline

TGF-α – Transforming Growth Factor alpha

TGN – trans-Golgi Network

TIRF – Total Internal Reflection Fluorescence

TNFα – Tumour Necrosis Factor-alpha

TRAPP – The TRAnsport Protein Particle

UV – Ultraviolet

VEGFR – Vascular Endothelial Growth Factor Receptor

VLC – Vacuole-Like Compartments

VPS – Vacuolar Protein Sorting

Acknowledgements

I would first like to thank my supervisors Steve Royle and Fred Bard for mentoring me throughout the PhD. They have given me constant support and guidance to help me complete this project and develop my scientific abilities. I would also like to thank the University of Warwick and the A*STAR research institute for funding this project and to the ARAP course directors Karuna Sampath and Meera Unnikrishnan.

I am grateful to the members of the Royle lab and Bard lab for the invaluable feedback in lab meetings and brainstorms. Particularly, I would like to thank Xavier Le Guezennec for helping me do the screen and for teaching me phage display, which has helped shape my project greatly. I would also like to thank Alexandre Chaumet and Trinda Anne Ting for training me thoroughly in many techniques including protein purification. Thanks to Laura Cooper and Eric Martins Ratamero for helping me automate the image analysis.

Moving halfway across the world is never easy, but doing it with Ewan and Ellie made it so much fun. Also, thanks to Monste and Méghane for listening to me talk about my project for hours! I would like to thank the many incredible friends I have made at Warwick and in Singapore, who have always encouraged me and believed in me. Finally, I would like to thank my parents and my brother for always supporting me, I would not be here without you.

Declaration

This thesis is submitted to the University of Warwick in support of my application for the degree of Doctor of Philosophy. It has been composed by myself and has not been submitted in any previous application for any degree.

The work presented (including data generated and data analysis) was carried out by the author except in the cases outlined below:

- Macro created by Eric Martins Ratamero for the quantification of co-localisation of vesicles in Figure 3.2
- Macro created by Laura Cooper to quantify the distance between vesicles and the mitochondria in Figure 5.8
- Custom Rab and SNARE siRNA libraries were printed into 384-well plates by Xavier Le Guezennec (Used in Figure 3.6 and 3.7)

Parts of this thesis have been published by the author:

- SHAH, P. et al. (2019) The NAE Pathway: Autobahn to the Nucleus for Cell Surface Receptors. Cells, 8(8), p. 915.

Abstract

The Nucleus-Associated Endosome (NAE) pathway is an endocytic trafficking pathway that provides a direct link from the plasma membrane to the nucleus of the cell. This study describes the development of a siRNA-based high-content imaging assay for the identification of regulators in the NAE pathway, using Pseudomonas Exotoxin A (PE), a cargo molecule that translocates to the nucleus, as a marker for NAE. Rab19, a member of the Rab GTPase family, was identified as a key player in the NAE pathway as knockdown of Rab19 resulted in a significant reduction in the number of PE-laden vesicles at the nucleus. High-resolution microscopy revealed that GFP-Rab19 localises to intracellular vesicles and the nuclear envelope, leading to the hypotheses that Rab19 functions at the vesicular level (NAE formation or translocation) or at the level of the nucleus (NAE docking or fusion). Rab19 vesicles were observed associated with large EEA1-positive early endosomes. Rab19-positive vesicular structures, containing PE, were also observed at the nuclear envelope. These structures were similar in size to the Rab19 vesicles associated with early endosomes. We propose a model that could explain the function of Rab19 in the NAE Pathway: Rab19 vesicles bud off from early endosomes and carry PE from the early endosome to the nucleus in NAE. The Rab19-vesicles then dock and fuse with the Rab19-positive nuclear envelope. Whether Rab19 is also required at the nuclear envelope to facilitate NAE docking requires further investigation.

Chapter 1: Introduction

1.1 Overview of Endocytic Trafficking to the Nucleus

1.1.1 Receptor Mediated Endocytosis

Endocytosis is an essential mechanism in all cells by which cargo such as extracellular ligands, cell-surface receptors and other macromolecules are internalised, allowing cells to interact with their environment and surrounding cells (Paolo, Fiore and de Camilli, 2001). Receptor-mediated endocytosis can involve ligand binding to a cell surface receptor, triggering internalisation of the cargo into coated vesicles (Roth and Porter, 1964). Upon uncoating, the vesicles are free to fuse with early endosomes (Figure 1.1), (Trahey and Hay, 2010). However, endocytosis of cell surface receptors does not only rely on ligand binding, as many cell surface receptors, such as Receptor Tyrosine Kinases (RTKs) are internalised constitutively. The rate of constitutive internalisation of RTKs is much slower than the recycling, and therefore the receptors and accumulate at the plasma membrane (Goh and Sorkin, 2013).

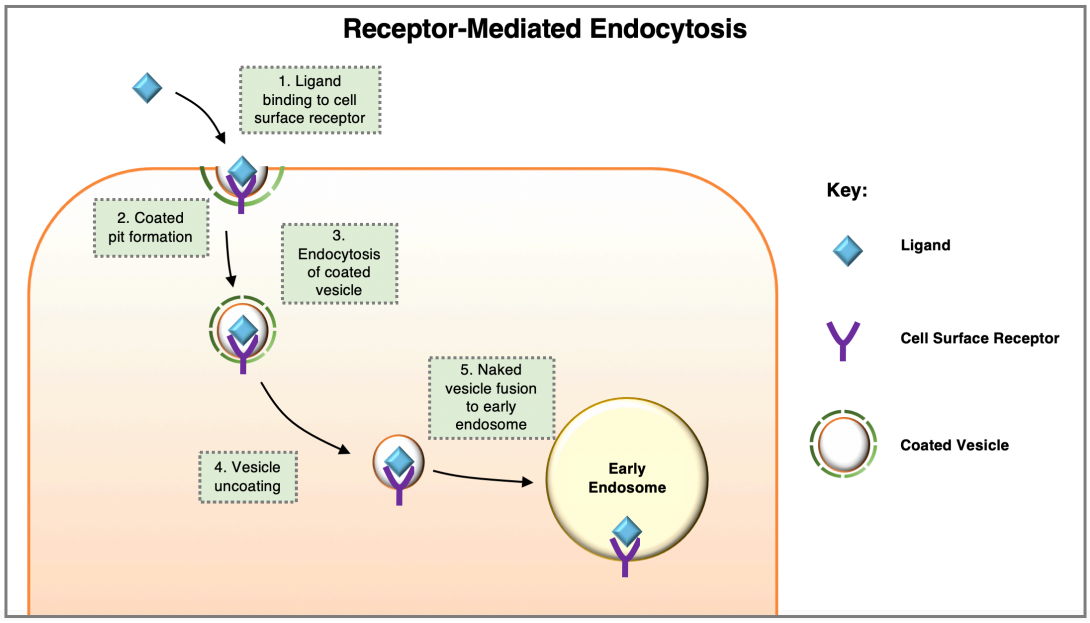

Figure 1.1 Stages of receptor-mediated endocytosis. Ligand binding to cell surface receptors triggers endocytosis into coated vesicles. Vesicle uncoating occurs and the cargo is transported to early endosomes.

Clathrin-Mediated Endocytosis (CME) is the major pathway for endocytic uptake of cargo in mammalian cells. Alternative clathrin-independent mechanisms also exist, such as caveolae-mediated endocytosis, which is dependent on a family of proteins called caveolins. Macropinocytosis, a non-selective mechanism for uptake of extracellular fluid, involves 'ruffling' of the cell membrane; this was first described in Lewis (1931). CME is the most studied and well characterised pathway of internalisation.

Clathrin is a protein that assembles into a triskelion structure. Clathrin consists of three heavy and light chains and forms a coat around the nascent vesicle (Kirchhausen and Harrison, 1981; Ungewickell and Branton, 1981; Royle, 2006). The internalised cargo has various functions such as nutrient uptake and cell signalling. Many of the proteins embedded in the plasma membrane have a transmembrane domain and a cytosolic domain. Internalisation through CME requires the recognition of endocytic motifs in the cytosolic domains of transmembrane proteins by adaptor proteins such as AP2 (Chen, Goldstein and Brown, 1990; Kozik et al., 2010; Traub and Bonifacino, 2013). AP2 and other accessory proteins recruit clathrin triskelia molecules to the endocytic site, promoting membrane curvature (Hinrichsen et al., 2006; Kelly et al., 2008; Zeno et al., 2021). Clathrin polymerises into a clathrin lattice, assembles the clathrin coat and forms the clathrin-coated pit. Dynamin, a large GTPase, is required for clathrin-coated pit maturation (Loerke et al., 2009). Dynamin is also involved in membrane scission, as it forms a helical structure at the neck of the clathrin-coated pit and breaks it, separating the clathrin-coated vesicle from the plasma membrane (Ferguson and de Camilli, 2012). Upon scission, the clathrin coat disassembles and the endocytic machinery can be recycled to the plasma membrane to be used for another endocytic event. Uncoating of clathrin coated vesicles is mediated by Rab5 effector hRME-6, which can dephosphorylate the μ2 subunit of the AP2 complex (Semerdjieva et al., 2008). This leaves the uncoated vesicle free to be transported towards and

fuse with early endosomes. From there, cargo can take several different trafficking pathways to reach different cell compartments.

1.1.2 Manipulation of Endocytic Pathways

Pathogens, such as viruses, and pathogenic substances, such as bacterial toxins, are capable of hijacking endocytic machinery to enter the cell. Endocytic mechanisms have also been manipulated for therapeutic purposes, by engineering peptides, viruses and liposomes for efficient delivery of molecules into cells.

Many intracellular bacteria hijack endocytic mechanisms and invade host cells for replication and evasion from the immune system. For all viruses, host cell entry is a necessity for their replication. Enveloped and non-enveloped viruses use host cell receptors to come into close proximity to the plasma membrane, where some viruses can be internalised by triggering endocytosis (Mercer, Schelhaas and Helenius, 2010). CME has been shown to be a main point of entry for many viruses, the best studied examples being influenza viruses, which have been shown to be localised in coated pits (Matlin et al., 1982), and Semliki Forest Virus (Helenius et al., 1980). Although, unlike Semliki Forest Virus, influenza viruses can also be internalised in the absence of clathrin, displaying fluidity in their mechanisms of entry (Sieczkarski and Whittaker, 2002). Internalisation into endosomes is an effective evasion strategy for viruses to avoid immune responses.

Studying bacterial toxins has helped shed light on many mechanisms of cellular trafficking. Bacterial toxins can use the endocytic trafficking pathway to reach different compartments of the cell to induce toxicity. The majority of these toxins act in the cell cytosol, where their substrates are typically found. Therefore, to induce toxicity, they must get access to the cytoplasm. Many toxins including Ricin, Diphtheria toxin, Shiga toxin and Pseudomonas exotoxin A (PE) target proteins that are required for protein synthesis, which

are localised to the cytoplasm, although the toxins take different routes to get there. Shiga toxin targets a ribosomal subunit, whereas the other two, Diphtheria toxin and PE, target the elongation factor EF2 (Olsnes et al., 1991). Diphtheria toxin is internalised into endosomes and undergoes a conformational change to form a pore in the endosomal membrane to escape (Murphy, 2011). Shiga, Ricin and PE can follow the retrograde trafficking route to travel from endosomes to the Golgi and then to the ER (Sandvig et al., 2010). The ER membrane has a mechanism to export misfolded proteins and target them for degradation called the ER-associated protein degradation pathway (ERAD). Proteins such as Shiga toxin can manipulate the ERAD pathway to gain access to the cytoplasm, whilst escaping ERAD-mediated degradation (Johannes and Römer, 2010). The cytoplasm is not the only destination for bacterial toxins. Many toxins target alternate organelles, for example Vacuolating cytotoxin A (VacA), secreted by *Helicobacter pylori* targets the mitochondria to induce cell death pathways (Rudel, Kepp and Kozjak-Pavlovic, 2010). Shiga toxin, produced by *Shigella dysenteriae serotype 1*, has been shown to localise to the nuclear envelope and nucleolus (Baibakov et al., 2010), where it can cause DNA damage (Brigotti et al., 2002).

1.1.3 Pseudomonas Exotoxin A in the Nucleus

Pseudomonas aeruginosa produces the lethal Pseudomonas Exotoxin A (PE), which has been shown to translocate to the nucleus (Chaumet et al., 2015; Borowiec et al., 2016). Subcellular fractionation and Electron Microscopy (EM) of MG63 cells were used to determine that PE accumulated in the nucleoplasm and in the lumen of the nuclear envelope within 1 hour of incubation (Chaumet et al., 2015). Investigating PE trafficking to the nucleus led to the discovery of a novel nuclear trafficking pathway discussed in Chapter 1.3. PE is a member of the AB toxin family, which are composed of an enzymatically active subunit (A) and cell surface binding subunit (B) (Figure 1.2).

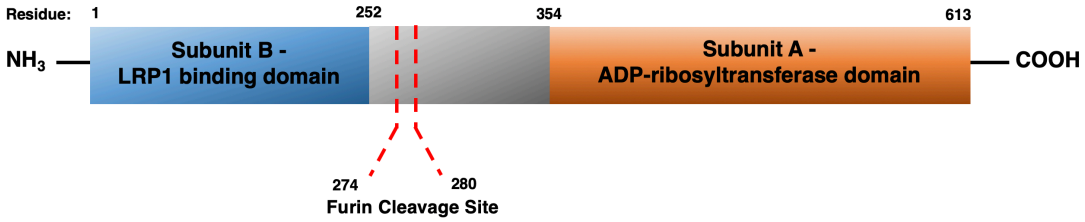

Figure 1.2 Schematic representation of the domains of Pseudomonas Exotoxin A (PE) Ligand binding domain (B) and ADP-ribosyltransferase (A) Furin cleavage site shown. Adapted from Michalska and Wolf (2015).

PE binds to cell surface receptor Low density lipoprotein receptor-related protein 1 (LRP1) and is internalised into clathrin-coated vesicles (Michalska and Wolf, 2015). It can undergo retrograde trafficking to reach the trans-Golgi Network (TGN). Retrograde trafficking from endosomes to Golgi is mediated by proteins that recognise motifs the cargo molecule such as the protein comples Retromer and SNX-BAR proteins (Tu et al., 2020). At the TGN PE is cleaved by Furin into an A_1 and an A_2 fragment, held together by a disulphide bond. The A_1 fragment domains encompasses the N-terminal ligand binding domain and a 37 kDa A_2 fragment contains the ADP-ribosylation activity. The 37 kDa fragment of PE is then transported to the ER, where it can escape to be free in the cytoplasm via the ERAD pathway (Michalska and Wolf, 2015). The ERAD pathway involves the transportation of misfolded proteins, recognised by chaperones, at the ER into the cytoplasm and targets them for degradation. The translocation occurs through a channel at the ER membrane, consisting of sec61 or derlin family of retrotranslocons (Vembar and Brodsky, 2008). The degradation is mediated by E3 ligases that recognised the ubiquitin modification in the misfolded protein. ADP ribosylation of eEF2 leads to inhibition of protein synthesis and host cell death (Iglewski and Kabat, 1975). Cytoplasmic PE has been shown to be cleaved, whereas PE in the nucleus is the full-length protein (Chaumet et al., 2015), supporting the hypothesis that PE translocation into the nucleus does not occur via retrograde trafficking. The full-length PE toxin cannot freely diffuse out of the nucleus due to its large size (66 kDa), therefore, it is unlikely to exhibit its toxic activity in the cytoplasm via the nuclear trafficking pathway.

A more direct pathway for PE intoxication has also been proposed by Alami et al. (1998). The low pH of endosomes exposes a normally hidden Tryptophan residue, enabling the insertion of PE into the endosomal membrane. This makes it feasible for PE to escape endosomes and directly gain access to the cytoplasm (Méré et al., 2005). Like the nuclear localised PE, cytoplasmic PE escaping directly from endosomes would also be the full-length protein. Morlon-Guyot et al. (2009) claim that the cytoplasmic full-length PE derived from endosomes is responsible for its cytotoxic activity, and that the cleaved form is unstable in the cytoplasm. This suggests that the full-length PE can be enzymatically active, however this is in conflict with previous studies that had claimed that mutant forms of PE that cannot be cleaved are non-toxic (Ogata et al., 1992). It is still unresolved whether full-length PE in the nucleus has an active function there, or whether its transportation into the nucleoplasm is a consequence of its corresponding cell surface receptor accumulation in the nucleus, a commonly described phenomenon discussed in Chapter 1.4.

Some reports have assumed that PE dissociates from the LRP1 receptor in the early endosome. Other studies claim that uncoupling of the ligand with its receptor occurs in the late endosomes/lysosomes due to its low pH, demonstrating there is limited and conflicting evidence to show precisely which stage LRP1 dissociates with its ligands (van Kerkhof et al., 2005; Laatsch et al., 2012; Scott, Vacca and Gruenberg, 2014; Mao, Xie and Pi, 2017).

1.1.4 Intracellular Delivery of Therapeutics

Manipulation of nuclear trafficking pathways has potential for the development of targeted intracellular delivery of therapeutics. Targeting drugs to the NAE pathway can help them gain access to the nucleus by bypassing the plasma membrane and nuclear envelope. The majority of patented drugs on the market are small molecules, produced by chemical synthesis (Makurvet, 2021). However, small molecules tend to have low specificity towards drug

targets, requiring administration of the drug in high doses (Rao et al., 2019). This can lead to off-target effects, cell toxicity and severe side effects in patients (Scheiber et al., 2009). Biologics, medicine derived from living cells, are larger, more complex molecules such as monoclonal antibodies. Biologics often display higher specificity and affinity towards the drug target and are capable of triggering immune responses (Makurvet, 2021).

Unlike small molecules, the larger size of biologics prevents them from readily crossing the cell membrane, therefore many antibody-based therapeutics mainly target cell surface proteins (Slastnikova et al., 2018). The discovery of cell-penetrating peptides (CPP) was promising for the intracellular delivery of therapeutics. The first CPP discovered was Trans-Activator of Transcription (TAT), a small peptide produced by Human Immunodeficiency Viruses (HIV), which was found to pass through the plasma membrane (Frankel and Pabo, 1988). TAT fusion proteins are effective at delivering various proteins into the cell (Fawell et al., 1994). A twelve amino acid sequence was identified required for its ability to penetrate the cell membrane, leading to the discovery or synthetic generation of a large variety of CPPs (Agrawal et al., 2016). The exact mechanism by which CPPs reach the cytoplasm is unclear. Whether it's by direct penetration of the cell membrane, internalisation into endosomes and subsequent endosomal membrane penetration, or another mechanism has not been determined (LeCher, Nowak and McMurry, 2017). It was first reported by Frankel and Pabo (1988) that cellular uptake of TAT was likely an endosomal independent process. Whilst CPP fusions can help with internalisation of drugs, there is growing evidence that they remain trapped in endosomes (Richard et al., 2003). This was dubbed the 'Endosomal escape problem', and likely leads to the majority of the drug subsequently being targeted for degradation in lysosomes. Current research focuses on reducing the levels of CPP that are targeted for lysosomal degradation, as increasing CPP-drug doses can lead to cellular toxicity. Strategies to optimise CPPs include enhancing its escape from endosomes or improving its specificity to target specific organelles such as the mitochondria. As of 2020, there have

been no CPP-based therapeutics that have been approved for use by the FDA (Xie et al., 2020).

The nuclear trafficking pathway was manipulated for the delivery of cargo into the nucleoplasm by Ting, Chaumet and Bard (2020). They used a truncated form of PE coupled to the c-myc inhibitor peptide H1 (PNDD1) to supress the oncogene. They demonstrated that PNDD1 is three thousand times more potent than a CPP conjugate for c-myc inhibition.

1.2 The Rab GTPases in Membrane Trafficking

1.2.1 Overview of the Rab GTPases

Endocytosis describes the process by which cells take up cell surface receptors and extracellular ligands. Membrane trafficking pathways ensure that the cargo is delivered to the correct subcellular compartment. The movement of cargo molecules between compartments is achieved with vesicular transport with intracellular membrane bound vesicles that deliver cargo from the donor to the target organelle (Figure 1.3). Membrane trafficking events are regulated by the Rab GTPases (Chavrier et al., 1990; Segev, 2001). The Rab GTPases are part of a superfamily of Ras small GTPases. There are four other members of the superfamily: the Ras, Rho, Ran and Arf subfamilies, which have roles in cell proliferation, cytoskeletal dynamics, nuclear import, cell cycle and in membrane trafficking. Five motifs have been identified that distinguish the Rab proteins from the other members of the Ras superfamily, termed RabF1-RabF5, located within different regions of the gene. For example, RabF4 motif is located in the hypervariable domain responsible for membrane targeting (Chavrier et al., 1991). The identification of these sequencing allowed the categorisation of Rabs into phylogenetic subfamilies, and the identification of new Rab proteins. (Pereira-Leal and Seabra, 2000).

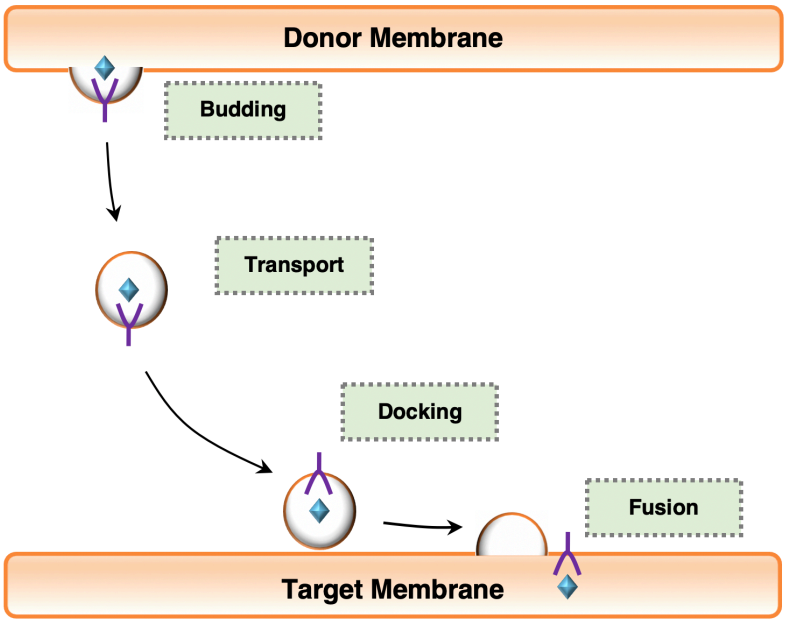

Figure 1.3 Vesicular transport between donor and target membranes. Membrane bound vesicles mediate transport of cargo between organelles.

The Rab GTPases proteins are known as the master regulators of intracellular membrane trafficking, as they regulate all events of membrane trafficking from vesicle formation and budding, transport, tethering/docking and fusion. With around 70 different Rab proteins found in humans, they are the largest subfamily of the Ras superfamily and they differentially localise to separate membranous compartments (Wandinger-Ness and Zerial, 2014). They are predominantly found on the surface of vesicles and organelles and can therefore be used as markers of vesicle transport (Hutagalung and Novick, 2011).

1.2.2 Rab GTPases act as Molecular Switches

GTPases are enzymes that can hydrolyse GTP to GDP (Figure 1.4). The Rab GTPases can be found in two states: a membrane-bound active state when bound to Guanosine-5'-triphosphate (GTP) and a cytosolic inactive state when bound to Guanosine diphosphate (GDP), therefore the Rabs can act as molecular switches. Exchange of GDP to GTP is catalysed by Guanine nucleotide Exchange Factors (GEFs), which recognises regions to facilitate

release of GDP. The release of GDP is quickly followed by a replacement with free GTP, because the cytosolic concentration of GTP is high. GTP hydrolysis is accelerated by GTPase Activating Proteins (GAPs), inactivating the Rab. Guanosine Dissociation Inhibitors (GDIs) solubilise the Rab and keep them in their inactive state by preventing the release of GDP and keeping them soluble in the cytoplasm (Stenmark, 2009; Barr, 2013; Zhen and Stenmark, 2015).

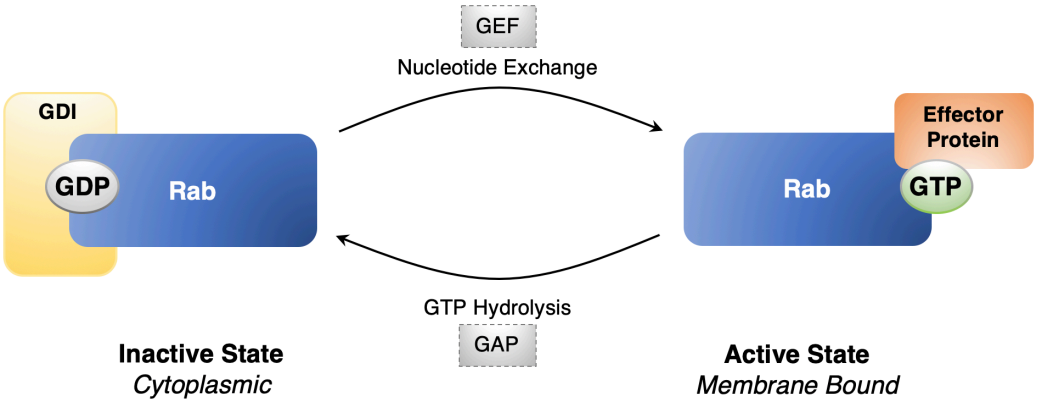

Figure 1.4 The Rab GTPases act as molecular switches GEFS exchange the GDP to a GTP to activate the Rab, which can bind effector proteins. Rab GAPs can accelerate GTP hydrolysis to inactivate the Rab. GDI keep the Rab in their inactive state.

Membrane insertion of Rabs requires modification by a geranylgeranyl transferase II, which adds two geranylgeranyl groups to the cysteine(s) at the C-terminus of the Rab protein (Pylypenko and Goud, 2012). The hypervariable C-terminal region of the Rab GTPase is responsible for its membrane targeting (Chavrier et al., 1991), however, this does not provide an explanation for how the Rabs are specifically targeted to different organelles. Blümer et al. (2013) demonstrated that upon artificial mistargeting of GEFs to the mitochondria, the correspondent Rab was recruited to the mitochondria as well. This suggests that GEFs are responsible for the specificity of the membrane targeting of Rabs. Pylypenko et al. (2006) have reported that GDIs rapidly mediate the membrane extraction and the membrane delivery of GDP-bound Rabs in the

absence of other factors. This led to the hypothesis that the Rab GTPase can reversibly 'sample' and be associated with various membranes. Activation by a site-specific GEF can prolong membrane contact and stabilise the Rab, leading it to be resistant to membrane extraction by a GDI, and resulting in the accumulation of the Rab at the appropriate membrane site (Barr, 2013). The active GTP bound Rab inserted into the membranes of organelles can recruit and bind to multiple effector proteins. Rab GAPs then inactivate the Rab, and this is followed by GDI mediated Rab extraction from the membrane (Ignatev et al., 2008; Gavriljuk et al., 2013).

The active Rab proteins have different effector proteins with a wide range of functions, for example adaptor proteins, tethering factors and kinases. The Rabs and their effector proteins control the trafficking of cargo from the point of internalisation into vesicles, to the delivery of the cargo to their final cellular destination.

1.2.3 Membrane Identity

The Rab GTPases are selectively distributed to membranes, making them ideal candidates for membrane identification. Early endosomes and late endosomes are defined by Rab5 and Rab7 respectively (Chavrier et al., 1990). How the cargo is transferred between these compartments could be explained by two hypotheses. The first hypothesis is that the cargo is transferred from a stable Rab5-positive early endosome to a Rab7-positive late endosome through vesicular transport. The second hypothesis is that there is maturation of the endosomal compartment itself from a Rab5-positive early to a Rab7-positive late endosome.

The early endosome is a highly dynamic compartment undergoing high levels of fusion and budding events. Key work from the Zerial lab has described that different Rab-GTPases can localise to the same organelle, providing evidence that endosomes can be compartmentalised into Rab-specific microdomains

(Sönnichsen et al., 2000). The early, late and recycling endosomes can consist of subdomains occupied by different Rabs. This finding supports both hypotheses, as both would require the presence of both Rab5 and Rab7 on the endosomal membrane. The intermediate stage of maturation could be captured, and only at a later stage would the complete disassembly of Rab5 from the endosomal membrane occur for replacement with Rab7. Rab7 microdomains that bud off from Rab5 positive early endosomes could also explain the presence of Rab5 and Rab7 on the same organelle.

Rab5 levels fluctuate on early endosomes, and as these compartments translocate towards the cell centre from the periphery, they lose Rab5 and acquire Rab7, arguing for a maturation step. This maturation/conversion requires the VPS/HOPS complex, which is a GEF for Rab7 and recruits Rab7 to the endosomal membrane (Rink et al., 2005). The Rab-defined microdomains in the endosomes are highly organised and interact with one another. Sönnichsen et al. (2000) provided evidence that receptors destined for recycling enter the Rab5 domain after internalisation, then are transferred to the Rab4 domain and then finally reside in the Rab11 domain for a longer period. Mono-ubiquitinated receptors destined for degradation are incorporated into intralumenal vesicles that leads to the formation of multivesicular bodies. These domains serve as a template for compartmentalisation of the endosomes, and allow for differential targeting of cargo. A single Rab protein has multiple sites that can bind to more than one effector protein, such as Rab5 which can bind EEA1 and APPL. EEA1 and APPL show limited colocalisation, providing further evidence for compartmentalisation within endosomes (Miaczynska et al., 2004). The early endosomal compartments can be composed of tubular extensions or vesicular structures and it is possible that these subdomains can hold the cargo that will be targeted to different pathways. For example, it is postulated that the tubular structures contain a higher level of cell surface receptors and cargo targeted for recycling (Jovic et al., 2010). It has been proposed that the tubular structures can become the endocytic recycling compartment (ERC) that

mediates slow recycling and the main vesicular compartment forms the multi-vesicular body (MVB) (Grant and Donaldson, 2009).

Cross talk between the domains was revealed upon the identification of a Rab effector proteins, Rabenosyn-5, which can bind to Rab4 as well as Rab5, at separate binding sites, revealing that two Rabs can bind to one effector. Increased Rabenosyn-5 expression lead to increased association between the Rab4 and Rab5 domains, and a decrease in Rab4 and Rab11 associated domains. Overexpression of Rabenosyn-5 also stimulated transferrin recycling. The authors proposed that this is due to an increase in fast recycling pathways, demonstrating that the interaction between these domains is important for the regulation of protein sorting and recycling (de Renzis, Sönnichsen and Zerial, 2002).

Following the identification of Rabenosyn-5, many effector proteins have been identified, which can also bind to multiple Rabs. This discovery led to the Rab cascade model becoming the general consensus for organelle maturation. This requires the template Rab(A) to recruit a GEF that can activate the next Rab(B). The newly recruited Rab(B) would recruit a GAP that would result in the disassembly of Rab(A) from the membrane. These series of reactions is responsible for the coordination of the events of trafficking and would ultimately result in a transition into different Rab compartments and maturation of the organelle (Rivera-Molina and Novick, 2009).

1.2.4 Rab5 and the Early Endosome

Following internalisation, incoming cargo is targeted to early endosomes (Mayor, Presley and Maxfield, 1993). The early endosome is a complex and dynamic organelle consisting of cargo that is sorted into many Rab-defined compartments within the endosomes itself (Jovic et al., 2010). Rab5 is the best characterised Rab GTPase with a diverse range of effectors with varying functions. Rab5 is localised to the plasma membrane, clathrin-coated pits and

early endosomes. Rab5 has been shown to be involved in almost all steps of early endosomal trafficking from CCV pit formation and uncoating to early endosomal tethering, fusion and maturation (Gorvel et al., 1991; Bucci et al., 1992; Zeigerer et al., 2012).

Rab5 has three differentially expressed isoforms: Rab5a, Rab5b, Rab5c (Bucci et al., 1995). Rab5 has been referred to as the master regulator in endocytic trafficking, due to the diversity in the functions of Rab5 and its effectors. There are some studies that suggest that the Rab5 isoforms are functionally redundant, due to the high sequence similarity between the isoforms and the evidence that the loss of each isoform individually does not interfere with EGFR internalisation (Chen et al., 2009). However, there has been evidence to show otherwise. The Rab5 isoforms are differentially phosphorylated (Chiariello, Bruni and Bucci, 1999), and Rab5a is the only isoform to be upregulated in response to cytokines (Alvarcz-Dominguez and Stahl, 1998; Wainszelbaum et al., 2006). Chen et al. (2014) suggest that Rab5 isoforms orchestrate a 'division of labour' for the early endocytic Rab5 pathways in vertebrates.

Rab5 is primarily involved in regulating steps of the early endocytic pathway by orchestrating events such as formation and uncoating of endocytic vesicles, through its many effector proteins. The first Rab5 effector that was identified was Rabaptin-5 (Stenmark et al., 1995). Depletion of Rabaptin-5 inhibits Rab-5 dependent early endosomal fusion. Rabex-5 is a GEF for Rab5, activating it and targeting to early endosomal membranes. Cytosolic Rabaptin-5 can form a complex with Rabex-5 and bind to the membrane-bound Rab5. This positive feedback loop stabilises the active form of Rab5, allowing further downstream effector recruitment. Effectors for Rab5 include kinases such as Phosphatidylinositol-3-OH kinase (PI3K). Vps34, a class III PI3K, phosphorylates phosphatidylinositol to PtdIns(3)P found in the early endosomal membrane. PtdIns(3)P is involved in early endosomal movement along microtubule tracks by the recruitment of the motor protein KIF16B

(Hoepfner et al., 2005). Proteins with FYVE finger domains, such as EEA1 can bind to PtdIns(3)P.

EEA1 is a long-coiled coil homodimer with a FYVE finger domain at its C-terminal, which is required for its endosomal targeting. Rab5 and EEA1 are both required for heterotypic fusion of CCV to early endosomes (Simonsen et al., 1998; Christoforidis et al., 1999). Whilst the presence of Rab5 is required on both membranes, the lack of EEA1 on the surface of CCV indicates its role in providing directionality for transport of cargo from the plasma membrane to early endosomes (Rubino et al., 2000). EEA1 also mediates tethering and homotypic fusion of early endosomes. Its N-terminal is responsible for binding Rab5. Unlike Rab5, which can be found on the membranes of multiple organelles, EEA1 is highly specific to early endosomes. The long extended EEA1 protein is ideal for the capture of vesicles. Rab5 can induce a conformational change in the protein to cause it to collapse and bring together the two membranes for the tethering and docking of vesicles (Murray et al., 2016). EEA1 binds to syntaxin6 and syntaxin13, both of which are SNARE proteins involved in early endosomal homotypic fusion (Simonsen et al., 1999; McBride et al., 1999).

The lipid PtdIns(3)P is enriched at early endosomes, which, through its FYVE finger domain, can recruit the enzyme PIKFyve. PIKFyve phosphorylates PtdIns(3)P to PtdIns(3,5)P_2, a lipid enriched on late endosomal membranes, and therefore it is important in the maturation of early endosomes to late endosomes (Kim et al., 2014).

1.2.5 A Novel Destination for Cargo at the Early Endosome

Following early endosomal sorting, cargo can be targeted to one of four different pathways: (1) Recycling pathways, (2) Retrograde trafficking, (3) Lysosomal degradation, (4) The NAE pathway (Figure 1.5).

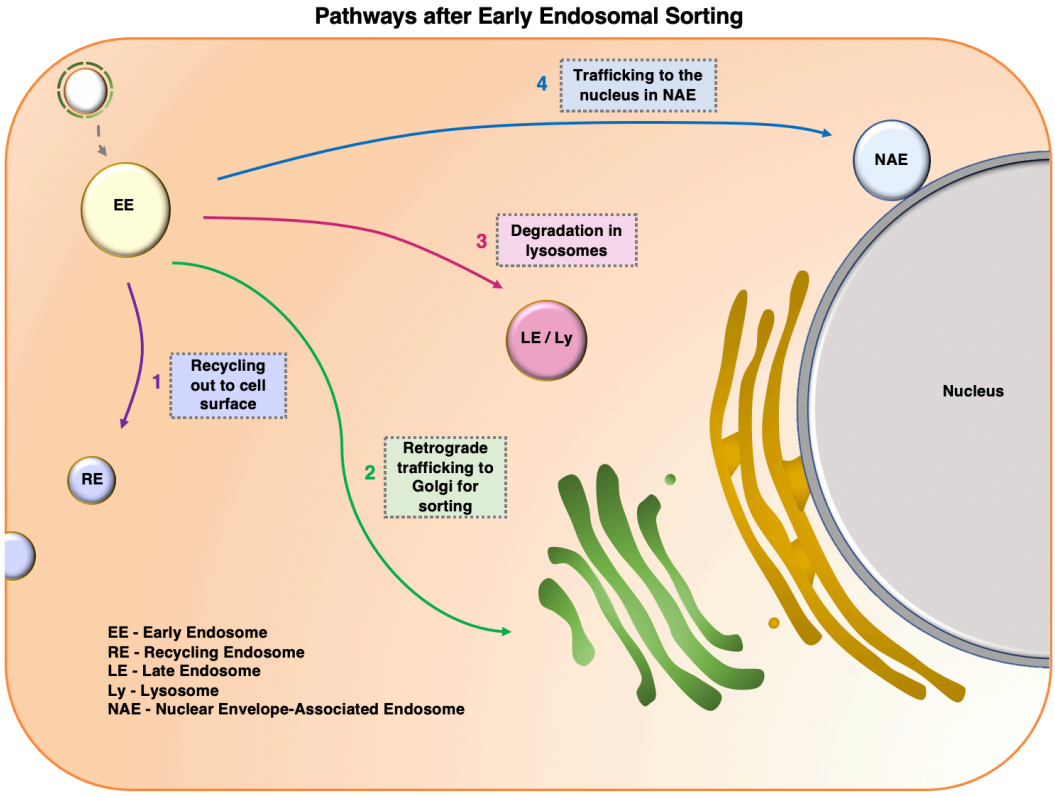

Figure 1.5 Destinations for cargo following early endosomal trafficking. Cargo can be targeted to four destinations after arrival at the early endosome: 1. Recycling back out to the cell surface; 2. Retrograde trafficking to the Golgi for sorting; 3. Degradation in lysosomes; 4. Trafficking to the nucleus in Nuclear envelope Associated Endosomes (NAE).

Cargo can follow the recycling pathways back to the cell surface. Internalised membrane bound receptors can be transported back to the plasma membrane, and the free endosomal cargo can be transported out of the cell in recycling endosomes. There are fast recycling pathways, mediated by Rab4, and that require the sorting of cargo from the Rab5 domain to the Rab4 domain rapidly within the same endosome, potentially mediated by the effector protein rabaptin5, which can bind both Rab4 and Rab5. Slow recycling pathways are mediated by Rab11 at the ERC (Sönnichsen et al., 2000).

Cargo can also be targeted to late endosomes for subsequent degradation in lysosomes. It had previously been thought that a lack of a degradation signal would result in the targeting of cargo to the recycling pathways (Gruenberg, 2001; Raiborg and Stenmark, 2009). However, ACAP1, a protein that mediates recycling was discovered. Blocking the association of ACAP1 with transferrin resulted in the delay of transferrin recycling (Dai et al., 2004). Since

then, many sorting signals found in the cytoplasmic tails of receptors have been identified (Kozik et al., 2010). Ubiquitination is a sorting signal for lysosomal degradation as well as proteasomal degradation (Hicke, 1999; Sigismund et al., 2013). The cargo is sorted to the lumen of the late endosome, and MVB formation occurs (Schmid et al., 1988; Piper and Katzmann, 2007). The fusion of the MVB to lysosomes result in the endolysosomal degradation of the cargo (Kornfeld and Mellman, 1989).

In the third pathway, cargo can follow retrograde trafficking pathways, in which cargo is transported to the Golgi for sorting. Retrograde trafficking is mediated by a retromer, which is composed of sorting nexins SNX1, SNX2, SNX5 and SNX6 and a cargo-recognition trimer composed of Vps26, Vps29 and Vps35. Retriever, a heterotrimer composed of DSCR3, C16orf62 and VPS29 can also facilitate cargo trafficking from endosomes to the TGN (Bonifacino and Hurley, 2008; McNally et al., 2017).

Recently, a fourth pathway was described by Chaumet et al. (2015). Following internalisation into early endosomes, cargo such as PE can be targeted to the nucleus in Nuclear Envelope-Associated Endosomes (NAE). This pathway provides a direct link for communication between the cell periphery and the nucleus, and an alternative to cell signalling pathways.

1.3 The NAE Pathway

1.3.1 Overview

A model describing the stages of the NAE pathway has been proposed (Shah et al., 2019). The NAE pathway can be broken down into six stages (Internalisation, Sorting and translocation, Docking, Fusion, Outer Nuclear Membrane (ONM) to Inner Nuclear Membrane (INM) Translocation and Receptor Extraction). Following internalisation of cargo into the early endosomes, a fraction of the cargo is sorted towards the nucleus. NAE can

translocate to the nuclear envelope where they dock and fuse with the outer nuclear membrane. Membrane-bound cargo can be transported from the ONM to the INM, where it is extracted to be free in the nucleoplasm (Figure 1.6).

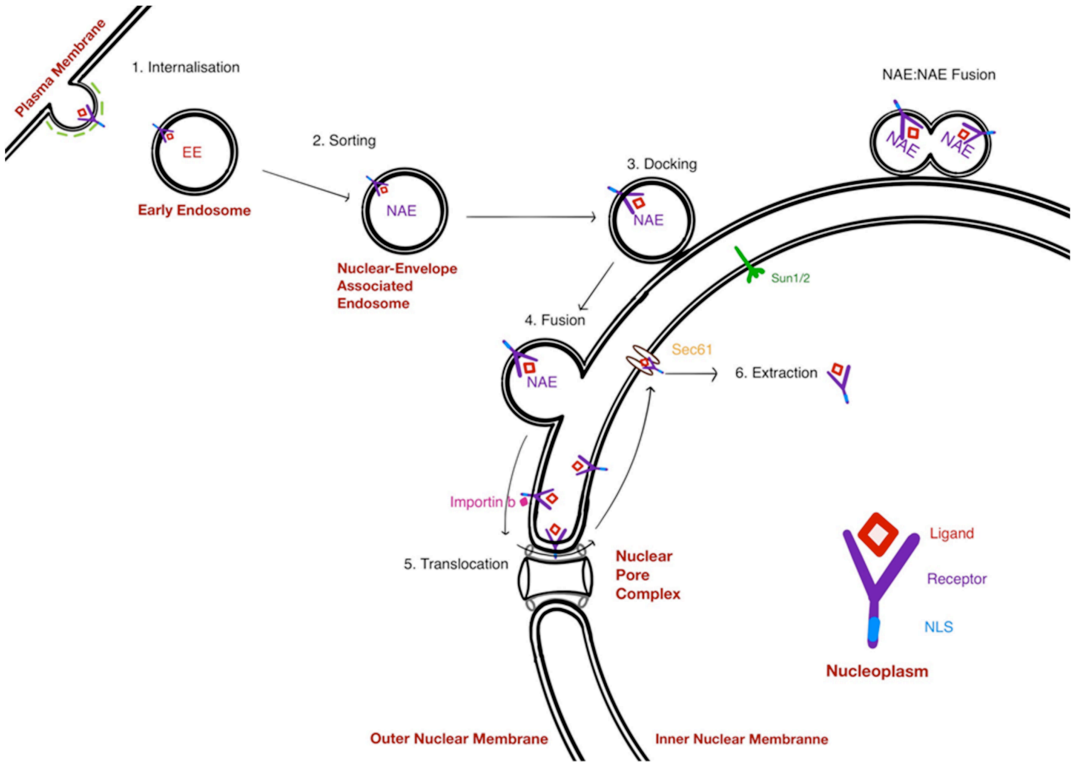

Figure 1.6 Stages of the NAE pathway. 1. Cargo is internalised into early endosomes; 2. Cargo can be sorted towards the nucleus in NAE; 3. After arrival at the nucleus, NAE dock at the nuclear envelope; 4. Fusion of NAE with the outer nuclear membrane occurs; 5. Membrane bound cargo is transported from the outer to the inner nuclear membrane; 6. Membrane bound cargo is extracted from the inner nuclear membrane to be solubilised in the nucleoplasm. SUN1/2 and sec61 are inner nuclear membrane localised proteins which have been proposed to be involved in the NAE Pathway. *Illustration from Shah et al. (2019).*

Cargo destined for the nucleus can have many different functions, and the specific function is unique to each cargo molecule. For example, nuclear EGFR is involved in the regulation of gene transcription, cell proliferation and DNA damage repair pathways (Lin et al., 2001; Dittmann et al., 2005; Brand et al., 2013). This can lead to consequences such as poor prognosis in cancer patients and resistance to cancer therapeutics (Xia et al., 2009; Hsu and Hung, 2016).

The conventional mechanism of how extracellular ligands can influence cell activity is typically through signal transduction pathways. Internalisation of cell surface receptors had been thought to be primarily a way for cells to down-regulate their signalling activity at the plasma membrane (Wiley et al., 1991; Nakamura et al., 1999). However, it has been shown that receptors can also continue to transmit signals after internalisation into endosomes, and even upregulate their own transcription upon translocation to the nucleus (Murphy et al., 2009; Domingues et al., 2011). The NAE Pathway describes an alternative mechanism to signal transduction for how extracellular ligands can directly influence cellular activities. This section will evaluate the literature on endosomal trafficking to the nucleus and postulate how each step of the pathway can be regulated.

1.3.2 Internalisation of Nuclear-Targeted Cargo

The cargo that can be translocated into the nucleus in NAE includes extracellular ligands, bacterial toxins and cell surface receptors, all of which require internalisation at the plasma membrane. There have been many different pathways of internalisation described for nuclear-targeted cargo. The majority of studies have shown ligand binding to the cell surface receptor is required for the nuclear accumulation of receptors. For example, it has been shown that EGFR translocation to the nucleus occurs via clathrin-mediated endocytosis, and is dependent on stimulation by the ligand EGF (de Angelis Campos et al., 2011). Nuclear targeted Insulin receptor can also be internalised in a caveolin dependent manner (Foti et al., 2007; Amaya et al., 2014). However, some studies have shown that stress such as UV ray and X-ray irradiation can also drive nuclear accumulation of EGFR. UV stimulation of EGFR was 1.7-fold greater than stimulation by EGF at driving the nuclear translocation of EGFR (Dittmann et al., 2005; Xu et al., 2009).

1.3.3 Sorting and Translocation of Cargo to the Nucleus

Following internalisation, incoming cargo is targeted to early endosomes. This has been demonstrated by visualising the co-localisation of cell surface receptors such as EGFR and PE with early endosomal markers (Chaumet et al., 2015). At the early endosome, a fraction of the cargo can be sorted to the nucleus. The sorting of cargo upon endocytosis is dependent on sorting signals present in the cytoplasmic tails of transmembrane proteins or post-translational modifications, such as phosphorylation, of the protein (Brodsky et al., 2001). Conventional endocytic sorting signals for cell surface receptors are encoded in their cytoplasmic tails that are recognised by adaptor proteins (Ohno et al., 1995). These small peptide sorting signals can determine the fate of the cell surface receptors (Pandey, 2010). The sorting signals to the nucleus have not yet been identified. Ligand binding has been shown to stimulate endocytic uptake and nuclear translocation of certain cell surface receptors. Whilst it is evident that ligand binding stimulates endocytic uptake and nuclear translocation of certain cell surface receptors, it has recently been shown that various EGFR ligands can cause differential translocation of the cell surface receptor. The ligands EGF, HB-EGF, TGF-α and β-Cellulin can induce the nuclear translocation of EGFR, whilst stimulation with amphiregulin and epiregulin did not (Faria et al., 2016). This highlights that ligand binding can indeed influence the fate of the receptor.

Nuclear-EGFR stimulated by irradiation has also been shown to require phosphorylation of the Thr654 residue, as deletion of this site blocked nuclear transport of EGFR (Dittmann et al., 2005). The post-translational modification process, SUMOylation, has also been implicated in nuclear targeting of cell surface receptor ErbB4 (Knittle et al., 2017). It is unclear whether traditional NLS, sorting signals or post-translational modifications of the cargo is required at the early endosomal level for sorting to the nucleus. The extent to which the ligand and its interaction with its corresponding receptor can determine the fate of the cargo remains unresolved.

Following cargo sorting, NAE must be translocated to come into proximity to the nuclear envelope. Whilst receptor translocation to the nucleus has been studied for decades, the proposal that this occurs directly through endosomal translocation is relatively new. Therefore, there is limited work on how the endosomes are translocated to the nucleus. Recently, Rab17 has been implicated in nuclear trafficking of EphA2-containing endosomes (Marco et al., 2021). However, the authors' model is that Rab17 is required for the internalisation of EphA2, and they did not test whether Rab17 can also drive endosomal translocation to the nucleus (Marco et al., 2021). Porcine Growth Hormone Receptor (GHR), has been reported to follow the NAE pathway and co-localise with early endosomal markers EEA1, Rab5 and Rab4 (Lan et al., 2018). Early endosomal transport along microtubules is bidirectional and regulated by Rab5 (Nielsen et al., 1999). It has been reported by Chaumet et al. (2015) that NAE can be derived from early endosomes, however the relationship between early endosomes and NAE requires further investigation. How NAE are translocated towards the nucleus also remains unresolved, and deciphering which cytoskeletal components or motor proteins are involved in NAE translocation will need to be investigated.

1.3.4 Docking of NAE to the Nuclear Envelope

Once NAE reach the nuclear periphery, they seem to dock at the nuclear envelope. Super-resolution and electron microscopy revealed that PE-containing vesicles are very closely associated with the nuclear envelope (Chaumet et al., 2015). Live imaging confirmed that NAE become less mobile when associated with the nuclear envelope. The average motility of cytoplasmic PE vesicles was three times that of the PE vesicles at the nucleus. Vesicles were seen transiting over the nuclear envelope and abruptly stopping, an indication that NAE becoming immobile is not due to spatial constraint, but rather translocating to the nucleus and docking. This could be an indication that they scan the nuclear envelope before docking (Chaumet et al., 2015).

Vesicular tethering is a reversible process, whereas subsequent docking is not (Ungermann, Sato and Wickner, 1998; Tamura and Mima, 2014). Tethering factors facilitate the long-range interaction that form a bridge between the membrane of the vesicle and target organelle (Gillingham and Munro, 2003). Once the vesicle is in close proximity, they can dock at the target membrane. Tethers tend to be long coiled coil proteins such as EEA1, which upon inhibition can perturb early endosomal docking (Christoforidis et al., 1999; Geumann et al., 2008). PE was shown to co-localise with EEA1, indicating that EEA1 may be present on NAE. Like early endosomes, NAE also undergo homotypic fusion, which could be the role for EEA1 on NAEs, and not necessarily to facilitate the tethering of NAE to the ONM (Chaumet et al., 2015).

The proteins SUN1 and SUN2 have been reported to be involved in the NAE pathway, as depletion of SUN1/2 led to a decrease in levels of PE in the nucleoplasm (Chaumet et al., 2015). SUN1/2 are proteins found on the inner membrane of the nuclear envelope. The N-terminus of SUN1/2 is in the nucleoplasm and its C-terminus is in the lumen of the nuclear envelope (Rajgor and Shanahan, 2013). The SUN2 proteins interact with the KASH domain on three independent nesprin proteins present on the outer nuclear membrane, forming the LINC complex (Sosa et al., 2012). The SUN1/2 proteins interact with the nuclear lamina and nesprins interact with actin filaments, intermediate filaments and microtubules. The interactions of the LINC complexes couple the nuclear envelope and the cytoskeleton of the cell. Studies have shown that SUN1 is required for the anchorage of Nesprin-1 and Nesprin-2 at the nuclear envelope and inhibition of this interaction can lead to the re-distribution of the nesprin proteins to the ER membrane (Padmakumar et al., 2005; Ketema et al., 2007). How SUN1/2 is involved in the NAE pathway and whether it is directly or indirectly involved is unclear. For example, it is possible that SUN1/2 proteins are simply required for the retention of nesprin at the nuclear envelope. The nesprin proteins are composed of spectrin repeats that can

form long coiled-coil structures, making them potential candidates for vesicular tethering at the nuclear envelope (Nicolas et al., 2014).

1.3.5 Fusion of NAE to the Outer Nuclear Membrane

Following the docking of NAE at the nuclear envelope, it has been proposed that NAE can fuse with the outer nuclear membrane. Fusion events are mediated by two types of SNARE proteins. Over 35 SNAREs exist in mammalian cells. v-SNAREs, typically on the membranes of vesicles, consist of a single polypeptide chain. t-SNARES, typically on target membranes, are formed from a complex of two or three proteins. When a v-SNARE and t-SNARE interact, they form the trans-SNARE complex that catalyse membrane fusion (Alberts, 2019).

There are three types of fusion that could occur between the NAE and the ONM: (1) Full fusion, (2) Kiss and Run, (3) Hug and Kiss. Full fusion would require the NAE to be fully incorporated with the ONM. Kiss and Run fusion was proposed to occurs at synapses, where a small pore is formed transiently, allowing discharge of cargo to occur for less than 6 ms (Stevens and Williams, 2000). However, vesicular PE signal at the nucleus was shown to progressively decrease, indicating the slow discharge of cargo from NAE (Chaumet et al., 2015). A similar mechanism dubbed the 'Hug and Kiss' type fusion was described by (Kurokawa, Okamoto and Nakano, 2014). The Hug and Kiss fusion describes a longer-term interaction between two membranes.

Vesicular fusion to the target membrane results in unloading of the vesicular cargo into the target compartment. The formation of a pore would allow for the translocation of the free cargo from NAE into the lumen of the nuclear envelope. This is supported by the evidence that PE can be detected in the lumen of the nuclear envelope (Chaumet et al., 2015). The transmembrane receptors present on the NAE membrane could be transferred to the ONM. Whilst the ONM is continuous with the ER membrane, the residing proteins

are different, indicating tight regulation of the protein present on the ONM (Schirmer and Gerace, 2005).

1.3.6 Translocation from Outer to Inner Nuclear Membrane

The nuclear envelope has a double membrane consisting of an outer and inner nuclear membrane. NAE fusion to the ONM does not explain how its contents end up in the nucleoplasm. Free cargo such as PE would have to gain access to the nucleoplasm from the lumen of the nuclear envelope through the INM. There would have to be a mechanism to shuttle the membrane-bound receptors from the outer to the inner nuclear membrane.

There have been some studies that can help explain how this may be possible. Whilst the Nuclear Pore Complex (NPC) is typically required for active transport from the cytoplasm into the nucleus, the NPC may also be involved in ONM to INM shuttling. Notably many studies have shown the involvement of importins and Nuclear Pore Complex (NPC) proteins in the nuclear translocation of many RTKs. NLS have been identified in many GPCRs and RTKs such as EGFR and ErbB2. Disruption of the NLS can lead to impaired nuclear translocation of the receptor (Chen et al., 2005; Y. N. Wang et al., 2010; Wang and Hung, 2012; Bhosle, Rivera and Chemtob, 2019). Fibroblast Growth Factor Receptor (FGFR) does not have a putative NLS and can translocate to the nucleus. In addition to this, higher molecular weight isoforms of the FGF ligand contains an NLS, however the 18 kDa isoform of the FGF ligand lacks the NLS, yet it can still trigger the nuclear translocation of FGFR (Reilly and Maher, 2001). This implies that there may be flexibility in the nuclear trafficking of these receptors, and there may be alternative pathways for how the receptors can be transported into the nucleus, discussed in Chapter 1.4.4.

Whilst there is evidence for involvement of the NPC in the nuclear translocation of certain cell surface receptors, how the receptor has access to

the NPC machinery in the cytoplasm remains unclear, arguing for a cytosolic route for the receptor trafficking into the nucleus. However, it is possible that membrane embedded proteins can be translocated from the ONM to the INM via a 10 nm peripheral channel of the NPC. Integral proteins destined for the INM use the NPC peripheral channel to gain access to the INM from the ER via the ONM. Proteins with nucleoplasmic domains of above 70 kDa do not accumulate at the INM, therefore it is possible that a cell surface receptor with a cytosolic domain that have molecular weights under this cut-off may be able to translocate to the INM using the peripheral NPC channel (Zuleger, Korfali and Schirmer, 2008). The cytoplasmic domain of EGFR is 61 kDa, and therefore could be translocated across the peripheral channel of the NPC (Hsu et al., 1990).

The INM-localised SUN2 protein contains an NLS at its nucleoplasmic N-Terminus, which reportedly mediates its targeting to the INM (Turgay et al., 2010). Therefore, it is possible that the NLS present on cell surface receptors such as EGFR, is required for the ONM to INM translocation of the receptor using the peripheral channel, rather than the classical nuclear import though the main channel of the NPC.

1.3.7 Receptor Extraction from Membrane

Once the membrane-bound cargo reaches the INM, it requires extraction from the INM to be free in the nucleoplasm. Aside from the SUN1/2 proteins, Chaumet et al. (2015) reported the involvement of sec61β in the NAE Pathway. Sec61β was also found to be involved in EGFR trafficking to the nucleus by Liao and Carpenter (2007), however, the authors proposed an alternative route to the NAE pathway, discussed in Chapter 1.4.2.

Sec61 is a heterotrimeric complex that resides in the ER membrane. Sec61α, Sec61β, and Sec61γ form a channel in the ER membrane to allow import and export of proteins from the ER. Surprisingly, several studies have found that

Sec61β also resides on the INM (Ying Nai Wang, Yamaguchi, et al., 2010; Chaumet et al., 2015). The authors claimed that the INM-localised Sec61β is involved in EGFR transport into the nucleus. Knockdown of Sec61β led to the accumulation of EGFR at the INM and a reduction in PE translocation into the nucleoplasm. (Ying Nai Wang, Yamaguchi, et al., 2010; Chaumet et al., 2015). This data suggests that Sec61β may have a role at the INM in the nuclear transportation of free cargo (for example PE) and transmembrane receptors (for example EGFR). It not known whether the Sec61α, Sec61γ proteins also localise to the INM or not. Or whether Sec61β can actually form a channel at the INM without its two other complex proteins. Whilst a potential role for Sec61β has been implicated in EGFR and PE transportation into the nucleus, how it may function in the extraction of membrane proteins or allow the translocation of free cargo across the INM requires examination. How the transmembrane domains of cell surface receptors can be soluble in the membrane required further investigations,

Following membrane extraction, either from the INM or elsewhere, the solubilised receptors and free cargo/ligands can be free in the nucleoplasm. Here the cargo can interact with many different factors and proteins leading to changes in cellular activity and many implications including cancer.

1.4 Cell Surface Receptors in the Nucleus

1.4.1 Cell Surface Receptors Localise to the Nucleus

Typically, growth factors and ligands have been thought to influence cellular activities through signal transduction such as EGFR receptors which trigger the Ras/Raf or PI3K/Akt cascades. Several studies in the 1980s had reported the nuclear translocation of exogenous growth factors (Rakowicz-Szulczynska et al., 1986; Raper et al., 1987). Following this, multiple studies have reported that cell surface receptors such as the insulin receptor and EGFR are also translocated to the nucleus with their corresponding ligand (Podlecki et al.,

1987; Kamio et al., 1990; Marti et al., 1991). These reports took decades to be widely accepted as it goes against the paradigm of cell surface receptor signalling at the plasma membrane, leading to questions on whether this phenomenon can occur under physiological conditions. Since then many receptor tyrosine kinases including ERB-2, FGFR-1, VEGFR1, PGDFR-b, EphA2 and many more have been found to translocate to the nucleus (Wells and Marti, 2002; Planque, 2006; Wang and Hung, 2012; Carpenter and Liao, 2013).

Many GPCRs have also been shown to translocate to the nucleus, where they can continue signalling (Boivin et al., 2008; Jong, Harmon and O'Malley, 2018; Bhosle, Rivera and Chemtob, 2019). Whilst several reports have claimed that some GPCRs localise not just to the nuclear membrane, but also in the nucleoplasm, no mechanism has been proposed for how GPCRs, that have seven transmembrane domains, could be solubilised to be free in the nucleoplasm (Lee et al., 2004; Jong, Harmon and O'Malley, 2018).

Various functions have been proposed for the cell surface receptors in the nucleus, suggesting that they actively function in this compartment by regulating gene transcription, independently to their cell surface signalling activities. Increased nuclear accumulation of cell surface receptors has also been implicated in many cancers. Several mechanisms have been proposed for how the cell surface receptors can reach the nucleus, many suggesting retrograde routes. The discovery of the NAE pathway provided a quick and direct route for cell surface receptors to the nucleus. The various trafficking routes, functions, and clinical relevance of the nuclear accumulation of cell surface receptors will be discussed in this section.

1.4.2 Different Routes to the Nucleus

The mechanisms for the nuclear translocation of cell surface receptors remain unclear, however, many models have been proposed. Here, we discuss the

four proposed models (Models A-D), all of which require endocytosis of the cell surface receptor at the plasma membrane. Models A and B described a retrograde trafficking route to the nucleus, whilst Models C and D describe direct delivery via endosomes (Figure 1.7).

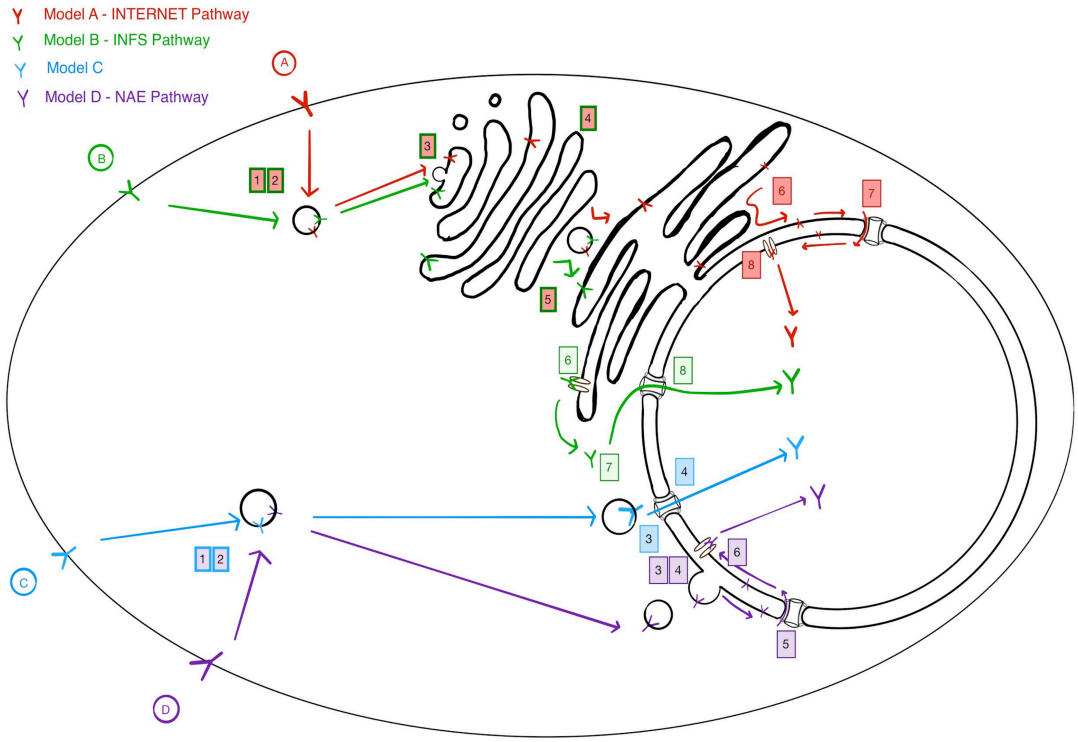

Figure 1.7 Routes to the nucleus for cell surface receptors. The current models to explain the nuclear translocation mechanism for cell surface receptors. The different steps required are numbered, 1: Endocytosis and 2: Sorting into the proper endosomal pathway are common to all models. Models A and B: Step 3: Targeting and fusion of endosomal carriers to Golgi membranes, 4: Retrograde Golgi traffic across the Golgi, 5: Transport from the Golgi to the ER. Model A: 6; diffusion of receptor to the outer nuclear membrane (ONM), 7: Transport across the Nuclear Pore Complex (NPC) to the inner nuclear membrane (INM), 8: Extraction to the nucleoplasm via an INM embedded channel. Model B: Step 6: Extraction to the cytosol via an ER embedded channel, 7: Binding to nuclear targeting factors, 8: Transport across the NPC. Model C: Step 3: Targeting to the nuclear envelope and interaction with the NPC, 4: Translocation and extraction across the NPC into the nucleoplasm. Model D: Step 3: Targeting and docking to the nuclear envelope, 4: Fusion of membranes and transfer of material to the outer nuclear membrane, 5: Transport across the NPC, 6: Extraction to the nucleoplasm via an INM embedded channel. *Illustration from Shah et al. (2019).*

Models A, INtegral Trafficking from the ER to the Nuclear Envelope Transport (INTERNET) and Model B, Integrative Nuclear FGFR-1 Signalling (INFS) describe a long retrograde trafficking route to the nucleus, in which cargo can

be transported in endosomes to the Golgi, followed by subsequent trafficking to the ER. Many cargo and toxins, including PE, use this route to gain access to the ER. The Golgi to ER translocation can occur through COPI vesicles, as EGFR has been shown to interact with γ-COP, a subunit of the COPI vesicle coat, providing evidence for a retrograde trafficking route for cell surface receptors (Ying Nai Wang, Wang, et al., 2010). Further evidence for the retrograde pathway for cell surface receptors comes from investigating the nuclear translocation of PDGFRβ. The authors provide evidence that the use of the Golgi-blocker BFA resulted in a slight decrease in nuclear PDGFRβ levels, indicating transit through the Golgi (Papadopoulos, Lennartsson and Heldin, 2018).

Once at the ER, the Model A and B diverge in their proposed routes to the nucleus. Wang et al. (2010) propose the INTERNET model (Model A) and argue that as the ER membrane is continuous with the ONM, receptors such as EGFR can be transported to the ONM from the ER. Then from the ONM, EGFR can be subsequently translocated to the INM through the NPC, akin to how resident proteins are targeted to the INM.

Model B, the INFS pathway, was proposed by Stachowiak, Maher and Stachowiak (2007) when investigating the nuclear translocation of FGFR1. They report that FGFR1 is released from the ER membrane into the cytosol, from where it can be imported into the nucleus through the NPC (Reilly and Maher, 2001; Stachowiak, Maher and Stachowiak, 2007). They state that FGFR1 import into the nucleus is mediated by importin-β, as it co-precipitated with importin-β despite lacking an NLS. EGFR was also shown to traffic to the ER to be released into the cytoplasm in a Sec61β dependent manner, perhaps by a mechanism similar to ERAD, as both translocations involve the sec61 proteins (Liao and Carpenter, 2007). This provides further evidence that the solubilisation of cell surface receptors can occur at the ER membrane.

Model C suggests that endosomes serve as vehicles to transport cell surface receptors into the nucleus and are transported across the NPC into the nucleoplasm. The authors showed the interaction of the ErbB-2 receptor with the early endosomal marker EEA1 and the requirement for the nuclear pore complex for the nuclear entry of the receptor (Giri et al., 2005). However, this model was not able to account for how the receptor escapes the endosomal membrane to have access to nuclear import machinery. This model was suggested by the authors who later postulated the INTERNET model.

Model D, the NAE Pathway, proposes a simple and more direct route to the nucleus. Chaumet et al. (2015) discovered that PE-labelled vesicles are closely associated with the nuclear envelope using 3D-SIM microscopy. PE and EGFR displayed co-localisation, suggesting that they are both localised to the same vesicle and may follow the same pathway to the nucleus. The revelation of the data that provides evidence that vesicles, termed NAE, can directly dock and fuse with the outer nuclear membrane, provides an explanation for how cell surface receptors are released from the endosomal membrane. Rather than release into the cytoplasm, as suggested in Model C, the fusion of NAE with the nuclear envelope can result in direct transfer of the cell surface receptor to the ONM. From the ONM, the cell surface receptor can be translocated from the ONM to the INM using the peripheral channel of the NPC, similar to the translocation proposed in the INTERNET pathway, Model A. Once at the INM, the receptor can be solubilised at the INM to be free in the nucleoplasm.

Whilst there is evidence that using the Golgi-blocker BFA results in reduction in nuclear levels of EGFR and PDGFRβ, PE vesicles at the nucleus were not affected upon BFA treatment (Ying Nai Wang, Wang, et al., 2010; Chaumet et al., 2015; Papadopoulos, Lennartsson and Heldin, 2018). Another study demonstrated that BFA treatment did not affect CD44 translocation into the nucleus, whereas treatment with nocodazole, a microtubule inhibitor did, implicating the endocytic pathway, but not the Golgi in the nuclear import of

CD44 (Janiszewska et al., 2010). The final argument in favour of the NAE pathway is the timing. Exogenous PE, EGF stimulated EGFR and biotinylated insulin receptor (biotinylating was used as an indication that the insulin receptor originated from the plasma membrane) can reach the nucleoplasm within ten minutes after stimulation at the plasma membrane (de Angelis Campos et al., 2011; Amaya et al., 2014; Chaumet et al., 2015). Whereas retrograde trafficking of toxins such as PE and ricin can take several hours (Braham et al., 1988; Moreau et al., 2011). However, these pathways are not mutually exclusive, as a long retrograde trafficking route and a short direct route are both feasible. Further investigations would be required to determine whether the pathway they take is dependent on the individual receptor, the stimulant or due to other cellular factors.

1.4.3 Functions of cell surface receptors in the nucleus

Many nuclear functions have been proposed for receptor tyrosine kinases, including activation of gene transcription. The genes that can be transactivated by the cell surface receptor seem to be correlated with the function of the receptor itself. For example, nuclear EGFR can upregulate genes associated with cell proliferation, insulin receptor can regulate the transcription of genes involved in insulin-related functions such as lipid metabolism and VEGFR can upregulate its own transcription to amplify angiogenic processes (Domingues et al., 2011; Brand et al., 2013; Hancock et al., 2019). Chromatin immunoprecipitation (ChIP) assays were used to determine that nuclear VEGFR2 binds to the Sp1-responsive region of the VEGFR2 proximal promoter (Domingues et al., 2011).

Increased levels of nuclear EGFR have been found in highly proliferative tissues, and can act as a transcription factor for an extensive list of genes, including cyclin D1, Aurora-A and b-Myb, all of which are involved in cell cycle progression (Lin et al., 2001). Whilst EGFR itself does not contain a putative DNA-binding domain, it can interact with co-factors such as Signal transducer

and activator of transcription (STAT5), STAT3 or E2F1 to activate transcription (Lo, Hsu, et al., 2005; Hanada et al., 2006; Hung et al., 2008).

Exposure to DNA-damaging reagents such as H_2O_2, heat or cisplatin induced the nuclear translocation of EGFR. Nuclear EGFR can function in DNA damage repair by interacting with DNA-protein kinase, which is involved in nonhomologous end joining of DNA following double stranded breaks (Dittmann et al., 2005). The role of nuclear EGFR in DNA damage repair was further solidified when it was revealed that EGFR can phosphorylate Tyr 211 on proliferating cell nuclear antigen (PCNA). Phosphorylation of this residue may stabilise PCNA interaction with chromatin, essential for the formation of the DNA clamp that can recruit proteins involved in DNA replication and DNA damage repair (Wang et al., 2006).

Whilst EGFR is the most widely studied example, other receptors also have a variety of functions in the nucleus. PDGFRβ is involved in chromatin re-modelling and controls proliferation by regulating p21 levels (Papadopoulos, Lennartsson and Heldin, 2018). The GPCR GABA-B has been shown to interact with transcription factors such as ATF (White et al., 2000). Nuclear FGFR has been reported to induce the expression of c-jun, a protein that forms the AP-1 transcription factor to regulate cell proliferation (Reilly and Maher, 2001). It is becoming evidently clear that the nuclear accumulation of RTKs can have vast implications in the regulation of cellular activity.

1.4.4 Clinical relevance of receptors in the nucleus

Once at the nucleus, cell surface receptors have functions including roles in cell proliferation, DNA damage repair and transcriptional regulation (Lin et al., 2001; Planque, 2006; Chen and Nirodi, 2007). The presence of receptors in the nucleus, such as EGFR, can have severe pathological implications. Nuclear EGFR is expressed in a large variety of cancerous tissues such as Non-small cell lung cancer, ovarian cancer and breast carcinomas. High levels

of nuclear EGFR have been correlated to poor prognosis in many cancers and has been inversely correlated with survival in patients (Lo, Xia, et al., 2005; Xia et al., 2009; Traynor et al., 2013; Wang et al., 2018).

EGFR has been identified as an oncogene leading to the development of many therapeutics targeting EGFR directly. Many EGFR inhibitors, such as gefitinib, a small molecule inhibitor that binds the ATP binding pocket required for EGFR activation, and cetuximab, a monoclonal antibody that binds the extracellular domain of EGFR to prevent ligand binding, have been approved for the treatments of cancer and have been shown to increase overall survival in patients (Minna, Peyton and Gazdar, 2005). Nuclear EGFR is associated with resistance to gefitinib and cetuximab (Li et al., 2009; Huang et al., 2011). Higher levels of nuclear EGFR, due to its roles in DNA damage repair, can lead to resistance to radiotherapy, making nuclear EGFR an attractive target for cancer therapeutics (Chen and Nirodi, 2007).

Trastuzumab, commonly known as Herceptin, is a monoclonal antibody against the ErbB-2 receptor (also known as HER2). Trastuzumab has had a high success rate, prolonging overall survival in HER2 positive breast cancers (Vogel et al., 2002; Moja et al., 2012). Higher levels of nuclear ErbB-2 receptor resulted lower overall survival in breast cancers and can be a biomarker for poor clinical outcome (Schillaci et al., 2012). Targeting nuclear ErbB-2 can overcome trastuzumab resistance and inhibit cancer cell growth (Cordo Russo et al., 2015). Identification of the key regulators and machinery involved in the NAE pathway, and finding out how the pathway is triggered may help to specifically block the pathway that is associated with the nuclear accumulation of cell surface receptors and its associated pathological condition.

1.5 Aims

A novel endosomal trafficking route to the nucleus was described by (Chaumet et al., 2015). The authors provided substantial evidence that endosomes, termed NAE, are closely associated with the nuclear envelope using electron and super-resolution microscopy. The authors also implicated the role of the NAE pathway in the translocation of cargo such as cell surface receptors from the cell surface to the nucleus. As this is a novel pathway, the first aim of this thesis is to visualise NAE and characterise the NAE pathway using PE as a marker for NAE. The second aim of the project is to develop an RNAi based assay for use in a high-throughput screening to screen for regulators of the NAE Pathway. The hits identified in the screen will be validated and the precise role of the regulator in the NAE pathway will be investigated.

Chapter 2: Methods

2.1 Cell culture

MG-63 cells (Sigma, 86051601), HeLa cells (HPA/ECACC, 93021013) and MDA-MB-231 (ATCC, HTB26) were grown in Hyclone high glucose Dulbecco Modified Eagle Medium (DMEM - Gibco) supplemented with 10% heat inactivated fetal bovine serum (FBS - Sigma). HeLa cells were additionally supplemented with 100 U/ml penicillin and 100 µg/ml streptomycin. Both cell lines were kept at 5% CO_2 at 37°C. Both cell lines were passaged twice per week and kept for a maximum of 30 passages.

2.2 Molecular Biology

DNA plasmids for overexpression of proteins in MG-63, MDA and HeLa cells were used in this study. Plasmids used were supplied by the Royle lab or generated for this study, for which the cloning method is shown in Table 2.1 if generated. Suitable vectors were selected for cloning using the restriction enzyme digestion method. If the insert did not have the selected restriction sites flaking the region of interest, then PCR amplification was used for the addition of the restriction sites. The primers used for restriction site insertion are listed in Table 2.2. The vectors and inserts were then digested, ligated using Quick ligase (NEB, M2200), and transformed into DH5α E. coli. Colonies were amplified and plasmid DNA was extracted using the GeneJET Plasmid Miniprep Kit (Thermo Sientific). Clones were checked by restriction digestion and sent for sequencing to Source BioScience. The verified clone was added to the Royle lab plasmid database.

Table 2.1 List of plasmids used in this study. Constructs were sourced from the Royle lab database, indicated by the plasmid ID number, or cloned for this study, for which the cloning method is stated.

Plasmid	Insert	Vector	Cloning Method	Plasmid ID	Source / Cloned by
GFP-Rab5a	Rab5a	pEGFP-C2	-	1905	Royle Lab
GFP-Rab7a	Rab7a	pEGFP	-	1907	Royle Lab
GFP-Rab9	Rab9a	pEGFP-C3	-	1910	Royle Lab
GFP-Rab5a-QL	GFP-Rab5a-QL	pEGFP-C2	-	2017	Royle Lab
GFP-Rab19	Rab19		-	1919	Royle Lab
GST-Rab19	Rab19	pGEX-6P1	-	2110	Royle Lab
GFP-EEA1	EEA1	pEGFP-C1	-	1121	Royle Lab
GFP-FKBP	FKBP	pEGFP-C1	-	1969	Royle Lab
pMito-mCherry-FRB	MitoTrap	pMito	-	681	Royle Lab
Stargazin-mCherry-FRB	Stargazin	mCherry-FRB	-	2270	Royle Lab
GFP-Rab19-QL	Synthesised from GenScript	GFP-Rab5a	BamHI / AgeI	2679	Poonam Shah
GFP-Rab19-TN	Synthesised from GenScript	GFP-Rab5a	BamHI / AgeI	2680	Poonam Shah

GFP-FKBP-Rab19	Rab19	GFP-FKBP	XhoI / SalI	2681	Poonam Shah
GFP-FKBP-Rab19-QL	Rab19-QL	GFP-FKBP	XhoI / SalI	2701	Poonam Shah
GFP-FKBP-Rab10-TN	Rab19-TN	GFP-FKBP	XhoI / SalI	2702	Poonam Shah
GFP1-10-NLS	GFP1-10	mCherry-NLS	NheI / XhoI	2703	Poonam Shah
GFP1-10-NES	G block NES	GFP1-10-Emerin	XhoI / BamHI	2704	Poonam Shah
GFP1-10-Emerin	GFP1-10	Emerin-EGFP-C1	NheI / XhoI	2705	Poonam Shah
GFP1-10-KASH	G block - KASH	GFP1-10-Emerin	XhoI / BamHI	2706	Poonam Shah
GFP11-Rab19	Rab19	GFP11	XhoI / SalI	2707	Poonam Shah
GFP11-Rab19-QL	Rab19-QL	GFP11	XhoI / SalI	2708	Poonam Shah
GFP11-Rab19-TN	Rab19-TN	GFP11	XhoI / SalI	2709	Poonam Shah
mCherry-Rab19	mCherry	GFP-Rab19	AgeI / BsrGI	2710	Poonam Shah

Sequences of primers used for the insertion of restriction sites for cloning are shown in Table 2.2. Sequencing primers for detection of the light and heavy chain regions for use in phage display experiments are also listed in Table 2.2, these primers were designed by Xavier Le Guezennec.

Table 2.2 List of primers used in this study.

Primer	Primer Sequence
Rab19Forward XhoI	GATCCCCCTCGAGGGATGCACTTCTCCAGC
Rab19Reverse SalI	CCGTCGAGGTCGACTTAGCAAGTGCAGTGG
GFP1-10Forward NheI	CAGATCTGCTAGCATGTCCAAAGGAGAAG
GFP1-10Reverse XhoI	GGCCCTCTAGACTCGAGTTCCGCCGCCACCTG

For the cloning of Rab19 constitutively active mutant, the plasmid was synthesised from Genscript with a codon optimised sequence of human Rab19. The amino acid at 76 position was substituted from glutamine to a leucine. For the dominant negative mutant, amino acid 31 was substituted from a threonine to an asparagine (Table 2.3). These GFP-tagged mutants were then sub-cloned into the vectors described in Table 2.1. Short sequences for the KASH and NES domains were generated using G block synthesis from IDT with flanking restriction sites suitable for sub-cloning into the appropriate vector (Table 2.1 and Table 2.3).

Table 2.3 Plasmid /Insert G block synthesis.

Plasmid	Supplier	Insert / G Block Sequence
GFP-Rab19-QL	Plasmid synthesis-Genscript	GFP-Rab19 (Q→L mutation) Vector - puc57
GFP-Rab19-TN	Plasmid synthesis-Genscript	GFP-Rab19 (T→N mutation) Vector - puc57
KASH	G block - IDT	GAGGAAGTGTACTCGAGGGCGCTCC TTCCTCTCAAGGGTGGTCCGGGCAG CCCTACCCCTGCAGCTGCTCCTCCT GCTGCTGCTGCTCCTGGCCTGCCTG CTGCCCTCCTCCGAAGAAGACTACA GCTGCACTCAGGCCAACAACTTTGC CCGGTCCTTTTACCCCATGCTGAGG

		TACACCAATGGGCCACCCCCCACAT AAGGATCCGAGGAAGTGGA
NES	G block - IDT	GGAGGAGTAGGATGAGTAGGAGGAA GTGGACTCGAGGGAGTGAGCTGCA GAACAAGCTGGAAGAGTTGGATCTG GACTCGTACAAGTAAGGATCCAGGA GTAGAAGTATGAAGTGGAGGAGGAG GA

2.3 DNA transfection

Transfection of MG63 and MDA cells was carried out using Lipofectamine 2000 (ThermoFisher UK). Cells were seeded on coverslips in 12-well plates 24 h before transfection at 50% confluency, 300,000 cells in 1 ml DMEM. The media was replaced with serum-free media (Opti-MEM) 2 h before transfection. A total of 0.5 µg DNA and 2.5 µl of lipofectamine in serum-free media was incubated for 15 min at RT. If two plasmids were co-transfected, 0.25 µg of DNA of each plasmid was used. This mixture was added to cells and incubated at 37°C for 6-8 h. The media was replaced with full fresh media the next day and cells were processed after 48 h post-transfection.

Transfection of Hela cells was carried out using GeneJuice (Merck UK). Cells were seeded in 12-well plates on coverslips 24 h before transfection at 50% confluency, 200,000 cells. The media was replaced with 1 ml fresh full media before transfection. In a 1.5 ml Eppendorf tube, 50 µl of serum-free media (Opti-MEM) and 1.5 µl of GeneJuice was added. The mixture was pipetted thoroughly. A total of 0.5 µg of DNA was added to the mixture, vortexed and incubated for 15 min at RT before adding to cells. Cells were incubated for 48 h at 37°C before processing.

2.4 siRNA transfection

siRNA transfection was carried out with Lipofectamine RNAiMAX (ThermoFisher) in 384-well plate for high-content screening and 6-well plate for cell fractionation. All siRNAs were supplied from Dharmacon, Horizon Discovery, in ON-TARGETplus (or Accell for GFP siRNA) and in SMARTpool or individual format, listed in Table 2.4. For custom Rab and SNARE library, 2.5 µl of 0.5 µM siRNA was dispensed into a 384-well plate, printed in IMCB, Bard lab by Xavier Le Guezennec. The libraries were sealed and stored at -80°C.

For RNAi in a 6-well plate format, 1.5 µl siRNA (50 µM), 4 µl Lipofectamine and 494.5 µl Opti-MEM was added to a 1.5 ml Eppendorf tube, incubated for 20 min at RT and seeded on a 6-well plate. Cells were seeded at a density of 200,000 in 2.5 ml per well and incubated for 72 h. For RNAi in a 384-well plate format for high content imaging, 2.5 µl siRNA (0.5 µM), 0.1 µl Lipofectamine and 7.4 µl Opti-MEM was added per well to a 384-well plate (Perkin Elmer, CellCarrier™ ultra) and incubated for 20 min at RT. Cells were seeded at a density of 2250 in 40 µl per well and incubated for at 37°C for 72 h. The siRNA/lipofectamine mixture was not removed from cells until ready for further processing. If DNA was also introduced, sequential transfection was carried out, with DNA transfection conducted 48 h after siRNA transfection.

Table 2.4 List of siRNAs used in this study.

Gene	Target Sequence
SNARE Library	On-Target Plus SMARTpool
Rab GTPase Library	On-Target Plus SMARTpool
Rab19 SMARTPOOL	On-Target Plus SMARTpool (Rab19 Si1- Rab19 Si4)
RAB19si1	CCUUGAUAUUGACGGCAAA
Rab19si2	AGACACAGCAGAACACGAU
Rab19si3	GCACACUGGCUGAGAAGUA

Rab19si4	UCACUGGAUUCAUGAGAUA
Rab19si5 3'UTR A	AGGAAAGGAGGAAGGCAAAUU
Rab19si6 3'UTR B	CAGGGAGAAUGGAACGAAAUU
NT	1: UGGUUUACAUGUCGACUAA 2: UGGUUUACAUGUUGUGUGA 3: UGGUUUACAUGUUUUCUGA 4: UGGUUUACAUGUUUUCCUA
SUN2	1: CCAGAGACUCAUCGCCACA 2: CCUGAGGGCCUUCGACAAA 3: GGAAACUGCUGCUCGCAUC 4: AGAGCUCGGUGGCGGAAGA
LRP1 SMARTPOOL	1: GCAAGAAGCCGGAGCAUGA 2: GAACAAACACACUGGCUAA 3: GCUAUGAGUUUAAGAAGUU 4: GCGCAUCGAUCUUCACAAA
PLK1	1: GCACAUACCGCCUGAGUCU 2: CCACCAAGGUUUUCGAUUG 3: GCUCUUCAAUGACUCAACA 4: UCUCAAGGCCUCCUAAUAG
GFP	GCCACAACGTCTATATCAT
Rab11B SMARTPOOL	1: CGAGUACGACUACCUAUUC 2: GACAGAAGCCCAACAAGCU 3: GGAUUCCACUAACGUAGAG 4: UAACGUAGAGGAAGCAUUC
Rab7A SMARTPOOL	1: CUAGAUAGCUGGAGAGAUG 2: GUACAAAGCCACAAUAGGA 3: AAACGGAGGUGGAGCUGUA 4: CGAAUUUCCUGAACCUAUC

2.5 Pseudomonas Exotoxin A (PE) Uptake

For PE uptake experiments, MG63 cells were incubated for the appropriate incubation period following siRNA and/or DNA transfection. A truncated version of PE (tPE26-389) recombinant purified protein was generated in the lab for use in optimisation experiments (Ting, Chaumet and Bard, 2020), and commercial full-length PE from Sigma was used in screening and follow up experiments. Media was removed from cells and 500 nM of PE in full DMEM was added. Cells were incubated for 30 min for rapamycin-induced protein re-routing experiments (Chapter 2.6) or for 1 h for NAE quantification experiments and subcellular fractionation (Chapter 2.8) at 37°C, 5% CO_2. Cells were washed twice in PBS before fixing and processing for subsequent immunofluorescence experiments was carried out.

2.6 Rapamycin-induced protein rerouting

Cells were seeded and co-transfected with FKBP and FRB tagged plasmids. The addition of rapamycin (Alfa Aesar), allows rapid re-routing of protein of interest with an FKBP to an anchor tagged to FRB, due to the dimerization of the FRB and FKBP domains. In this study, MitoTrap (mitochondria with the yeast outer membrane protein) (Robinson, Sahlender and Foster, 2010) was used as a mitochondrial anchor, tagged with FRB and mCherry. This allowed the re-routing of GFP-FKBP, GFP-FKBP-Rab19, GFP-FKBP-Rab19-QL and GFP-FKBP-Rab19-TN to the mitochondria, illustrated in Figure 2.1. Figure 2.1 also illustrates that two pools of Rab proteins can be potentially be re-routed, a cytosolic GDP-bound Rab pool or a membranous-GTP bound Rab pool.

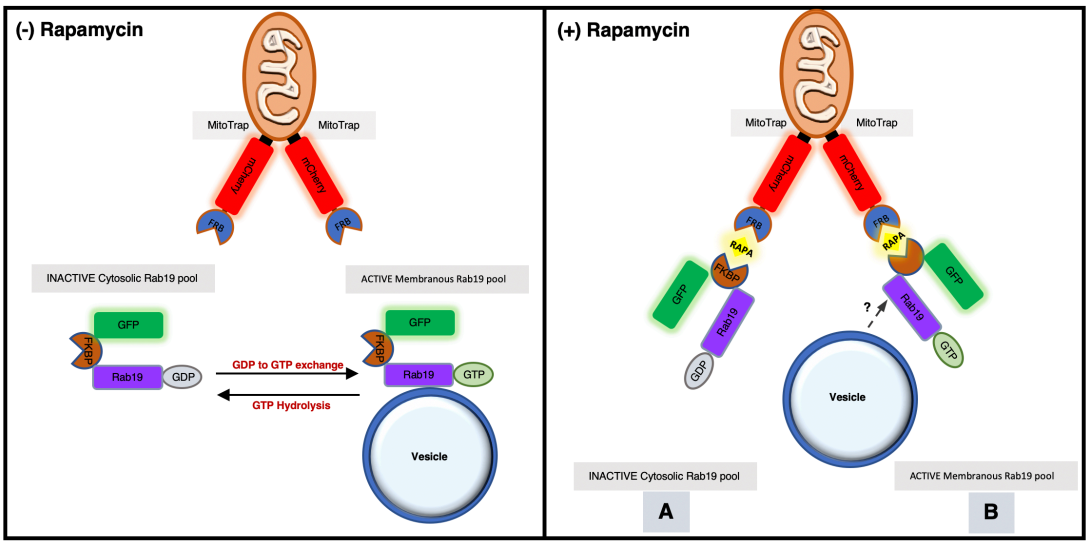

Figure 2.1 Schematic illustration of rapamycin-induced re-routing of the active and inactive pools of Rab19. FKBP tagged Rab19 re-routes to FRB tagged mitochondrial anchor upon addition of rapamycin. The FKBP tagged Rab protein could originate from (A) the inactive cytoplasmic pool of GDP bound Rab19 or (B) the membranous pool of GTP bound Rab19 prior to re-routing. Membranous pool of Rab19 could be extracted from vesicular membrane upon addition of rapamycin or vesicular re-routing occurs.

For live cell imaging, 48 h after transfection, the media of cells seeded on fluorodishes (World Precision Instruments) was replaced with 0.5 ml of L-15 supplemented with 10% FBS and 2 drops of NucBlue™ (Molecular Probes) and incubated at 37°C for 0 h 20 min. Cell were imaged on a Nikon CSU-W1 confocal microscope with SoRa upgrade using a 100X oil objective. Cells were imaged at 5 frame/s. A minimum of 3 frames were acquired before the addition of rapamycin. A 2X concentration of 400 nM rapamycin (resulting in a final concentration of 200 nM rapamycin) or control DMSO (Sigma) in 0.5 ml L-15 media supplemented with 10% FBS was added to cells. Rapamycin/DMSO was added whilst continuing image acquisition.

For fixed cells seeded on coverslips on a 12-well plate, 48 h after transfection, 0.5 ml of 200 nM rapamycin in L-15 media supplemented with 10% FBS was added to cells and incubated for 30 min at 37°C. The media was removed and 0.5 ml of 500 nM PE ligand in full DMEM was added to cells and incubated for 1 h at 37°C. Cells were washed for 5 min in PBS twice before fixation and processing for immunofluorescence.

2.7 Immunofluorescence

For immunofluorescence experiments in a plate format, cells were fixed 48 or 72 h post transfection with 4% PFA, 3% Sucrose in PBS at RT for 15 min. Cells were permeabilised and blocked for 20 min in 2% FBS, 0.2% Triton X-100 in PBS (blocking/permeabilization solution). Cells were incubated with primary antibodies in blocking/permeabilization solution for 4 h (Table 2.5). Cells were washed in PBS for 5 min 3 times. Cells were incubated with secondary antibodies conjugated to Alexa-fluor 488, 568 or 647 (Life technologies) diluted to 1:500, and with Hoechst 33342, trihydrochloride, trihydrate (10 mg/ml in water diluted to 1:10,000) in PBS for 45 min. Cells were washed 3 times in PBS and stored at 4°C before imaging.

For immunofluorescence of cells plated on coverslips, cells were fixed with 4% PFA, 4% Sucrose in PBS at RT 15 min. Cells were permeabilised with 0.5% Triton X-100 in PBS for 10 min and blocked in 3% BSA, 5% Goat Serum in PBS for 1 h. Cells were incubated with 80 µl primary antibodies in blocking solution overnight (Listed in Table 2.5). Cells were washed in PBS for 5 min 3 times. Cells were incubated with 400 µl secondary antibodies conjugated to Alexa-fluor 488, 568 or 647 (1:500) in blocking solution. Cells were washed in PBS for 5 min 3 times. Coverslips were dipped in molecular grade water and left to dry for 30 min. Coverslips were mounted on slides with 8 µl Vectashield medium (Vector laboratories) with DAPI and sealed with nail varnish. Slides were stored at 4°C in the dark before imaging.

Table 2.5 List of antibodies used in this study

Primary Antibody	Species	Supplier	Working Concentration / Dilution
Anti-Pseudomonas Exotoxin A	Rabbit	Sigma-Aldrich (P2318)	1:200 (IF) 1:2000 (WB)

Anti-SUN2	Rabbit	Sigma-Aldrich (HPA001209)	1:500 (IF) 1:2000 (WB)
Anti-GAPDH	Rabbit	Abcam (ab181602)	1 µg/ml (WB)
Anti-MAX	Mouse	Abcam (ab53570)	0.1 µg/ml (WB)
Anti-Calnexin	Rabbit	Abcam (ab10286)	1:5000 (WB)
Anti-LRP1	Rabbit	ThermoFisher	0.5 µg/ml (WB)
Anti-EEA1	Mouse	BD Biosciences	1 µg/ml (IF)
Anti-TGN	Sheep	BioRad	0.5 µg/ml (IF)
Anti-Rab5	Rabbit	Cell Signalling	1:200 (IF)
Anti-Lamin A/C	Mouse	Abcam (ab8984)	1:500 (IF)
Anti-GFP	Rabbit	Invitrogen	1:2000 (WB)
Alexa-fluor 488	Goat anti-rabbit	Life Technologies	1:500 (IF)
Alexa-fluor 561	Goat anti-rabbit	Life Technologies	1:500 (IF)
Alexa-fluor 647	Goat anti-mouse	Life Technologies	1:500 (IF)
M13 HRP	Mouse	Invitrogen (A5B3)	0.2 µg/ml (ELISA)
Anti-GST HRP	Mouse	Sigma (A7340)	1:10000 (WB)
Anti-tubulin HRP	Rabbit	Invitrogen	1:30000 (WB)
Anti-myc HRP	Mouse	ThermoFisher	1:1000 (WB)
Anti-Rab19	Rabbit	Invitrogen	1 µg/ml (WB)

2.8 Subcellular Cell Fractionation

MG-63 cells transfected with siRNA in a 6-well plate format (as described in chapter 2.4) in replicates of two, one for total cell lysate and one for cell fractionation. Cells were incubated with PE toxin in full DMEM for 1 h at 37°C

at a final concentration of 200 nM. Media was removed and cells were washed with PBS twice. Cells were collected in an Eppendorf tube using a cell scraper in 0.5 ml ice-cold PBS and kept on ice. Cells were centrifuged at 1500 g for 15 min and supernatant was removed. Cell pellets were stored on ice. Total lysate was obtained by adding 200 µl RIPA buffer to one cell pellet. Cells were fractionated with Cell Surface Protein Isolation Kit (#89881, Thermo Fisher Scientific) according to manufacturer's instructions. An additional spin of 15 min at 1500 g was conducted after the first spin of the cytoplasmic fraction purification to increase the fraction purity and remove membranous compartment contaminants. The rest of the steps were followed as instructed to obtain a cytoplasmic, membrane and nuclear fractions of cells. Fractions were analysed by Western blotting.

2.9 PE toxin purification

Truncated Pseudomonas Exotoxin A (tPE26-389) purification was carried out with bacterial protein expression in BL21 cells. A 5 ml pre-culture cells in LB + 100 µg/ml ampicillin was grown overnight at 37°C at 200 RPM. Pre-culture was used to grow 60 ml of culture until an OD of 0.4-0.6 was reached. Protein expression was enhanced by 0.1 mM IPTG (Thermo Scientific) induction. Ni-NTA beads were washed in lysis buffer (50 mM Tris pH8, 170 mM NaCl, 0.5% NP40, 6 M urea). Centrifugation of media at 10,000 g for 10 min to pellet cells. Lysis of bacteria was carried out with sonication in lysis buffer for 10 s with 10 s pause for 2 min 30 s on, at 200-300 W. Sonicated samples were centrifuged for 30 min at 15,000 RPM at 4°C. Supernatant was transferred to beads topped up with 10 ml lysis buffer and beads were placed on roller overnight at 4°C. Three washes were carried out with wash buffer (100 mM Tris pH8, 500 mM NaCl, 0.5% NP40, 6 M urea, 40 mM Imidazole). Protein was eluted with 2 ml elution buffer (100 mM Tris pH8, 500 mM NaCl, 0.5% NP40, 6 M urea, 1 M Imidazole). Slide-A-Lyzer Dialysis Cassette, 3 ml capacity and 100,000 MWCO (Thermo Scientific) was used for dialysis of eluted proteins. Samples were loaded into the cassettes with a 3 ml syringe. PBS was changed

3 x with 4 h incubations at 4°C under gentle shaking. BCA assay was used to determine protein concentration. Coomassie stain and western blot to confirm protein size.

2.10 Coupling of PE to dye

Pseudomonas Exotoxin A (Sigma) at 1 mg/ml was coupled to HiLyte™ Fluor 594 acid using the Alexa Fluor™ 594 Antibody Labelling Kit SE (AnaSpec, A20185). HiLyte Flour 594 dye was resuspended in 55 µl DMSO. 100 µl Reaction buffer was added to 1 ml PE toxin. 10 µl of the dye/DMSO mix was added to PE and incubated for 1 h at 4°C. Free dye was eluted in Millipore 15 MWCO size exclusion columns.

2.11 Rab19 protein purification

Pre-culture of GST-Rab19 in LB media + ampicillin was grown overnight at 37°C 200 RPM. 10 ml of the pre-culture was added to 390 ml LB + 100 µg/ml Ampi + 1% glucose, and incubated at 37°C at 200 RPM until an OD of 0.6-0.8 was reached. 1 mM of IPTG induction was carried out and incubated at 220 RPM at 25°C overnight (9 h). The culture was centrifuged at 10,000 g for 10 min at 4°C, and pellets were stored at -80°C until ready for purification. Glutathione Sepharose™ 4B (GE Healthcare) were washed with lysis buffer (25 mM Tris, 140 mM NaCl, 3 mM KCl, protease inhibitor tablet, 0.1 mM PMSF, 0.1% Triton X-100, 1 mg/ml lysozyme, pH 8) and prepared to give 50% slurry. Bacterial cell pellets were resuspended in 20 ml lysis buffer and sonicated for 10 s with 10 s pause for 2 min 30 s on at 200-300 W on ice. Samples were centrifuged for 30 min at 10,000 g 4°C. The supernatant was added to 800 µl slurry Glutathione Sepharose™ 4B and incubated at 4°C for 2 h with gentle agitation. Beads were centrifuged at 500 g for 5 min and washed with wash buffer 1 (25 mM Tris, 140 mM NaCl, 3 mM KCl, protease inhibitor tablet, 0.1 mM PMSF, 0.1% Triton X-100, pH 8). The wash was repeated, and the third final wash was carried out in a high salt wash buffer

(25 mM Tris, 500 mM NaCl, 3 mM KCl, protease inhibitor tablet, 0.1 mM PMSF, 0.1% Triton X-100 pH 8). Samples were eluted in Elution buffer (25 mM Tris, 140 mM NaCl, 3 mM KCl, 50 mM glutathione, pH 8). Slide-A-Lyzer Dialysis Cassette, 0.1 – 0.5 ml capacity and 10,000 MWCO (Thermo Scientific) was used for dialysis of eluted proteins. Samples were loaded into the cassettes with a 1 ml syringe. PBS was changed 3 x with min 4 h incubation at 4°C under gentle shaking. BCA assay was used to determine protein concentration. Coomassie stain and western blot to confirm protein size.

2.12 Phage Display - Panning

TG1 cells were grown in YT Media at 37°C overnight. Three rounds of pannings were carried out to enrich for phage that bind to GST-Rab19. Removal of non-specific phage binding was carried out by depletion against BSA/milk and recombinant GST protein (SinoBiological). Nunc MaxiSorp™ flat-bottom (ThermoFisher) 96-well plates were coated with 1% BSA / 1% milk in PBS, 1 µg of recombinant GST in 50 mM $NaHCO_3$ pH 9.6.and 1 µg of GST-Rab19 in 50 mM $NaHCO_3$ pH 9.6, sealed and stored at 40°C overnight. The wells were washed with PBST (PBS + 0.05% Tween) three times. 50 µl of phage library in 150 µl blocking buffer (PBST with 2% Milk) was added well containing BSA/ milk, and 200 µl of blocking buffer was added to wells coated with recombinant GST and GST-Rab19 and incubated for 1 h. Blocking buffer was removed from the GST coated well, and phage were transferred from BSA well to GST well and incubated for 1 h. Blocking buffer was removed from GST-Rab19 well and phage were transferred from GST well to GST-Rab19 well and incubated for 2 h. 5 washes of wells were carried out using 400 µl PBST.

2.13 Phage Display - Amplification and Elution

Bound phage were eluted from the GST-Rab19 well with 150 µl High-grade trypsin (Sigma) 10 µg/ml at 37°C 400 RPM for 30 min. TG1 cells were grown in YT media so that an OD of 0.4 was reached towards the end of the phage elution incubation period. Transduction of phage eluate was carried out with 150 µl TG1 cells (OD=0.4) at 37°C for 30 min, static. Transduce along with input phage library. Serial dilutions of 2 µl input and eluate phage in 18 µl YT media were spotted on large YT Ampi + 1% glucose agar dishes, along with the rest of the eluate phage (2 large plates) and incubated at 37°C overnight. Cells were scraped in 1.5 ml YT media from the agar plate of eluate phage and 2 ml glycerol stocks of first panning round were made and stored at -80°C. Input and output cfu were calculated form serial dilution titration plates.

2.14 Phage Display - Phage Purification

YT Ampi +1% glucose culture was started with 50 µl of glycerol stock from panning round and grown at 37°C until an OD of 0.4 was reached. $5x10^{10}$ helper phage M13K07 (Invitrogen) was added to 10 ml culture and incubated at 37°C water bath for 30 min. Culture was centrifuged at 3000 g for 10 min. Pellet was resuspended in 50 ml YT media + 100 µg/ml ampicillin + 30 µg/ml kanamycin + 0.1% glucose and incubated at 30°C overnight at 220 RPM. Overnight culture was centrifuged at 3000 g for 15 min. Phage containing supernatant was centrifuged at 10800 g for 10 min at 4°C. 10 ml 20% PEG 6000 2.5 M NaCl was added to 40 ml of supernatant, mixed well and incubated on ice for 2 h on shaker. Sample was centrifuged at 10800 g for 30 min. The supernatant was discarded and tube containing pellet was centrifuged at 10800 g for 5 min. The supernatant was discarded and white pellet was resuspended in 1 ml PBS + 15% glycerol and incubated on shaker for 10 min. Sample was centrifuged at 11600 g for 10 min and supernatant containing phage was kept at 4°C for next round of panning. Phage binding, elution and amplification was repeated for three rounds of total panning.

2.15 Phage Display - Monoclonal Selection

Glycerol stocks from the third round of panning was spread onto a large YT Ampi + glucose agar plate, diluted accordingly to obtain single colonies. 235 individual colonies were picked and placed into a 96-well plate containing 100 µl YT Ampi + 1% glucose per well. Plates were incubated at 37°C at 250 RPM. Glycerol stocks of each colony were taken, sealed and stored at -80°C. 2 µl of overnight culture added to 200 µl YT Ampi 1% glucose in a 96-well deep volume plate. Cultures were grown for 2 h at 37°C 300 RPM until an OD of 0.4 was reached. M13K07 helper phage in YT Ampi/glucose solution was prepared and added to each well and the plate was incubated at 37°C for 1 h at 250 RPM. Plates were centrifuged at 1800 g for 10 min. Supernatant was discarded and pellet was resuspended in 200 µl YT ampicillin (100 µg/ml), kanamycin (50 µg/ml) and incubated at 30°C overnight. Phage plated were centrifuged and 50 µl of supernatant was used to conduct ELISA assay for monoclonal phage. Positive clones were sent for sequencing.

2.16 Phage Display – Purification of ScFv

For generation of single chain antibody only (excluding the phage fragment) HB2151 cells were used instead of TG1. ScFv is encoded upstream of an amber stop codon and the phage sequence. Unlike the TG1 strain, HB2151 does not supress the amber atop codon, resulting in amplification of the ScFv peptide only. Clones grown in HB2151 cells, infected with helper phage were grown and amplified as in TG1 cells. Single colonies grown in YT ampicillin 1% glucose media were grown overnight. Glycerol stocks of colonies in HB2151 were taken. Pre-culture was added to a 500 ml TB media + ampicillin + 1% glucose and incubated at 37°C until an OD of 0.4-0.6 was reached. Samples were centrifuged at RT 3500 RPM for 30 min. Pellets were resuspended in 500 ml TB high sucrose media and grown at 25°C for 1 h. Induction of protein expression for 20 h overnight was carried out with 1 M IPTG. Samples were centrifuged at 6000 g for 30 min at 4°C. Pellet was dried

and resuspended in periplasmic buffer (Protease inhibitor cocktail (Roche) with 50 ml buffer – Tris-EDTA sucrose). Resuspended pellet was placed on shaker on ice for 30 min. 25 ml of ice-cold water was added to periplasmic extract and placed back on shaker for 2 h and centrifuged for 30,000 g for 30 min at 4°C. Periplasmic extract was dialysed using PBS using snakeskin tubing with 10,000 MWCO. 1 mM PMSF was added to supernatant. Supernatant was centrifuged at 20,000 g for 45 min 4°C. Supernatant was filtered with 0.2 µm filter. Ni-NTA beads were prepared and washed to give 50% slurry. Filtered supernatant was added to slurry and incubated overnight. Three washes and elution using imidazole was carried out and snakeskin was used for dialysis. Affinity of ScFv binding to Rab19 was carried out using ELISA and western blot with an anti-myc tag antibody against recombinant GST, GST-Rab19, cell lysate and cell lysate with overexpression of GFP-Rab19.

2.17 Phage Display - ELISA:

A Maxisorp plate was coated with 100 ng of antigen (GST and GST-Rab19) and BSA/Milk. Blocking with was carried out for 1 h, and washed with PBST. From each round of panning, 5 µl of phage (or 50 µl supernatant for monoclonal phage) with 95 µl PBST + 2% milk was added to antigen coated wells and incubated for 1 h. Wells were washed five times with 400 µl PBST. M13 HRP antibody was added to each well for 1 h and washed three times with PBST. For visualisation, 100 µl of TMB was added to each well and upon turning blue, the reaction was stopped with 100 µl 1 M HCl. Optical absorbance at 450 nm was measured.

2.18 Protein Gel Stain and Western Blot

Cells were scraped and resuspended in 1 ml ice cold PBS in an Eppendorf tube. Cells were centrifuged at 8000 g for 15 min at 4°C. Supernatant was removed and pelleted cells were resuspended in 200 µl RIPA buffer.100 µl

cell suspension was added to 100 µl Laemmli blue (+ β-Mercaptoethanol) and boiled at 95°C, 800 RPM for 5 min. 30 µl sample was loaded on to NuPAGE™ 4-12% Bis-Tris gel, 1.5 mm x 15 well, (Invitrogen) along with 5 µl PageRule Plus Prestained Protein Ladder (ThermoFisher), and run at 200 V for 40 min. For protein staining, One-Step Blue® Protein Gel Stain (Biotinum) was added to gel for 1 h and de-stained with water for 1 h before detection on Azure Biosystems 300 imager. For western blot, the proteins were then transferred to a 15-well nitrocellulose membrane on the Trans-Blot Turbo (BioRad) for 13 min. Membranes were blocked in 5% milk in TBST for 30 min. Primary antibodies were diluted in milk or TBST overnight. The membranes were washed for 5 min 3 times. HRP conjugated secondary antibodies were diluted 1:10,000 for 45 min. The membranes were washed for 5 min 3 times. The membrane was placed onto black plastic holder and coat with ECL-bright (Sigma) and detected on Azure Biosystems 300 imager.

2.19 Automation for High Content Screening:

Pre-printed siRNA plates were thawed at RT for 30 min in a sterile cell culture hood. Once thawed, the plates were centrifuged for 500 g for 5 min. The foil seal was removed and the lid was placed back onto the plate. An automated pipeline was used to dispense reagents into 384-well plates (Perkin Elmer, CellCarrier™ ultra). Small tube plastic tip dispensing cassette (Thermo Scientific) or was loaded onto the Thermo Scientific™ Multidrop™ Combi Reagent Dispenser. The dispense was set to 15 mm above the plate, set to dispense into 384 well plate at medium speed. The tubes of the dispensing cassettes were soaked in 70% ethanol for 5 min. 30 ml of ethanol was flowed through the dispenser tubes followed by 30 ml sterile filtered water. The tubes were emptied to ensure no ethanol residues or water remain. The tubes were then placed in a 50 ml falcon tube containing the reagent that is to be dispensed into the 384-well plate. For the dispensing of larger volumes (> 10 µl) Multidrop™ Combi, 384 and DW Reagent Dispenser Accessories was used. The washing steps were followed as above, but with larger volumes of

ethanol and water. Washing steps were carried out before, after and in between changing the reagents being dispensed. Opti-MEM, RNAiMAX mixture and PE ligand were dispensed using the Long small tube plastic tip dispensing cassette (Multidrop Combi). Cells in media, PBS washes, PFA, permeabilization and blocking buffers, and primary and secondary antibodies were dispensed using the Multidrop™ Combi, 384 and DW Reagent Dispenser Accessories.

2.20 High-Content Image Acquisition

For acquisition of high content images, Opera Phenix Plus High-Content Screening System (Perkin Elmer) was used. 63 X water immersion objective, with confocal imaging mode. Fixed cells were imaged in 384-well plate (Perkin Elmer, CellCarrier™ ultra). Two colour image channels were acquired with 405 and 488 lasers at 50% laser power. Exposure times were 40 ms for the blue channel and 100 ms for the green channel. Three z slices were acquired at positions (-1, 0 and 1) 0.5 µm apart and 35 fields were acquired per well. Channels were acquired sequentially.

2.21 SORA Confocal Microscopy

Live cells were imaged on fluorodish™ at 37°C. Media was exchanged for Leibovitz L-15 CO_2-independent medium (Gibco) before imaging, 2 drops per ml of media of NucBlue (Molecular Probes) was added 30 min before imaging. Fixed cells on coverslips were imaged on mounted on slides. For acquisition of single cell high-resolution imaging, spinning disk confocal microscope (CSU-W1-SoRa Nikon) was used. 100 X oil objective and Len-switched light path of 2.8 x SoRa magnification. Exciting was with SORA 405, 488, 561, 647 nm lasers. 95B Prime (Photometrics) camera was used, operated on NIS elements system (Nikon). Acquisition was in 16-bit images with no binning, 4,000 RPM disk speed. Pixel size was 0.039 µm.

2.22 High-Content Imaging Analysis

High content image analysis was carried out on the Columbus™ software (Perkin Elmer). Maximum projection of the 3 z slices, and basic flatfield correction was applied. To identify the nuclei, Method B with an intensity threshold of 0.4 was used. Objects with an area of > 50 μm^2 were selected to create masks around individual nuclei. Within the nuclei masks created, spot detection was carried out using Method A, with a relative spot intensity threshold of 0.115 and a splitting coefficient of 1. Well data included - Number of Nuclei, area of nuclei (μm^2) [sum per well], Number of spots and total spot area [sum per well]. Cytoplasmic masks and spots could also be identified using a mask created with a non-nuclear segmentation. This dataset was used to calculate the spot coverage index. Individual spot object data was also obtained, to calculate individual spot intensity and spot sizes and raw spot count for individual nuclei.

2.23 Confocal Image Analysis

Co-localisation of PE ligand and vesicular markers was analysed on ImageJ. Three colour thresholded images were used for co-localisation calculations. DAPI staining using the blue channel was used to create an ROI around the nucleus and create a nuclear and non-nuclear binary mask around the cell. The ImageJ plugin ComDet v0.5.0 (https://github.com/ekatrukha/ComDet) was used for detection of particles in the red and green channels. Co-localisation was calculated with the number of colocalised yellow particles as a percentage of total red particles in the nuclear and cytoplasmic masks. A macro created by Eric Martins Ratamero was used to automate the ROI detection, thresholding and quantification of colocalisation.

Nuclear Envelope ring intensity was calculated using a z-slice through the middle of the cell, identified manually. Nuclear ring ROI was created using the DAPI channel, with a pixel width of 5. The Multiplot tool in the ROI manager of

ImageJ was used to measure the intensity along the ROI region. This dataset was used to calculate an average intensity along the nuclear ring. Total cell intensity was used for normalisation of transfection levels. For GFP-FKBP and MitoTrap transfected cells, areas overlapping with mitochondrial signal were removed before ring intensity quantification. For live movies, bleach corrected was corrected and background signal was subtracted.

A macro created in Image J by Laura Cooper was used to quantify the distance between vesicles and the mitochondria. The red channel was used to create a binary mask of the mitochondria, and a distance map was created (ranging from 0-255). Vesicles were detected using 'Analyze Particles' feature, with a radius of 5 pixels and directed to the distance map to give a distance value from mitochondria. Vesicles within in the -10 range were classified as 'in proximity' to the mitochondria.

Vesicles beneath the nuclei were detected using the ImageJ plugin ComDet v0.5.0. The total particle area and nucleus area was measured to give a nuclear spot coverage index as in Chapter 2.22.

Chapter 3: High-Content Imaging Identifies Regulators of the NAE Pathway

3.1 Introduction

Nuclear-Envelope Associated Endosomes (NAE) were first described by Chaumet et al. (2015). The NAE pathway is involved in the translocation of cargo such as PE from the cell surface into the nucleus. It has been proposed that once at the nucleus, NAE dock and fuse with the nuclear envelope, releasing their contents into the nucleoplasm. Relatively little work has been done to characterise these endosomes or the mechanisms of the pathway.

Without a unique membrane marker to define NAE, designing an assay to detect changes in NAE is a challenging task. NAE can be distinguished by their characteristic of being 'associated' with the nucleus. However, using super resolution or live cell microscopy to identify fused or docked vesicles at the nuclear envelope is not feasible in a high throughput manner. Another approach to defining NAE could be done by labelling cargo that translocate to the nucleus. It is possible that a large variety of cargo - receptor tyrosine kinases, GPCRs and associated ligands - can translocate to the nucleus in NAE, but it is unknown whether different proteins can use differential routes or a different subset of nuclear vesicles for their translocation (Shah et al., 2019). Recently, the receptor EphA2 has also been proposed to follow the NAE pathway (Marco et al., 2021), providing evidence that the NAE pathway is not a PE specific event or that PE is the sole cargo for NAE. Many of these cargo proteins destined for the nucleus also have alternate subcellular destinations, making it difficult to detect and identify NAE specific cargo.

A fraction of PE labelled vesicles translocate from the cell surface to the nuclear envelope. The heterogenicity in the size, morphology, intensity levels

and variation in the number of PE vesicles, indicate that much of the internalised PE can be trafficked to different compartments and subsets of vesicles. This only further adds to the complexity of defining NAE, making it more difficult to distinguish between NAE and other compartments that PE localises to. Although not specific to NAE, PE was used as a marker for NAE in this study. This, together with its proximity to the nucleus, can be used as criteria to define a subset of PE positive vesicles which may be NAE or precursor NAE vesicles.

The Rab GTPases are known as the master regulators of membrane trafficking. They facilitate each step of trafficking, from vesicle formation to fusion. The Rab GTPases have a largely conserved structure and have domains characterised for functional activity. The Rab proteins cycle between two states, an active GTP-bound state normally localised to the cytoplasm, and an inactive GDP-bound state that can be inserted into membranes and recruit effector proteins. Single amino acid substitutions in the active sites of the Rab proteins lead to the proteins being locked in either their GTP or GDP bound state, creating constitutively active or dominant negative mutants of the Rab protein. Whilst the Rab proteins direct intracellular traffic by interacting with a range of effector proteins, the SNARE proteins mediate membrane fusion (Alberts, 2019).

The aim of this study was to identify regulators of the NAE Pathway using an imaging-based RNAi screen. High-content imaging is a powerful tool to identify phenotypic changes in the cell, which uses automated microscopy to acquire images of cells in a high-throughput manner. A library of pre-printed siRNA plates can be used to detect and quantify the effect of the knockdown of certain genes on the phenotype of a cell. High-content imaging can allow for the testing of the effect of thousands of conditions in a fast and efficient manner. The NAE quantification assay, used to identify changes in NAE, was optimised and automated for use in a 384-well plate format. This study tested the knockdown of 48 SNARE proteins and 60 Rab GTPases for their phenotypic

effects on PE vesicles in MG63 cells. This assay could in principle be used for large scale testing of other siRNA libraries in the future, including genome-wide screens.

3.2 Characterisation of NAE

NAE were discovered when imaging PE internalisation pathways, where it was found that a fraction of PE vesicles were closely associated with the nuclear lamina (Chaumet et al., 2015). To validate this, confocal microscopy was used to visualize PE vesicles in MG63 cells, detected by indirect immunofluorescence (Figure 3.1).

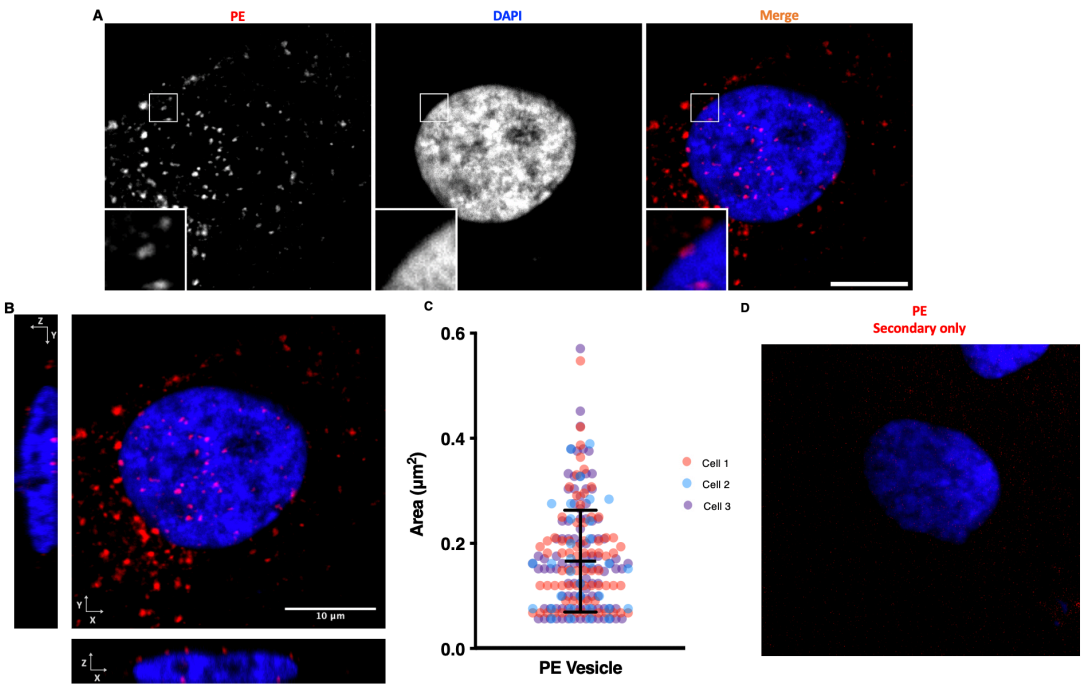

Figure 3.1 A fraction of PE vesicles are in close proximity to the nucleus. (A) Confocal Imaging of PE vesicles in fixed MG63 cells, nucleus stained with DAPI. PE vesicles stained with anti-pseudomonas exotoxin primary antibody and anti-rabbit Alexa-fluor-568 secondary. Scale bar 10 µm. 3X magnification zoom inset. (B) Z slices (0.2 µm) of PE vesicles presented in XY and orthogonal views, ZY and XZ. (C) Quantification of PE vesicle size at the nuclear level across three representative cells. Error bars show mean and standard deviation. (D) control image of cell with secondary antibody only.

Confocal 3D imaging confirmed that PE labelled vesicles were in proximity to the nucleus (Figure 3.1A). Nucleus-associated PE vesicles can be detected at

the periphery of the nucleus across multiple z slices, as well as above and below the nucleus, as depicted in the orthogonal views displaying the YZ and XZ views (Figure 1B). Due to the shape of the cell and nuclear positioning, a uniform layer of PE vesicles can be best detected and quantified below the nucleus in a single z slice. This, along with the evidence provided in Chaumet et al. (2015), that PE vesicles dock and fuse with the nuclear envelope, indicate that these vesicles seen in proximity to the nucleus are NAE.

To characterize the morphology of NAE, the size of the PE vesicles detected within the nuclear area was measured. Nuclear PE vesicles displayed substantial heterogenicity in vesicular size, ranging from 0.1 to 0.5 μm^2 in area, with the average vesicle being 0.16 μm^2 in size (Figure 3.1C). Heterogenicity in nuclear PE vesicular size could be an indication that either NAE vary in size or that a fraction of the PE vesicles detected are a different subset of vesicles. A caveat of using immunofluorescence / confocal microscopy to detect NAE is that the resolution of the microscope is high not enough to distinguish between NAE or PE labelled vesicles that are co-incidentally peripheral to the nucleus. The focal plane imaged beneath the nucleus may also encompass sections of the cytoplasm, ER and plasma membrane, however this visualised region will be referred to as proximal to the nucleus in this thesis.

Chaumet et al. (2015) stated that NAE are derived from early endosomes because PE vesicles co-localise with the early endosomal marker EEA1 but not the late endosomal marker Rab7. I therefore set out to further characterise PE vesicles by testing for co-localisation with an extensive list of Rab GTPases, hoping to find a Rab GTPase that could be a unique marker for NAE (Figure 3.2), (Table 3.1).

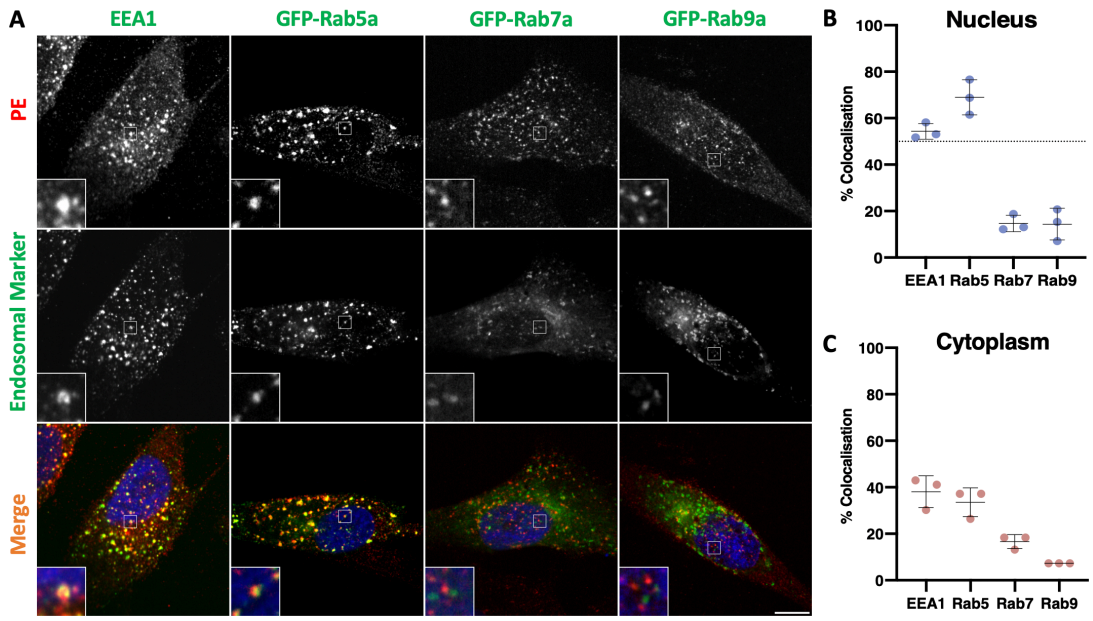

Figure 3.2 PE vesicles co-localise with early endosomal markers. (A) MG63 cells were transfected with GFP-Rab5a, GFP-Rab7a or GFP-Rab9a or immunostained with an EEA1 antibody. 500 nM of PE ligand was added for 1 h, cells were fixed, permeabilised and labelled with a PE antibody. Co-localisation of PE is seen with Early endosomal markers EEA1 and GFP-Rab5 but not with late endosomal markers GFP-Rab7a and GFP-Rab9a. (B,C) Quantification of colocalisation between PE and Endosomal markers at the level of the nucleus and cytoplasm. Error bars show mean with standard deviation. Scale bar is 10 µm. 3X magnification zoom inset.

PE partially co-localised with early endosomal markers, with an average of 38% and 34% of PE vesicles co-localising with EEA1 and Rab5 respectively. This establishes that PE is internalised and is delivered into early endosomes. There is less co-localisation between PE and late endosomal markers, with only 16.5% and 7% co-localisation with PE vesicles and Rab7 and Rab9 in the cytoplasm, suggesting that small amounts of PE end up in late endosomes, and that only a small fraction is likely to be targeted for degradation in lysosomes (Figure 3.2).

Co-localisation of PE and endosomal markers in proximity to the nucleus was also quantified, using confocal microscopy to image PE vesicles in the z slice just beneath the nucleus. Here, over 54% and 69% of PE vesicles co-localised with EEA1 and Rab5, respectively. PE showed little co-localisation with late endosomal markers at the level of the nucleus, with only 15% and 14% of PE vesicles co-localising with Rab7 and Rab9, respectively (Figure 3.2B). This

indicates that NAE are derived from early endosomes. Since PE also co-localises with early endosomal markers at the nuclear level, it suggests that a maturation step could occur for early endosomes to develop into NAE. PE vesicles displayed varying degrees of co-localisation with many different Rab GTPases in cytoplasmic or nuclear regions (Table 3.1). This demonstrates that PE is trafficked through various intracellular compartments. Although we did not find a unique marker for NAE, PE vesicles close to the nucleus can be used as a marker to study NAE pathway regulation. It must be noted that it may be possible that more early endosomes present nuclear mask, due to the presence of the plasma membrane in the slice images beneath the nucleus, and this may lead to an increase in co-localisation of early endosomal makers with PE at the nucleus.

Co-localisation of Rab GTPases with PE

Rab GTPase	Summary of Co-localisation with PE
Rab1b	No colocalisation observed
Rab2	No colocalisation observed
Rab3a	No colocalisation observed
Rab4	Partial Co-localisation
Rab5a	Partial Co-localisation
Rab6	No colocalisation observed
Rab7	Co-localise with very few PE vesicles
Rab8a	No colocalisation observed
Rab9	No colocalisation observed
Rab10	No colocalisation observed
Rab11	Partial Co-localisation – mainly cytoplasmic
Rab12	No colocalisation observed
Rab13	No colocalisation observed
Rab14	Partial Co-localisation – mainly cytoplasmic
Rab15	No colocalisation observed
Rab17	No colocalisation observed

Rab18	No colocalisation observed
Rab19	Co-localise with very few PE vesicles
Rab20	No colocalisation observed
Rab21	Co-localise with very few PE vesicles
Rab22	Co-localise with very few PE vesicles
Rab23	No colocalisation observed
Rab24	No colocalisation observed
Rab25	No colocalisation observed
Rab26	No colocalisation observed
Rab27a	No colocalisation observed
Rab28	No colocalisation observed
Rab30	No colocalisation observed
Rab32	No colocalisation observed
Rab33a	No colocalisation observed
Rab33b	No colocalisation observed
Rab34	No colocalisation observed
Rab35	Co-localise with very few PE vesicles
Rab36	No colocalisation observed
Rab37	No colocalisation observed
Rab38	No colocalisation observed
Rab39a	No colocalisation observed
Rab40a	No colocalisation observed
Rab43	No colocalisation observed
Rab45	No colocalisation observed
RabL4	No colocalisation observed
RabL5	No colocalisation observed
RabL7	No colocalisation observed

Table 3.1 Summary of co-localisation of Rab GTPases with PE. Co-localisation status of Rab GTPase with PE.

3.3 Design and Development of the NAE Quantification Assay

To identify regulators of the NAE Pathway, we designed an siRNA-based assay to determine changes in PE vesicles in proximity to the nucleus (Figure 3.3). The assay conditions were optimised and its suitability for high-content screening was assessed using the Z′ factor (Figure 3.4). Z′ factor and Z′ robust are statistical tests commonly used to evaluate the quality of the assay for use in high throughput screening. A Z′ factor considers the dynamic range and variation between the data, using the mean and standard deviation of the positive and negative controls. Recently a robust Z′ factor was defined using the median and median absolute deviation to account for outliers adversely skewing the Z′ factor coefficient, and is reportedly better suited to assess the quality of more complex cell-based assays (Atmaramani, Pancrazio and Black, 2020). A Z′ factor coefficient of above 0.5 is considered an 'excellent' assay (Zhang, Chung and Oldenburg, 1999). Suitability of the assay for use in high-content screening allows for the detection of phenotypic changes in thousands of conditions in an efficient manner.

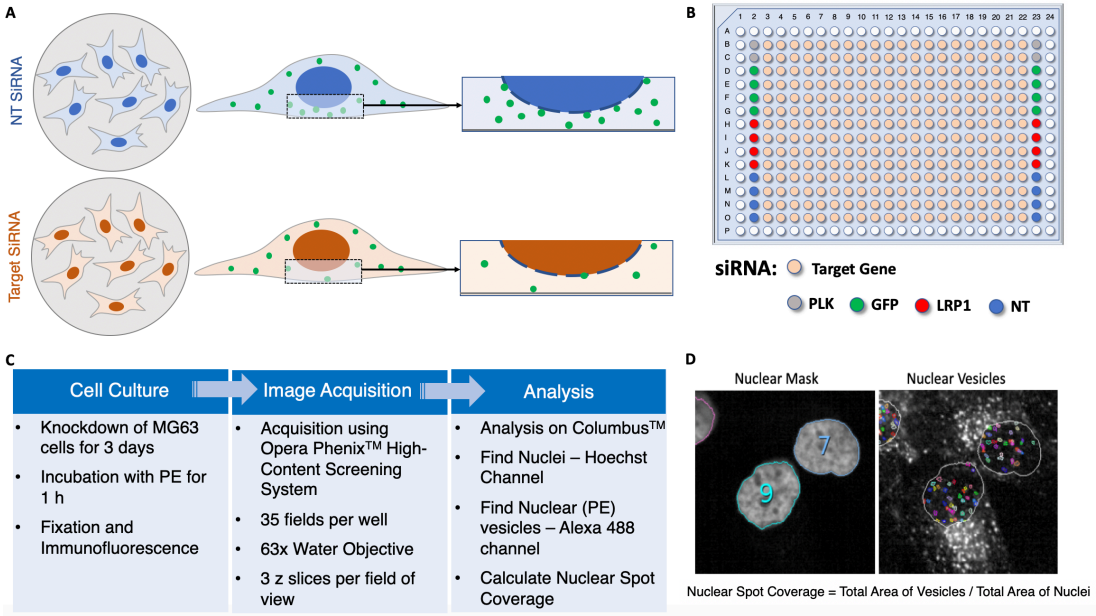

Figure 3.3 Design and development of NAE quantification assay (A) Illustration of principle behind the NAE quantification assay. (B) 384-well plate layout for screen, indicating controls used in screen. (C) Workflow for cell culture, image acquisition and analysis of NAE

quantification assay (D) Typical image of nuclear masks (blue channel) and ROI PE 'spots' that coincided with this mask in the green channel.

A phenotypic assay was designed to determine proteins that regulate PE trafficking to the nucleus using high-content confocal imaging. The principle being, that the knockdown of an essential regulator of the NAE pathway would lead to a reduction in the number of nuclear associated PE vesicles, which can be detected using a confocal high-content screening system (Figure 3.3A). The screen will be conducted in a 384-well plate format, with the controls placed in columns 2 and 23 of the plate and target siRNAs placed in the columns in-between (Figure3.3B). Images can be taken using a maximum projection of three z slices beneath the nucleus. The workflow for this assay includes the detection of the nucleus, and the PE vesicles in the Region of Interest (ROI) beneath the nucleus (Figure 3.3C). This can be quantified to give a 'spot coverage index'. The spot coverage index is calculated by dividing the area of the vesicles by the total area of the nuclei to give a percentage of the nuclear area that is covered in vesicles (Figure 3.3D).

It should be noted that the nuclear spot coverage index does not consider any changes in the total spot coverage in the cell, therefore any upstream regulators will also be picked up in this assay. Disruptions in the endosomal trafficking network may also lead to false positive hits, as these may not necessarily regulate trafficking to the nucleus. Secondary assays that include quantification of the cytoplasmic spot coverage (Figure 3.11) or subcellular fractionation measure changes in total lysate, cytoplasmic or membranous compartments (Figure 3.14) will be considered for hit validation.

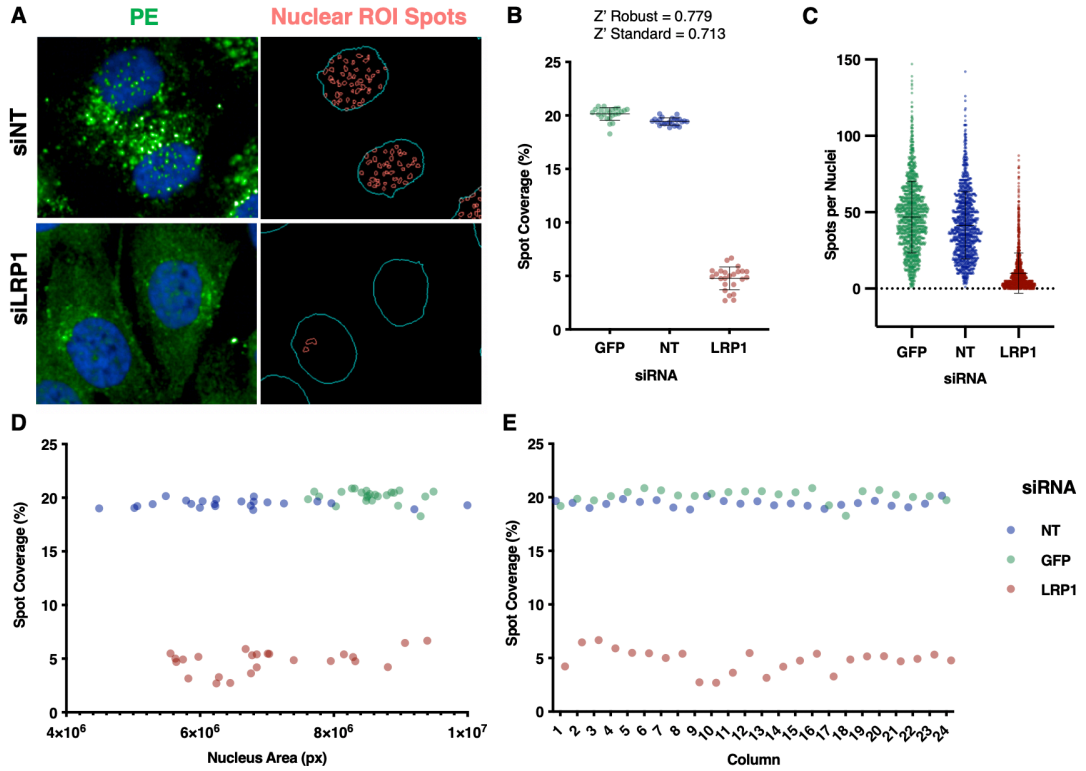

Figure 3.4 Optimisation and controls tested for screening. (A) MG63 cells were transfected with NT and LRP1 siRNA. Left Panel shows PE vesicles in each control, with the nuclei stained with Hoechst. Right panel displays the nuclei mask ROI detected in blue channel and 'spot' ROIs detected in the green channel. (B) Spot Coverage index calculated for condition with siRNA against controls GFP, NT and LRP1. (C) Raw spot count per nuclei detected for GFP, NT and LRP1 siRNA control conditions. Error bars show mean and standard deviation. (D) Spot coverage index plotted again average nuclei size (pixels). (E) Spot coverage index plotted along every column in 384 well plate.

To ensure the NAE quantification assay was suitable for use in high-content imaging, pilot experiments were carried out to determine the sensitivity and dynamic range of the assay. Non-targeting (NT) siRNA or GFP siRNA were used as negative controls. siRNA against LRP1, which is the cell surface receptor required for PE internalisation, was used as a positive control. Knockdown of LRP1 blocks PE entry into the cell and leads to a reduction in the total number of PE vesicles detected (Figure 3.4A-C). Knockdown of LRP1 leads to a significant reduction in PE vesicles in the cell (Figure 3.4A), with the average spot coverage decreasing from 20% in the GFP and NT controls to below 5% for the LRP1 control, showing the dynamic range of this assay. The Z′ factor for this assay using the NT and LRP1 controls gave a coefficient of

0.713, and a Z′ robust of 0.779, indicating suitability of this assay for high-content imaging.

As the spot coverage calculations are measured as an average per well, with each well containing 800-1600 cells, it is also important to look at individual cell data. There was large variability in NAE number between cells, ranging from 0 to 150 NAE per cell with siNT and an average NAE count of 40 per cell. Upon LRP1 knockdown, this range is shifted, with a higher number of cells with a low number of NAE. The average NAE count per cell upon knockdown of LRP1 is 10. This confirms that knockdown of LRP1 is effective at inhibiting PE entry and significantly lowering PE vesicular count.

As the spot coverage measurement considers the size of the nuclei and the vesicles, we needed to ensure that nuclei size would not cause a significant effect on the spot coverage readout i.e. bigger nuclei would not lead to a higher readout in the spot coverage index. Whilst the nuclei size varies upon treatment of cells with NT and GFP siRNA, the average spot coverage does not substantially change and remains at around 20% in both of the negative control conditions (Figure 3.4D). This demonstrates that nuclear morphology does not affect the final spot coverage measurement. To ensure that the positioning of conditions on different wells of the plate does not affect the readout, NT, GFP and LRP1 siRNA conditions were plated across every column on the 384-well plate (Figure 3.4E), the spot coverage readout remained at around 20% with the negative control conditions across the plate. This data determines that nuclear size and well-positioning of the condition on the plate does not affect the readout of this assay. These controls, together with the high sensitivity of the assay, as validated by the Z′ factor, to detect changes in nuclear PE vesicles, suggest that the NAE quantification assay is suitable for use in an automated high-content screen.

As the efficiency of knockdown of expression for every gene cannot be tested in the screen, I tested the transfection conditions used in the screen to

determine the knockdown efficiency of two example proteins. The expression level of SUN2, a nuclear envelope protein, and the number of viable cells following knockdown of Polo-Like Kinase 1 (PLK1), was assessed by confocal microscopy. PLK1 is an enzyme involved in cell cycle regulation. Knockdown of this gene results in cell cycle arrest and apoptosis in cancer cells, leading to a reduction in cell count which can be quantified (Spänkuch-Schmitt et al., 2002; Liu and Erikson, 2003). Therefore, PLK siRNA transfection followed by cell counting can be used as an indicator of successful transfection and delivery of siRNA into cells (Figure 3.5)

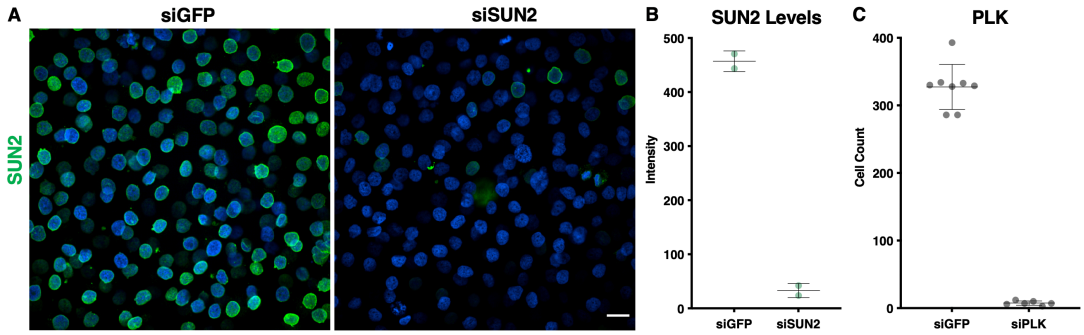

Figure 3.5 Knockdown efficiency in MG-63 cells. (A) MG63 cells were transfected with a siRNA against GFP or siSUN2. Confocal Images show SUN2 staining (green) upon knockdown, nuclei are shown in blue. Scale bar 50 µm (B) Quantification of SUN2 intensity (C) Cell number following transfection of MG63 cells with GFP or PLK siRNAs. Error bars show mean and standard deviation of triplicate wells.

Experimental conditions resulted in >90% reduction in SUN2 levels upon transfection with SUN2 siRNA. Treatment with PLK siRNA lead to over 97% reduction in cell count compared to the GFP siRNA control, indicating successful knockdown of SUN2 and efficient delivery of PLK siRNA to MG-63 cells. Knockdown of PLK was used as a control in subsequent screening assays, because cell counting will be calculated as part the assay conditions, thus saving on the extra steps and reagents for immunofluorescence experiments, and time required to acquire an extra channel necessary for the quantification of SUN2 levels.

3.4 NAE Quantification Screen Results

The NAE quantification assay was semi-automated for use in high-content imaging. This involved the use of robotics for high-speed microplate reagent dispensing in a 384 well plate, minimising human error and maintaining experimental consistency. The screen was composed of a plate of siRNAs against the SNARE proteins (Figure 3.6) and Rab GTPases (Figure 3.7). The pre-printed siRNA plate had 4 quadrants. siRNA against 48 or 60 SNARE or Rab proteins respectively, in replicates of 4 across the quadrants were tested. Wells with a cell count of below 700 were excluded from the plot, as low cell count indicates that the cells were subjected to high levels of toxicity. The lower threshold for the identification of down-regulators, and upper band for the identification of up-regulators of the NAE pathway was set according to the mean of the NT siRNA control.

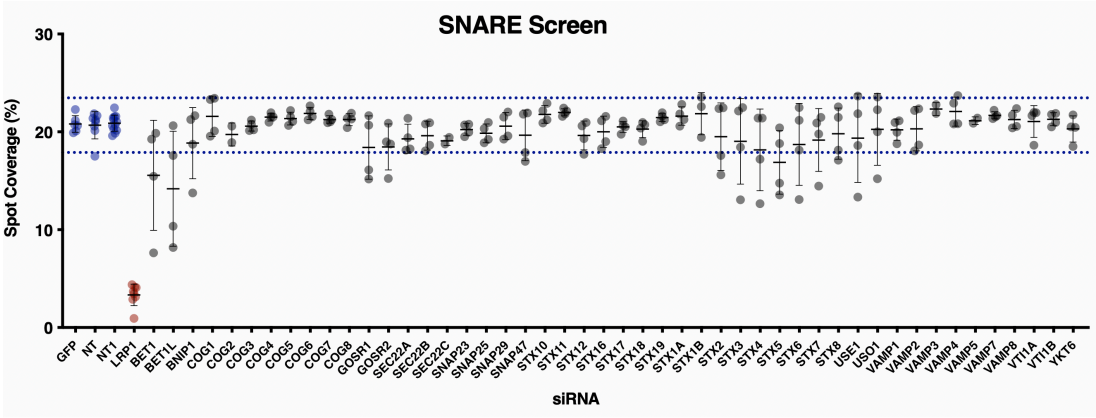

Figure 3.6 SNARE screen results. Average spot coverage per well upon knockdown of 48 SNARE proteins. GFP, NT and NT1 siRNA negative controls and LRP1 siRNA positive control plotted. Upper and lower dotted line plotted two SD above and below mean of NT control. Error bars show mean and standard deviation of triplicate wells, n=1. Wells with a cell count of below 700 were excluded.

Spot coverage index from the SNARE screen results show that upon knockdown of LRP1, the average spot coverage was 3%, compared to 21% in the negative NT control. However, no hits were identified in the SNARE screen, with only a few conditions that showed an average reduction below the lower threshold set. These conditions, BET1, BET1L and STX5, were

disregarded due to the high standard deviations. The conditions that had a high standard deviation between the replicates, was because of incorrect toxin dispensing due to technical issues with the nozzle on the reagent dispenser, as these conditions were positioned on the same row. The lack of hits could be interpreted as a limitation of the sensitivity of the assay. The knockdown of the positive control, LRP1, results in a reduction in total internalized PE, giving a much higher reduction in PE vesicular count that we could expect with intracellular regulators.

However, it is still possible that the assay is able to detect the minor changes in nuclear PE levels. This, combined with the multiple reports that state that the SNARE proteins have a high tendency for redundancy (Liu and Barlowe, 2002; Bethani et al., 2009; Kim and Bassham, 2013), we decided to conduct another screen using a different set of membrane trafficking regulators, the Rab GTPases, to test for their involvement in the regulation of the NAE pathway (Figure 3.7).

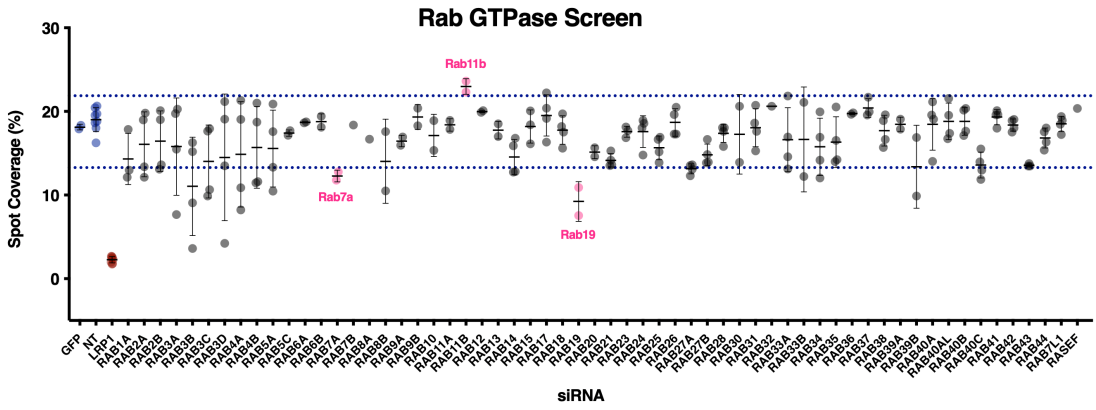

Figure 3.7 High-content imaging identifies Rab7a, Rab11b and Rab19 as regulators of the NAE pathway. Dots show average spot coverage per well upon knockdown of Rab GTPases. GFP and NT siRNA negative and LRP1 positive controls plotted. Rab7a, Rab11b and Rab19 hits obtained are highlighted and labelled with pink symbols. Upper dotted line plotted two SD above mean of NT control. Lower dotted line plotted four SD below mean of NT control. Error bars show mean and standard deviation of triplicate wells, n=1. Wells with a cell count of below 700 were excluded.

The Rab GTPase siRNA screen identified three regulators of NAE pathway: an up-regulator, Rab11b, with the average spot coverage increasing from 19% to 23% compared to the non-targeting control; a down-regulator, Rab7a, which resulted in a decrease in spot coverage from 19% to 12.3%; and another down-regulator Rab19, in which the knockdown resulted in nearly a 50% decrease in the spot coverage index, reducing it from 19% with siRNA NT to below 10% with siRNA against Rab19 (Figure 3.7). Whilst the threshold for the for the down-regulators was set four standard deviations below the mean, the threshold for the up-regulators was set two standard deviations above the mean to allow for the capture of hits that increase in NAE, as the assay and was set up and optimised to identify down-regulators.

Whilst the spot coverage index quantified from the screen revealed what is happening to the population of cells in a single well, investigating the individual cell data allows us to evaluate the spread of NAE numbers at a single cell level. Individual cell data of selected hits Rab19, Rab11b and Rab7a with the two controls (NT and LRP1) was quantified, showing the NAE count for each individual cell (Figure 3.8A).

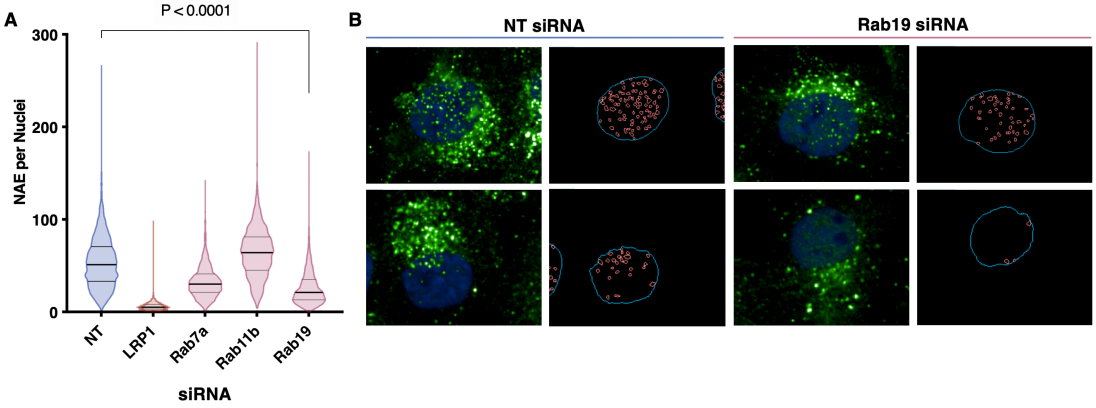

Figure 3.8. NAE per nuclei upon LRP1, Rab7a, Rab11b and Rab19 knockdown. (A) Violin plot of raw NAE count per nuclei of each cell in the siLRP1, siRab7a, siRab11b and siRab19 conditions compared to the siNT control. Lines show 25th, 50th and 75th percentile. (B) Typical images to depict heterogenicity in NAE number per cell within the same field. Error bars show mean and standard deviation of triplicate wells.

The distribution of the data was altered in each of these conditions compared to the siNT control. Knockdown of Rab7a led to a significant shift to a

population of cells with fewer NAE, and Rab19 knockdown shows a similar trend, but to a larger extent. The median NAE count of cells treated with NT siRNA was 54 NAE per cell. The median NAE count upon knockdown of Rab7a and Rab19 was 33 and 26 NAE per cell respectively. Knockdown of Rab11b led to a slight increase in the number of cells with a higher number of NAE, with a median of 64 NAE per cell. The single cell data displays the heterogenicity of NAE count between individual cells, with cells in each condition ranging from 0 to over 200 NAE per cell even within the same condition and field (Figure 3.8B). This data however does not account for NAE size or intensity levels, as the cells with fewer NAE could have larger and more dense vesicles.

The images of the hits identified from the screen were examined to determine whether the knockdown had observable phenotypic effects. To determine the phenotypic effects upon knockdown of Rab7, we examined the cellular and PE vesicular morphology (Figure 3.9). Detection of nuclear PE vesicles upon knockdown of Rab11b and Rab19 are shown (Figure 3.10).

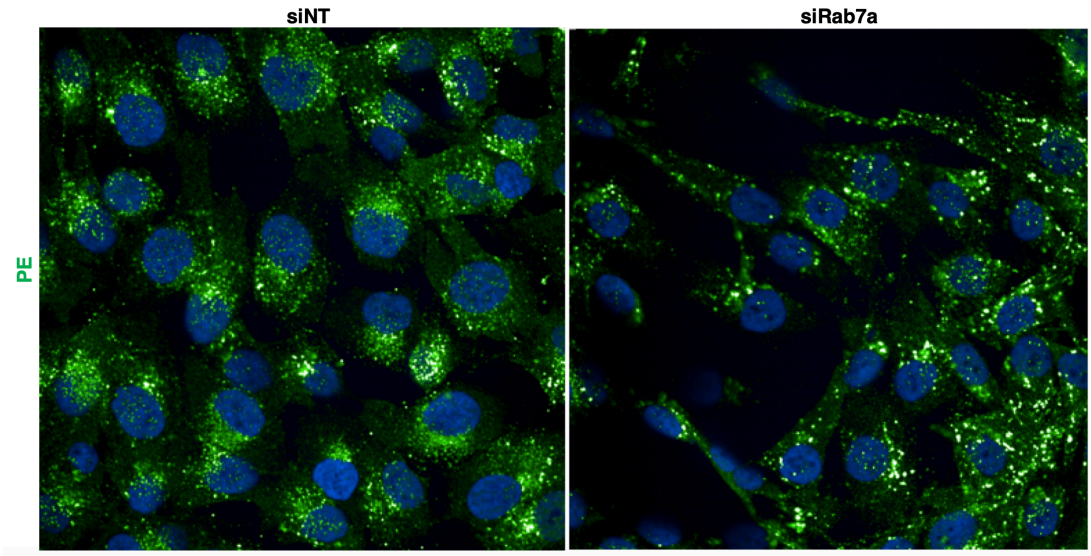

Figure 3.9 Effect of Rab7a knockdown on PE trafficking. Representative confocal images cells treated with siRNA against Rab7a and a non-targeting control siRNA. PE vesicles detected in the green channel and nuclear staining in the blue channel.

Images of PE vesicles show there is a reduction in NAE upon knockdown of Rab7a (Figure 3.9). Images also revealed that there is a change in the

morphology of the cells upon Rab7a knockdown. PE vesicle trafficking also seems to be altered, with a change in the morphology of the PE vesicles, leading to larger and brighter vesicle formation, indicating higher levels of PE cargo in the vesicles. Rab7a is not likely to be a direct regulator of the NAE pathway, as knockdown of Rab7a leads to significant effects on cytoplasmic PE trafficking resulting in the phenotype observed.

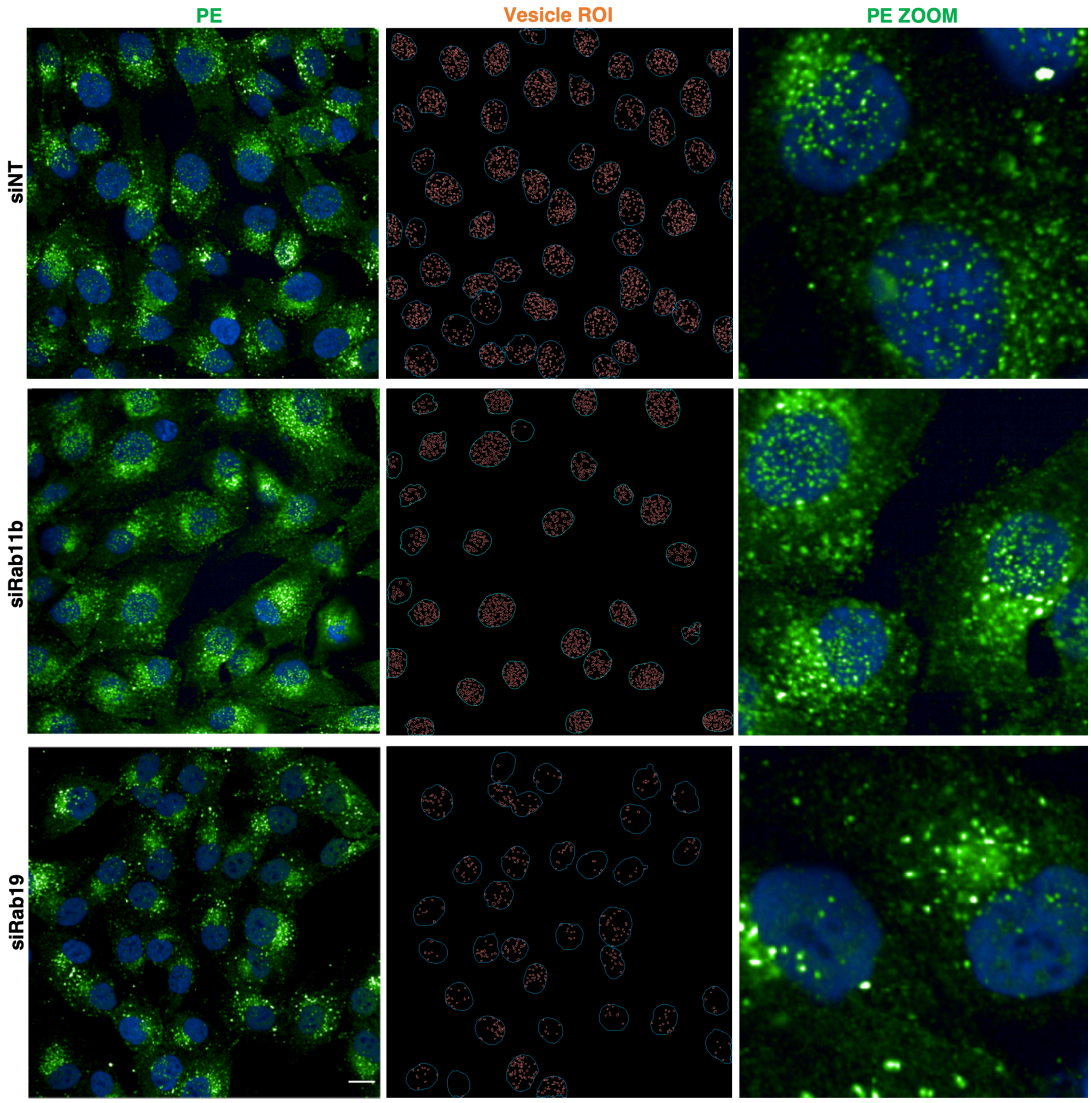

Figure 3.10. Effect of Rab11b and Rab19 knockdown on NAE. Left panels show images of a typical field of cells in the NT siRNA control and Rab11b and Rab19 siRNA treated wells. Scale Bar 50 µm. Middle panels show overlays of the nuclear mask and ROI nuclear vesicles. Right panels show zoomed views. PE vesicles detected in the green channel and nuclear staining in the blue channel.

Knockdown of Rab11b and Rab19 did not lead to an altered PE vesicular morphology or the formation of the large vesicular structures as seen with the knockdown of Rab7a. The up-regulation of NAE count in cells depleted of Rab11b can be observed in the confocal images (Figure 3.10). As Rab11 is involved in the slow recycling pathways (Ullrich et al., 1996), its depletion leads to a disruption in the recycling of cargo back out to the cell surface. A disruption in recycling pathways could prevent the recycling of PE back to the plasma membrane, resulting in an increase in PE vesicles overall in the cell and even potential re-sorting of PE vesicles, that cannot be recycled, towards the nucleus.

Depletion of Rab19 led to a significant decrease in the number of vesicles found at the nucleus, depicted in the confocal images in Figure 3.10. Unlike Rab7a, which led to altered trafficking of PE throughout the cell, Rab19 did not seem to have an observable effect on the cellular or PE vesicular morphology.

Determining whether there are changes in cytoplasmic PE vesicles would indicate whether the hit acts directly at the nucleus or upstream and could give further insight into the function and the stage of the pathway the regulator acts at. A change in cytoplasmic coverage index could also indicate that a non-specific effect of general trafficking disruption may be occurring, which needs to be considered. Therefore, cytoplasmic spot data was extracted from the images from the screen. A mask for the non-nuclear segment can be created and cytoplasmic spot coverage could be calculated (3.11).

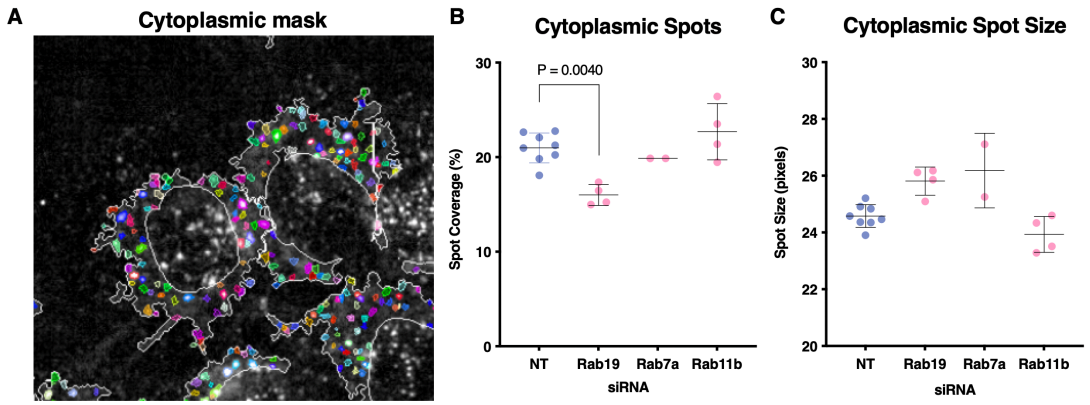

Figure 3.11 Quantification of cytoplasmic PE spots after knockdown of Rab19, Rab7a and Rab11b. (A) Confocal image visualising the non-nuclear mask segmentation and vesicular ROI detected. (B) Quantification of cytoplasmic spots detected upon knockdown of Rab19, Rab7a and Rab11b. Knockdown of Rab19 lead to a decrease in cytoplasmic spot coverage index. (C) Quantification of average spot size per well of cells with Rab19, Rab7a and Rab11b knockdown. Error bars show mean and standard deviation.

Masks created for cytoplasmic segments are not as accurate as the nuclear mask, since cell outlines were difficult to establish without a marker for the cell surface. Classification of spot identification was also more difficult to determine than for the nuclear spots, as images taken were a maximum projection of three z slices beneath the nucleus, and the density of vesicles was lower and the vesicles were more uniformly layered beneath the nucleus. Therefore, the cytoplasmic vesicular signal had more noise due to higher density of vesicles and variable arrangement (Figure 3.11A).

Knockdown of Rab19 led to a small but significant change in cytoplasmic spot coverage, with an average spot coverage index of 16% compared to 21% in the NT control (Figure 3.11B), highlighting that the role of Rab19 in the NAE pathway could be at the nuclear level or upstream. Changes to cytoplasmic spot size upon knockdown of each hit were non-significant (Figure 3.11C). These data suggest that Rab19 may function upstream of NAE docking, or that knockdown of Rab19 leads to a general disruption of endosomal trafficking leading to changes in nuclear and cytoplasmic vesicles.

3.5 Validation of Rab19 as a regulator in the NAE Pathway

Rab19 was an interesting hit, as it did not cause the formation of the large structures observed upon knockdown of Rab7a (Figure 3.9). Rab19 has also not been linked to recycling pathways. Both of these would provide an explanation for the change in nuclear PE vesicles. Therefore, we chose to further investigate and validate the role of Rab19 in the NAE pathway. In order to validate the results from the screen, we repeated the knockdown of Rab19 and tested for changes in nuclear spot coverage index, using the SMARTpool Rab19 siRNA (a pool of 4 different siRNAs) as used in the screen as well as the individual siRNAs. (Figure 3.12).

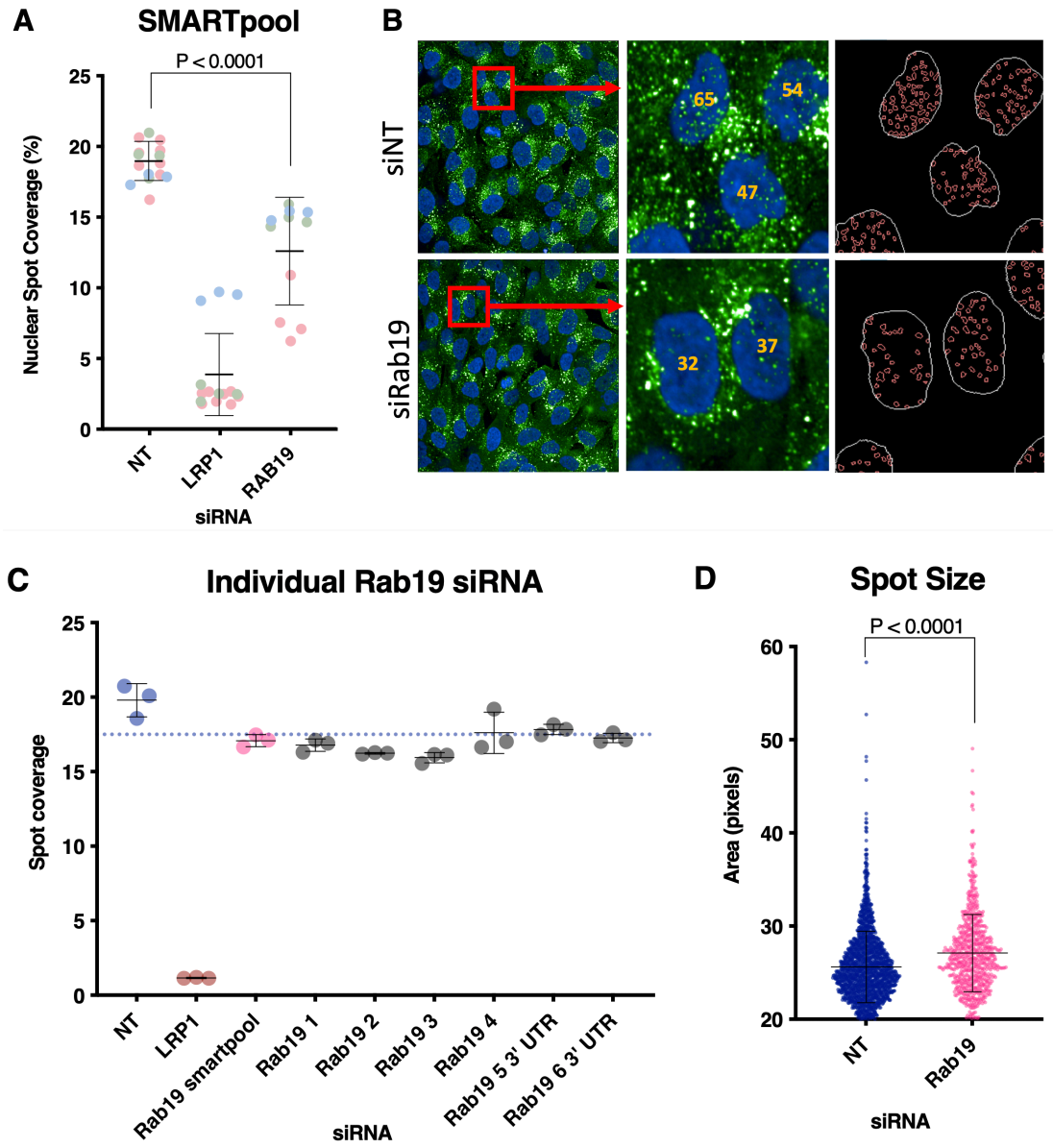

Figure 3.12 Rab19 is a key player in the nuclear PE vesicular trafficking (A) Three biological replicates (each presented in orange, green and blue symbols) of the NAE quantification assay depicted by changes in nuclear spot coverage index upon knockdown of Rab19 compared to the positive control LRP1 and a non-targeting negative control. n=3 (B) Representative images displaying the number of NAE in control sample and Rab19 knockdown. PE vesicles detected in the green channel and the nucleus in the blue channel (C) Effect of Rab19 SMARTpool and individual Rab19 siRNA knockdown on spot coverage index plotted with the NT and LRP1 controls. (D) Spot size of PE vesicles in NT and Rab19 siRNA conditions. Error bars show mean and standard deviation of triplicate wells.

In three biological replicates, we confirmed that the knockdown of Rab19 leads to a reduction in nuclear spot coverage from 19% spot coverage in the NT control to 12.5% upon knockdown of Rab19 (p value of < 0.0001) (Figure 3.12A). Following this, each siRNA from the SMARTpool as well as custom

designed siRNA against the 3' UTR region of Rab19 was individually tested for its effects on NAE. Although there was a slight reduction in nuclear spot coverage index upon knockdown of Rab19 using the 6 individual siRNAs that target different regions of Rab19, the effect size was not as prominent as in previous experiments (Figure 3.12C). Each individual siRNA however did show a minor decrease in nuclear spot coverage that was similar to the SMARTpool in this experiment, with an average spot coverage index of 17% upon knockdown of Rab19 compared to 19.8% in the NT control.

To determine the effect the knockdown has on the morphology of nuclear PE vesicles, data for individual spots was extracted, quantifying the spot size of each individual PE vesicle upon treatment with NT or Rab19 siRNA. PE vesicles were slightly larger upon knockdown of Rab19. Spot size upon knockdown of Rab19 was an average of 6% larger than PE spot size upon treatment with NT siRNA (Figure 3.12D).

We wanted to test whether expression of the constitutively active (GFP-Rab19-QL) or dominant negative (GFP-Rab19-TN) mutants of Rab19 could affect NAE, allowing the use of alternative method to RNAi to test for NAE modulation (Figure 3.13). There are several limitations of siRNA-based methods, as multiple studies have reported that a range of off-target effects can occur using RNAi from mistargeted mRNA degradation to the stimulation of immune responses (Jackson et al., 2003; Lin et al., 2005). Unlike the RNAi based method, which can only test for phenotypic affects upon the depletion of Rab19, DNA transfection of the constitutively active Rab19 mutant would in addition allow us to test for the effects on NAE upon overexpression of Rab19, and whether this can lead to the up-regulation of the NAE pathway.

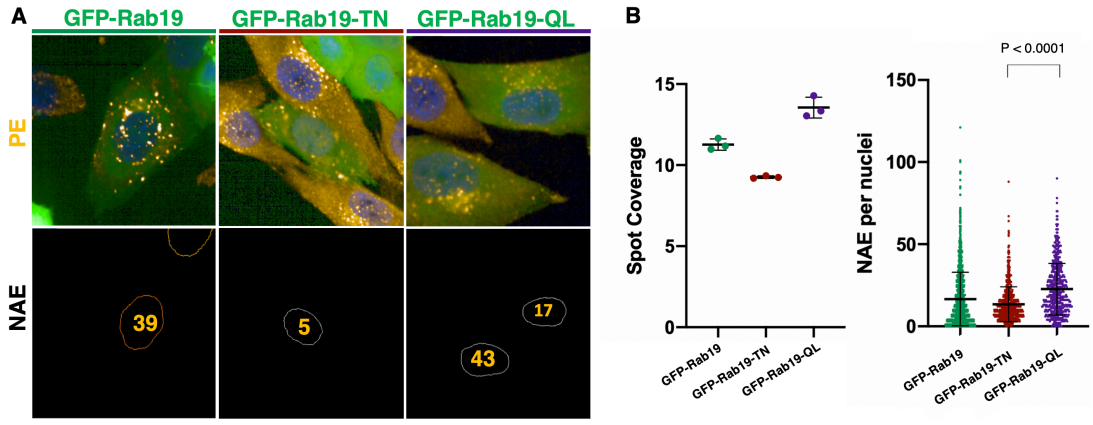

Figure 3.13. The effect of Rab19 activity on the number of nuclear PE vesicles (A) Representative images of PE labelled vesicles in MG6-63 cells transfected with GFP-Rab19, GFP-Rab19-TN and GFP-Rab19-QL. GFP transfected cells are in green, PE vesicles in yellow and nucleus stain in blue. Nuclear Mask and ROI spot count depicted in lower panel. (B) Quantification of nuclear spot coverage and (C) raw NAE spot count per cell in cells transfected with GFP-Rab19, GFP-Rab19-TN and GFP-Rab19-QL. Error bars show mean and standard deviation of triplicate wells, n=1.

We determined that NAE were detected in cells expressing GFP-Rab19, GFP-Rab19-QL and GFP-Rab19-TN. Quantification of NAE demonstrated that cells expressing the GFP-Rab19-TN mutant resulted in a decrease in PE vesicles with an average spot coverage index of 9% compared to 11.5% with cells expressing GFP-Rab19. Expression of the active GFP-Rab19-QL mutant, resulted in an increase in NAE, with an average spot coverage index of 13%. Individual cell data displayed that expression of GFP-Rab19-TN led to a shift in the population of cells with fewer PE vesicles, and that the expression of GFP-Rab19-QL led to a shift in the population of cells with a higher number of PE vesicles. These results, together with the siRNA experiments, demonstrate that depletion of Rab19 or expression of the dominant negative mutant leads to a reduction in the number of NAE, and overexpression of the active mutant leads to an increase in NAE.

As we have confirmed that depletion of Rab19 can result in a decrease in vesicles at the nucleus, we wanted to test whether the depletion of Rab19 could also affect PE delivery into the nucleus. An assay to test the role of Rab19 in the NAE pathway was conducted using subcellular fractionation. Cells were treated with NT, LRP1 and Rab19 siRNA and subjected to PE

incubation for 1 h before subcellular fractionation was carried out. PE levels in each cell compartment were then tested by western blotting (Figure 3.14).

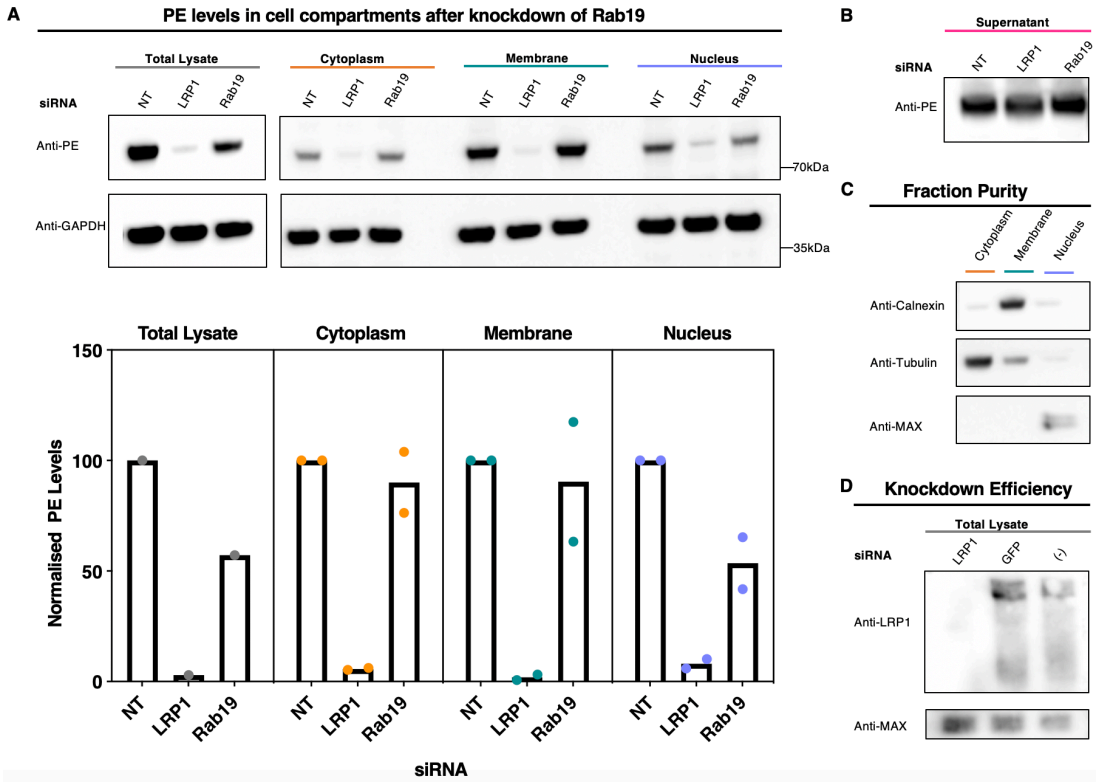

Figure 3.14 Knockdown of Rab19 leads to a reduction in PE levels in the nuclear fraction. (A) Western blot and quantification of PE levels after subcellular fraction of MG63 cells incubated with PE ligand for 1 h. PE levels in the cytoplasm, membrane and nuclear fraction and total lysate was detected in cells treated with non-targeting, LRP1 and Rab19 siRNA. GAPDH was used as a loading control. Quantification of PE levels was normalised to NT in each fraction. Bar chart shows mean of two biological replicates. (B) PE levels in supernatant of MG63 cells. (C) Fraction purity depicted by staining calnexin, tubulin and MAX in the cytoplasmic, membrane and nuclear fraction. (D) LRP1 levels of cells treated with LRP1 siRNA, GFP siRNA and non-siRNA treated cells. n=2.

In agreement with the imaging experiments, there was almost a 40% reduction in nuclear PE levels upon knockdown of Rab19 compared to the NT control (Figure 3.14A). An unexpected finding was that there was also a reduction in PE levels in the total lysate. We hypothesised that blocking nuclear entry of PE, the cell machinery would re-direct PE to be recycled back out via recycling endosomes. We tested the supernatant for levels of PE upon each knockdown condition, however, due to a lack of loading control for the supernatant fraction, no conclusions can be made from this result (Figure 3.14B). Another reason

for the decrease in PE levels in the total lysate could be explained by the possible role of Rab19 in PE internalisation. If Rab19 is involved in the internalisation of PE destined towards the nucleus, then this implicates the role of Rab19 in NAE formation rather than its role at the level of the nucleus. Antibodies to detect calnexin, tubulin and MAX, predominantly found in the membrane, cytoplasmic and nucleus respectively, were detected in each fraction to demonstrate moderate levels of fraction purity (Figure 3.14C). Levels of LRP1 were also tested by western blot upon treatment with LRP1 siRNA, verifying sufficient knockdown of LRP1 (Figure 3.14D).

3.4 Discussion

Visualisation of PE vesicles with high-resolution confocal microscopy confirmed that they are in close proximity to the nucleus, suggesting that these vesicles are NAE. A high-content imaging screen led to the identification of three Rab GTPases as regulators in the NAE Pathway, Rab7a, Rab11b and Rab19. The most interesting hit identified was Rab19, which is relatively understudied compared to the other Rab proteins identified in the screen. We determined that the depletion of Rab19 lead to a significant reduction in the number of PE-vesicles at the nucleus, as well as a reduction in nuclear PE levels by subcellular fractionation. A fraction of PE vesicles also displayed co-localisation with GFP-Rab19 vesicles (Table 3.1).

To characterise morphology of the changes in NAE, we measured the spot size of PE vesicles upon knockdown of Rab19. Larger PE vesicles were detected at the nucleus upon knockdown of Rab19. Understanding the reason for the change in PE spot size can be explained by differing causes dependent on the precise function and level that Rab19 acts at in the NAE pathway. The Rab GTPases are known to function at every step of membrane trafficking from vesicle formation to translocation, docking and fusion. If Rab19 is involved in the docking and/or fusion, then the depletion of Rab19 would inhibit NAE fusion to the nuclear envelope. This would lead to the accumulation of

cargo in NAE due to failure of the delivery of PE into the nucleoplasm, resulting in an increase in NAE size. Rab19 could also be involved upstream than at the level of the nucleus, i.e NAE vesicle formation or delivery, also leading to an increased detection in larger PE vesicles. For example, depletion of Rab19-positive PE containing vesicles could also lead to the accumulation of PE in larger non-NAE structures detected in the screen, as one of the limitations of the screen is that PE-labelled vesicle detection cannot differentiate between docked PE containing NAE and other PE labelled structures. A reduction in cytoplasmic PE vesicles and decrease in PE levels in the total lysate upon knockdown of Rab19, supports the model that Rab19 could be acting upstream than at the level of the nucleus i.e vesicle formation or NAE translocation.

In addition to the knockdown experiments, we identified that expression of the constitutively active mutant (GFP-Rab19-QL), led to an increase in nuclear PE vesicles compared to cells expressing the wild type GFP-Rab19 expressing cells. A minor decrease was seen in cells expressing the dominant negative mutant (GFP-Rab19-TN). An explanation for there being only a minor decrease upon expression of GFP-Rab19-TN could be due to the expression of endogenous Rab19 levels. Although these GDP locked Rabs are dubbed as ‘dominant-negative’, it is unclear how they act and whether they are able to supress the function of an endogenous Rab. Reports have stated that this is likely due to the sequestration of endogenous GEFs, required to catalyse the conversion of Rabs from their GDP to GTP bound states and thus supressing endogenous Rab activity (Gabe Lee, Mishra and Lambright, 2009). The sequestering of endogenous GEFs was not measured and therefore the dominant negative activity of GFP-Rab19-TN was not validated in this study. It could also be due to the low levels of GFP-Rab19-TN transfection, leading to only partial inhibition of endogenous Rab19 activity. Although these results suggest that active Rab19 expression leads to an increase in PE vesicles at the nucleus, it does not resolve which step of the PE trafficking pathway Rab19

actively functions. We further investigated the precise role of Rab19 in the NAE pathway in Chapter 5.

A limitation of siRNA-based trafficking assays, is that it can lead to the identification of non-direct regulators, such as Rab7a and Rab11b. Altering one pathway of membrane trafficking can affect others. The late endosomal marker Rab7a was identified as a hit in the Rab GTPase screen. Knockdown of Rab7a lead to the formation of enlarged PE structures observed in MG-63 cells. The phenotype of these enlarged structures seen after knockdown of Rab7 have been described previously by Vanlandingham and Ceresa (2009). They describe that cells depleted of Rab7 have an increased number of enlarged late endosomes/multi-vesicular bodies (MVBs), implicating a role of Rab7 in the exiting of cargo, such as EGF, from these structures and transfer to lysosomes. Furthermore Girard et al. (2014), provided evidence that depletion of Rab7 leads to enlargement of both early and late endosomal structures. Depletion of Rab7 leads to retention of selective cargo at the early endosome, providing an additional function of Rab7 in cargo sorting at the early endosomal level. This suggests that the large PE structures observed upon knockdown of Rab7a could be either enlarged early or late endosomes/MVBs. The retention of PE in these structures could lead to less PE being directed towards the nucleus and fewer NAE present. As the depletion of Rab7a severely disrupts the general trafficking processes of the cell, we concluded that it is not likely to be a direct regulator of the NAE pathway.

The sole up-regulator identified in the screen was Rab11b. Depletion of Rab11b resulted in an increase in the number of PE vesicles at the nucleus. This phenotype is likely to be due to indirect effects as Rab11b is involved in slow recycling pathways (Ullrich et al., 1996). LRP1 has been reported to localise to Rab11 marked recycling endosomes (Muratoglu et al., 2010). Furthermore, Rab11b co-localises with PE (Figure 3.2). It can be concluded that Rab11b depletion would affect the trafficking of both LRP1 and PE.

Knockdown of Rab11b blocks recycling pathways and could block PE recycling back out to the cell surface, resulting in an increased overall detection in the cytoplasmic and nuclear PE vesicles. Depletion of Rab11b has been reported to cause an increase in the internalisation of cell surface receptors and therefore a decrease in cell surface levels of the receptors, including receptors such as β1 Integrin and the receptor tyrosine kinase Fibroblast growth factor receptor 4 (FGFR4), (Haugsten et al., 2014; Howe et al., 2020). Grimsey et al. (2016) stated that the depletion of Rab11b caused an increase in intracellular levels of GPCR PAR, and also that this resulted in enhanced lysosomal degradation of PAR1, indicating that blocking the recycling pathways can lead to the re-sorting of internalised cargo. Therefore, it is also possible that perturbing the recycling pathway could result in increased sorting to the nucleus. We concluded that the increase in nuclear PE vesicles is due to indirect effects of the disruption of Rab11b pathways.

Prior to the Rab GTPase screen, a SNARE screen was conducted, and we found no evidence for their involvement in the association of PE vesicles with the nucleus. A total of 48 SNAREs were tested and no hits were found, despite a good Z′ factor for the assay. A lack of hits identified in this pilot screen could be due to a few factors. A redundancy in SNARE proteins has been reported by multiple studies. This redundancy can be a consequence of residual activity upon knockdown of SNARE proteins. Bethani et al. (2009) stated that just 10% of SNARE protein levels were sufficient to compensate for the loss of SNARE activity to maintain endosomal fusion activity, resulting in a phenotype similar to wild type cells. Another cause for redundancy has been explained by Kim and Bassham (2013), in which they describe trans-Golgi network resident SYP4 family of SNARE proteins. Members of this family can substitute for another in *Arabidopsis thaliana*, arguing for redundancy and overlap in function. They also demonstrated that SYP4 members can interact with different members of the VTI1 family of SNAREs, hypothesizing that the specificity of the SNARE proteins in membrane fusion events is likely to be due to their cellular localization rather than biochemical and structural

properties. The redundancy of SNAREs has also been observed in yeast (Liu and Barlowe, 2002). These redundancies, combined with the possibility that the assay may not be sensitive enough to pick up minor changes in NAE would explain for a lack of hits identified in this screen. It cannot be concluded that SNAREs are not involved in the NAE pathway, because an unidentified SNARE or one that was not tested in this screen could regulate the homotypic fusion of NAE or that of NAE to the nuclear envelope. Another rationale for the lack of hits could be due to a limitation of this assay in testing for SNARE function. It is possible that even if the knockdown of a SNARE protein resulted in the prevention of endosomal fusion to the nuclear envelope, that these endosomes would stay tethered to the nucleus. This would result in an unaltered readout in NAE count due to the function of the SNARE protein acting downstream to the observable phenotype quantified in this assay.

Some of the challenges and limitations of the NAE quantification screening assay are due to the ambiguity in defining NAE. The lack of a unique membrane marker necessitated the use of PE as a marker for NAE. Images of PE with Rab GTPases showed varying degrees of co-localisation, indicating that whilst PE is found in NAE, it is also localised to various intracellular compartments such as Rab5 and EEA1 positive early endosomes. Reviews such as Leonard et al. (2008)and Naslavsky and Caplan (2018) discuss the role of the early endosome in early cargo sorting, assessing the role of Rab5 and EEA1 in this process. High levels of co-localisation observed between PE and early endosomal markers suggests that a sorting event could take place at the early endosomal level, and that a fraction of these PE-labelled vesicles are directed towards the nucleus, where they can be defined as NAE. It is possible that a fraction of PE contained early endosomes are sorted towards the nucleus and mature into NAE.

The confocal images also revealed the large variation in the size, intensity and number of PE vesicles in each cell and at the level of the nucleus. This heterogeneity could be a result of the variation in the levels of the receptor

LRP1 present on the cell surface, affecting PE internalization. The large range in PE vesicle count in each cell could also be due to the cells being in different cell cycle stages or other factors that affect endocytosis, such as the machinery available for endocytosis. Reports have shown that clathrin-mediated endocytosis is inhibited during mitosis due to an unmet actin requirement (Fielding et al., 2012; Kaur et al., 2014). Reports have also stated that membrane size and tension can affect the rate of endocytosis (Raucher and Sheetz, 1999; Djakbarova et al., 2021). These factors contribute to differential levels of internalised cargo and could lead to variation in size and numbers of NAE present in cells. The variation in PE levels between cells, therefore PE vesicle morphology, made it difficult to distinguish whether the heterogenicity in PE vesicles was indicative of the heterogenicity of the nature of NAE or whether a subset of these nuclear PE vesicles detected were not NAE, but are in proximity to the nucleus by chance.

The assays described in this chapter validate the involvement of Rab19 in the NAE pathway, but do not help resolve which step of the pathway Rab19 actively functions. The role of Rab19 in the NAE pathway could be upstream than at the level of the nucleus, such as its involvement in the formation and translocation of NAE to the nucleus. It could also be involved at the level of the nucleus, in the docking and/or fusion of NAE to the nuclear envelope. The next two chapters will aim to design experiments to decipher the precise role of Rab19 in the NAE pathway.

Chapter 4: Using Phage Display to screen for a Single-Chain Variable Fragment against Rab19

4.1 Introduction

The data presented so far in Chapter 3 revealed a role for Rab19 in the NAE pathway. We showed that knockdown of Rab19 led to a significant decrease in the number of PE vesicles at the nucleus. The development of assays to investigate the role of Rab19 in the NAE pathway was essential. Many of these assays would involve the use of an antibody. For example, an antibody against Rab19 would allow testing for endogenous levels of the protein by western blot. Immunofluorescence experiments followed by microscopy would allow us to test for the endogenous intracellular localisation of Rab19. Pull-down experiments could be carried out to identify Rab19 effector proteins and binding partners. If an antibody with inhibitory action can be identified, then the antibody, tagged with cell penetrating peptides, could be delivered into intracellular compartments, and the phenotype of Rab19 inhibition could be studied. Obtaining a Rab19 antibody would broaden the range of experiments that could be carried out to help us study and gain insight into Rab19 function.

Antibodies are Y-shaped proteins with two heavy and two light chain polypeptides held together by disulphide bonds (Edelman and Gally, 1962). Mammalian antibodies consist of five classes, IgA, IgD, IgE, IgG and IgM, each defined by their class of heavy chains α, γ, δ, ε and μ respectively. The two light chain polypeptides have λ and κ subtypes. Both the light and heavy chains consist of constant and variable regions, with the variable regions giving rise to the diversity of the antigen binding sites. Each light chain consists of a variable region (V_L) and a constant region (C_L). The heavy chain has one variable (V_H) and three or four constant (C_H) regions (Figure 4.1). Only a 5-10 amino acid sequence contained within the hypervariable regions form the antigen-binding site. The binding site is sandwiched between the hypervariable domains of the heavy and light chain, giving two antigen-binding

sites per antibody (Alberts, 2019). The hypervariable regions form loops termed complementarity determining regions (CDRs) that determine antigen recognition whilst the constant region is involved in mediation of effector activation (Sela-Culang, Kunik and Ofran, 2013). Non-CDR regions called Framework Regions (FR), have been thought of as scaffolds for CDRs, but studies have shown that they can contribute to antigen recognition (Sedrak, Hsu and Mohan, 2003).

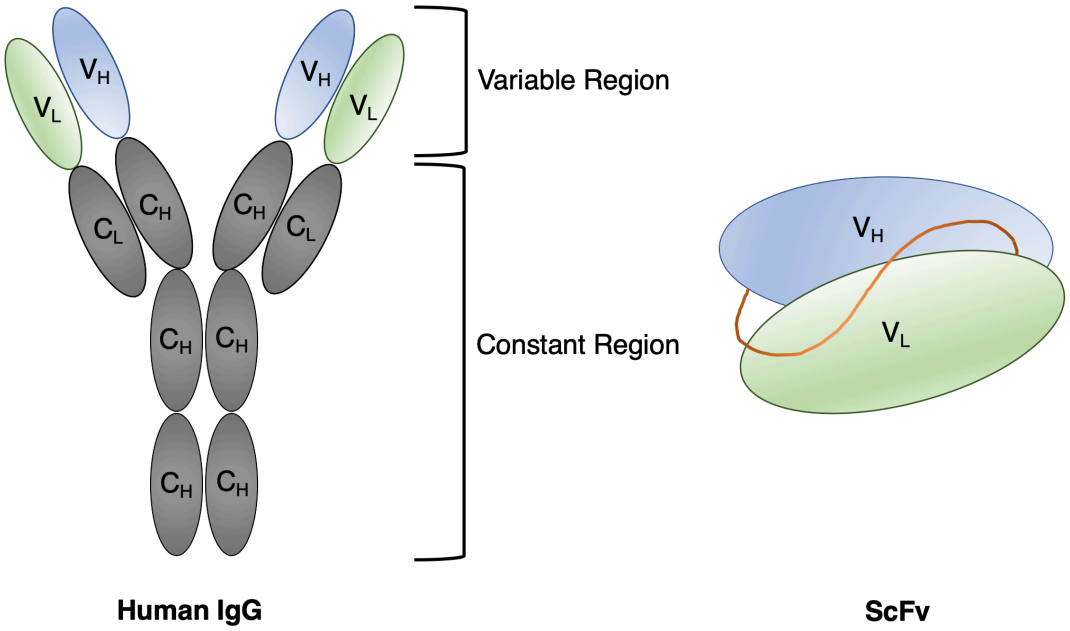

Figure 4.1 Illustration of the Structure of a Human IgG and ScFv fusion protein. Illustration of the variable (V_L and V_H) and constant (C_L and C_H) regions of the light and heavy chains in of a human IgG. Also shown is an illustration of the composition of synthetic fusion protein Single Chain Variable Fragment (ScFv) connected by a linker peptide.

A Single Chain Variable Fragment (ScFv) is a fusion protein of the variable regions (V_L and V_H) connected by a flexible linker peptide (Ahmad et al., 2012), illustrated in Figure 4.1. The engineered fusion protein can be produced in bacterial expression systems and has been widely used in phage display technology.

The development of phage display technology as a technique to screen for antibodies has revolutionised drug discovery methods, leading to the approval

of many antibody-based treatments for use in therapeutics (Barbas et al., 1991). With success stories such as adalmumab, which became the first fully human monoclonal antibody approved for use in medicine for the targeting and inhibition of tumour necrosis factor-alpha (TNFα), it is clear that is a promising and powerful technique for pharmaceutical drug development (Barderas and Benito-Peña, 2019). This technology is based on the work carried out by George Smith and Sir Gregory Winter, awarded the 2018 Nobel prize in chemistry for demonstrating that phage can be manipulated to display genetically encoded antibody fragments on the surface of bacteriophage. Variable regions of antibodies can be amplified from B cells and cloned into expression vectors fused to the phage coat protein, allowing the screening and selection based on their antigen binding activity(McCafferty et al., 1990).

The experiments conducted in this chapter will use a pre-existing naive library expressing 10^{10} independent phage clones (Dorfmueller et al., 2016) to screen for a ScFv that binds to Rab19.

4.2 Purification of GST-Rab19

Before considering the use of phage display technology to search for a Rab19 binding ScFv, a commercially available anti-Rab19 antibody (Invitrogen) was tested. I tested whether this antibody could detect endogenous levels of Rab19 in MG-63 and MDA cells, as well as cells overexpressing GFP-Rab19 by western blot (Figure 4.2).

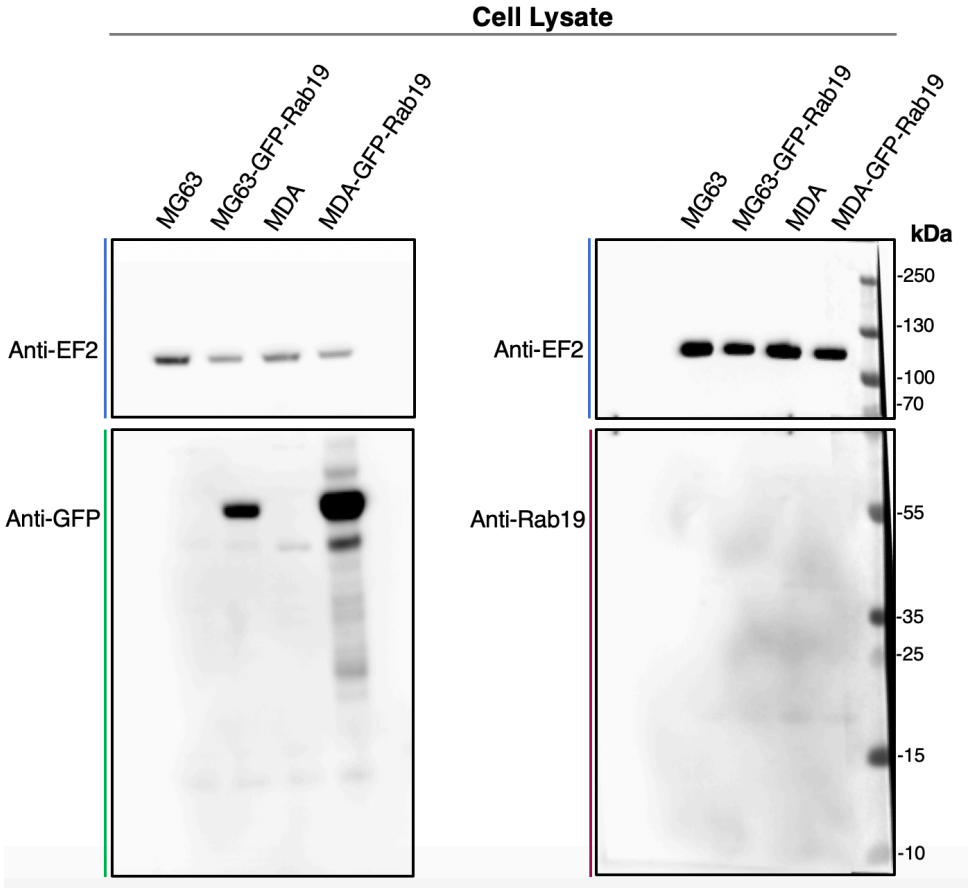

Figure 4.2 Testing the ability of a commercial Rab19 antibody to bind Rab19. Western Blot of MG-63 and MDA cells lysates and cell lysates of MG-63 and MDA cells transfected with GFP-Rab19.EF2 used as loading control. (A) Proteins detected by anti-GFP antibody staining to confirm expression of GFP-Rab19 in transfected cells (B) Staining with anti-Rab19 antibody to test its ability to detect Rab19 in cell lysates.

To ensure successful efficiency of GFP-Rab19 transfection, an anti-GFP antibody was used to detect GFP-Rab19 levels and an anti-rabbit HRP-linked secondary antibody. The GFP-Rab19 fusion protein has a molecular weight of 57 kDa, with a band detected at the predicted size in the GFP-Rab19 transfected MG-63 and MDA cells and not the wild type cells. We then tested the ability of the polyclonal Rab19 antibody to bind (GFP)-Rab19 in cell lysates, using 1 µg/ml working concentration, incubated on with the membrane overnight. Endogenous Rab19 has a molecular weight of 29 kDa. A band of this size was not detected in wild type MG-63 and MDA cells, suggesting low affinity of the antibody to Rab19 or that endogenous levels of Rab19 are too low to be detected by this antibody by western blot. We also tested the capability of this antibody to bind GFP-Rab19 in cell lysates, once again, no

bands were detected in this blot. This strongly suggests that Rab19 cannot be detected using this antibody. Although it cannot be ruled out that the fusion of Rab19 to GFP prevented the antibody to bind Rab19. Regardless, this antibody is not suitable for use to detect Rab19 levels, and I therefore turned to phage display technology to search for a Rab19-binding ScFv.

To select for phage encoding an ScFv that bind Rab19, purification of the Rab19 antigen was carried out using affinity chromatography. Recombinant GST-Rab19 was purified from bacterial BL-21 cells. Following IPTG induction, cells were lysed and the soluble fraction was incubated on glutathione sepharose beads and the beds were washed three times in wash buffers. GST tagged proteins bound to the beads were eluted with glutathione ligand. Samples were taken at each step of the purification process and visualised with a protein binding stain. The final eluted protein was tested by western blot using an anti-GST antibody (Figure 4.3).

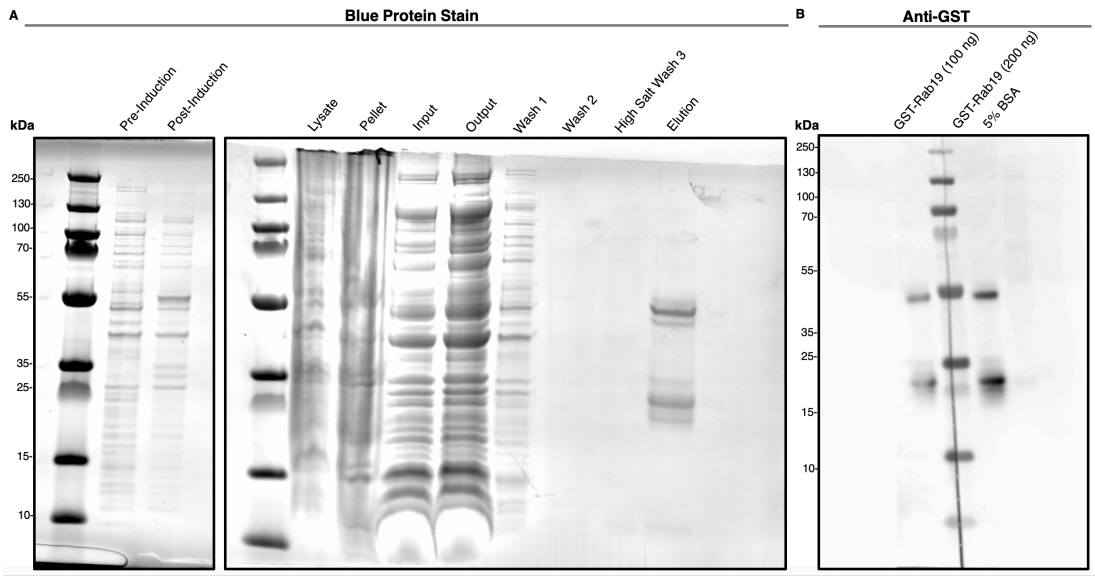

Figure 4.3 Protein Purification of GST-Rab19. (A) One-Step Blue stain of proteins taken from each step of the protein purification steps. (B) Western blot of proteins detected with Anti-GST antibody on 100 or 200 ng of GST-Rab19 recombinant protein and 5% BSA in PBS.

The GST-Rab19 fusion protein has a molecular weight of 55 kDa. An enrichment of the protein can be seen in the post-induction sample, adjacent to the 55 kDa ladder marker. The final eluted sample shows a band at 55 kDa,

indicating successful purification of the GST-Rab19 protein. A band was also detected at 25 kDa, we anticipated that this was sole expression of the GST tag. We tested this by western blot using an anti-GST antibody, and confirmed that the band observed at 26 kDa was indeed GST tag expression, which can be due to the cleavage of GST from the protein of interest in bacteria or due to proteolysis during the purification. A band at 55 kDa was also observed, confirming the purification of GST-Rab19.

4.3 Phage Selection

Purified GST-Rab19 protein was immobilised on plates, and the phage library added. Before addition, the library was depleted of any phage that bound to BSA, to remove non-specific binders. An extra depletion step against recombinant GST protein was also done, to remove phage that bound to the GST tag. The library was then finally added to the GST-Rab19 antigen, and extensive wash steps were conducted to ensure non-specific and low affinity phage were removed. Only high affinity phage were retained and subsequently eluted from the antigen containing plate. This library of eluted phage were then transduced and amplified, and the phage were purified. This pool of phage was then used as a library to once again select for Rab19-binding in the second round of panning. A total of three rounds of pannings were carried out, and phage binding was assessed for each panning round using ELISA (Figure 4.4).

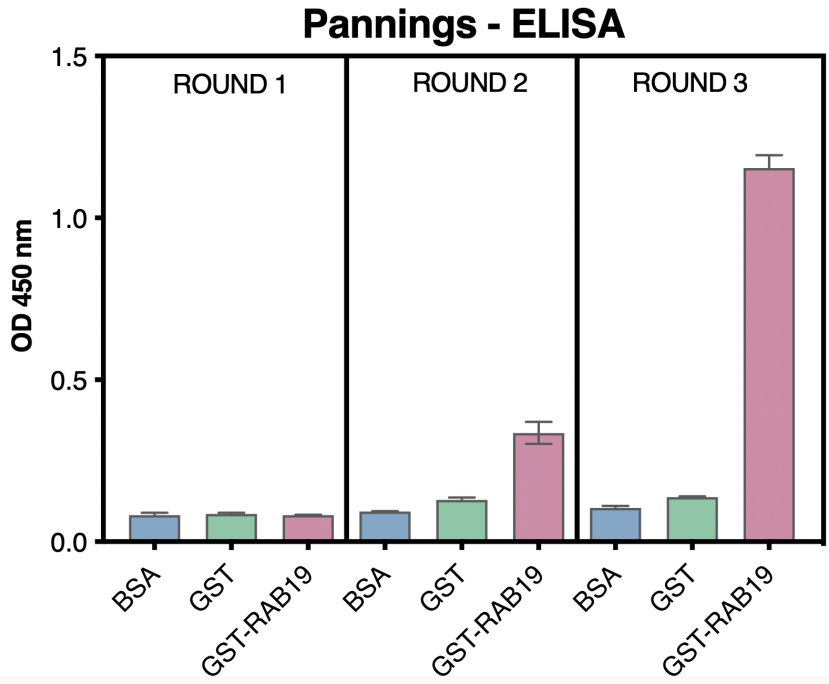

Figure 4.4 Binding of phage library from each of three rounds of pannings. ELISA test to show phage library from panning rounds 1, 2 and 3 against BSA, recombinant GST protein and recombinant GST-Rab19 protein. Phage were detected with anti-M13 antibody. Error bars show standard deviation across the three technical replicates conducted for each condition.

ELISA was used to detect phage that bound to BSA, GST and GST-Rab19. Phage were detected using a HRP-linked antibody that recognises the coat protein (pVIII) of the M13 phage. ELISA from test shows that with each round of panning, there was an enrichment of phage that bound to GST-Rab19. Phage that bound to BSA did not show any enrichment to binding BSA, giving an OD of 0.08 across all three panning rounds. There was a slight increase in phage binding to the recombinant GST protein, with the OD increasing from 0.09 in round 1 to 0.3 in round 3. The enrichment of phage binding to Rab19 is evident showing a 10-fold increase in phage binding, with the OD increasing from 0.11 in round 1 to 1.15 in the final round of panning.

Following the successful rounds of panning, we proceeded with the monoclonal selection of phage that bind to GST-Rab19. The transduced phage pool from round 3 was plated out onto agar plates and individual colonies were picked, with each colony expressing a different clone of the

phage. Purified phage from each clone were tested for its affinity to BSA, GST and Rab19 by ELISA (Figure 4.5).

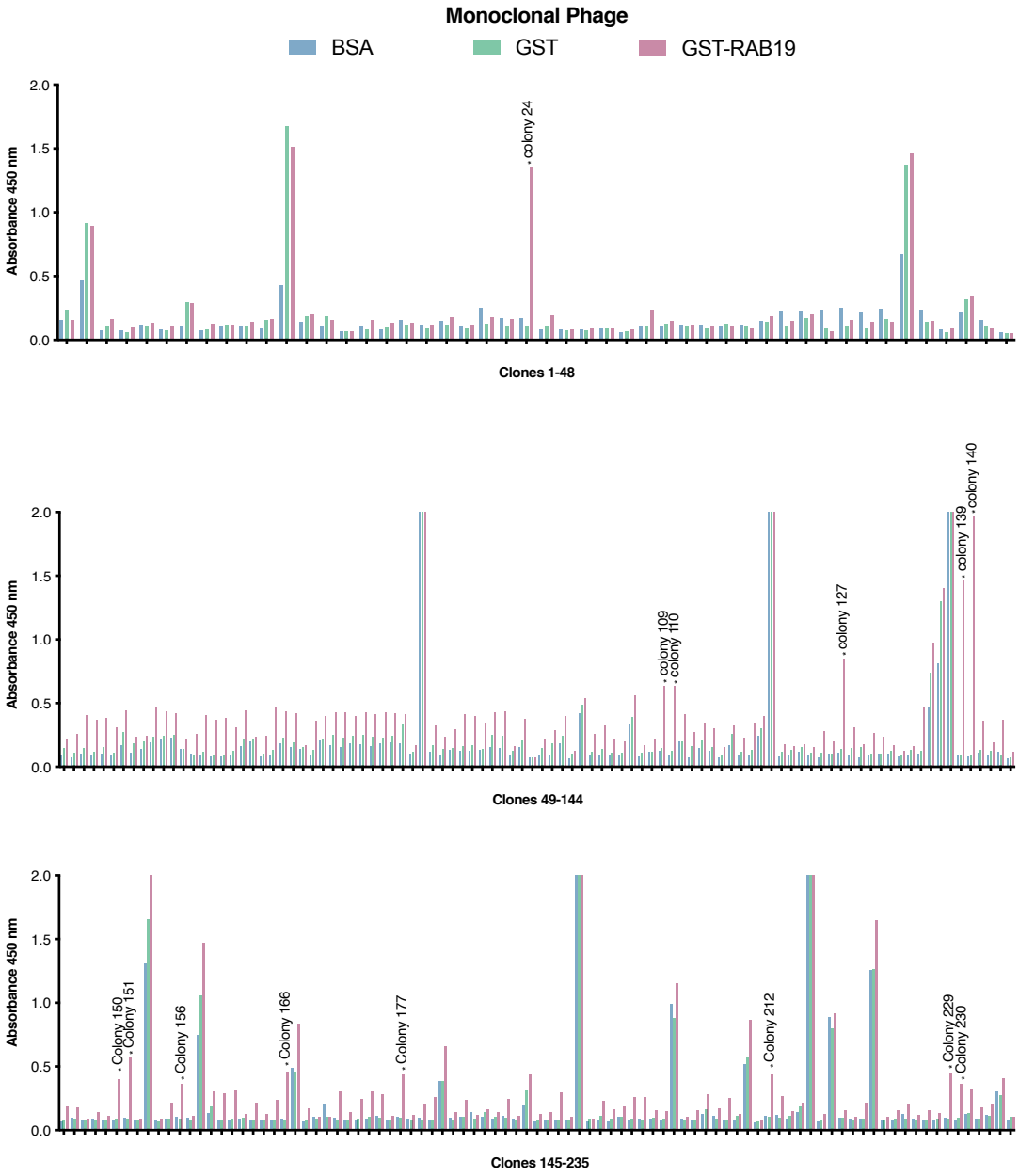

Figure 4.5 Monoclonal Selection of phage binding to BSA, GST and GST-Rab19. ELISA test to show monoclonal phage binding against BSA, recombinant GST protein and recombinant GST-Rab19 protein. Phage were detected with anti-M13 antibody.

235 individual clones were tested for their affinity to bind BSA, GST and GST-Rab19. Many clones, such as clone 12, that displayed high levels of phage binding to GST-Rab19 but also to recombinant GST or BSA were rejected. Only clones that showed a significant enrichment in binding to solely to GST-

Rab19 were selected for further experiments. A total of 14 clones (24, 109, 110, 127, 139, 140, 150, 151, 156, 166, 177, 212, 229 and 230) were selected for subsequent experiments.

4.4 Phage Sequencing

The 14 clones selected from the monoclonal stage were sent for sequencing using primers against the V_L and V_H region. Sequence analysis of phage was carried out on AbYsis (Swindells et al., 2017), a system used for the analysis of antibody sequence and structure. The sequencing results from each clone were input into the system to align and identify the CDR and FR regions of the light and heavy chain of the ScFv, listed in Table 4.1 and Table 4.2 respectively.

V_L Region Sequencing

Colony	Leader	LFR1	CDR-L1	LFR2	CDR-L2	LFR3	CDR-L3	LFR4	Tail
24	N/A								
109	RD	RRSDDQSPSSLSASVG DRVTITC	RASQSISSYLN	WYQQKPGKAPKLLIY	YASNLQS	GVPSRFSGSGSGTDFTLTI SSLQPEDFATYYC	QQSDTSPTT	FGQGTKVEIKRAA	AHHHHH H
110	GR	TSVLTQPPSVSAAPGQ KVTISC	SGSSSNIGNNHVA	WYQQYPGEAPKLLIY	DNNKRPS	GIPDRFSGSKSGTSASLAIS GLQSEDEADYYC	AAWDDSLSAGV	FGGGTKLTVLGAA	AHHHHH H
127	TVD	PSVLTQPPSVSGAPG QRVTISC	TGGSSNIGAGYDVH	WYQQLPGTVPKVLIY	GSTYRPS	GVPDRFSGSKSDTSASLA ITGLQAEDEADYYC	AAWDDSLNGY V	FGTGTKVTVLGAA	AHHHHH H
139	QIGVQ	SSVLTQPPSASGTPGQ RVTISC	SGSSSNIGMNSVN	WFQQLPGAAPKLLIY	DNNKRPS	GIPDRFSGSKSGTSAALGI TGVQTWDEADYYC	ATWDSSLSVYV	FGTGTKVTVLGAA	AHHHHH H
140	TVD	PSVLTQPPSVSGAPG QRVTISC	TGGSSNIGAGYDVH	WYQQLPGTVPKVLIY	GSTYRPS	GVPDRFSGSKSDTSASLA ITGLQAEDEADYYC	AAWDDSLNGY V	FGTGTKVTVLGAA	AHHHHH H
150	N/A								
151	N/A								
156	RAI	SSELTQDPAVSVAVGQ TVRITC	QGDILRKYYAS	WYQLQPGQAPVLVIY	GQNNRPS	GISDRFSGSNSGNTASLTI AGAQAEDEADYYC	NCRDKNYNHW V	FGGGTKVTVLGAA	AHHHHH H
166	N/A								
177	N/A								
212	STOP CODON								
229	N/A								
230	YRD	RIVLTQSPPSLPVTPGE PASISC	RSSQSLLHSTAYNYLD	WYLQKPGQSPQLLIY	LGSSRAS	GVPDRFTGSGSGTDFTLKI SRVEAEDVGVYYC	MQGLQSPIT	FGQGTKVEIKRAA	AHHHHH H

Table 4.1 Summary of sequence variation of light chain regions of monoclonal phage clones. AbYsis was used to align sequencing results with the variable loops and CDR regions of the light chain. Highlighted in green are the two clones used in further ScFv purification experiments. N/A indicates that sequencing results did not in a clear read.

V_H Region Sequencing

Colony	Leader	HFR1	CDR-H1	HFR2	CDR-H2	HFR3	CDR-H3	HFR4	Tail
24	N/A								
109	N/A								
110	ATAAILFQETVIMKYL LPTAAAGLLLLAAQP AMA	QVQLVQSGGGLVKPGGSLR LSCAASGFTFS	SYSMN	WVRQAPGKGLEWVS	SISSSSSYIYYADSVKG	RFTISRDNAKNSLYLQMN SLRAEDTAVYYCAR	GYYGMDV	WG	
127	NLHAILFQETVIMKY LLPTAAAGLLLLAAQ PAMA	QVQLVQSGGGLVQPGGSL RLSCAASGFAFS	SYAMS	WVRQAPGKGLEWVS	SISASGGATYYADSVKG	RFTTSRDNSKNTLYLQV NSLRDEDTAVYYCVT	GGGALGV	WGQGTTV TVSS	GGGG
139	N/A								
140	IAACILFQETVIMKY LLPTAAAGLLLLAAQ PAMA	EVQLVESGGGLIQPGGSLR LSCEVSGFTVS	STFMS	WFRQAPGKGLEWVS	LIYSTGETYYAESVKG	RFTISRDNSKNTLYLQM NSLKTEDTAVYYCTT	GWGYGDY	WGQGTLV TVSS	GGG
150	LLHAILFQETVIMKYL LPTAAAGLLLLAAQP AMA	QVQLVQSGGGLVQPGRSLR LSCAASGFTFD	DYAMH	WVRQAPGKGLEWVS	CISWNSGSIGYADSVKG	RFTISRDNAKNSLYLQMN SLRAEDTALYYCAR	GPVPRAFDI	WGQGTM VTVSS	GGGG
151	MAACILFQETVIMK YLLPTAAAGLLLAA QPAMA	QVQLVQSGGGLVQPGRSLR LSCAASGFTFD	DYAMH	WVRQAPGKGLEWVS	GISWNSGSIGYADSVK G	RFTISRDNAKNSLYLQMN SLRAEDTALYYCAR	GPVPRLLISG ARTMVTVST		
156	KHACNSISGDSHNEI PIAYGSRWIVITRGP AGHA	QVQLLQSAGEVKKPGESLKI SCRGSGYIFT	SQWIG	WVRQMPGKGLEWM G	ITYPGDSDTRYSPSFQD	QVTISADKSINTAYLQWN SLKASDTAMYYCAR	HVETGESDY	WGQGTLV TVSS	GGGG
166	SCMHAILFQETVIM KYLLPTAAAGLLLLA AQPAMA	QVQLVQSGGGLVQPGRSLR LSCAASGFPFN	NYAMS	WVRQAPGKGLEWVS	SIIASGGATYYADSVKG	RFTTSRDNSKNSLYLQVN SLRDEDTAVYYCVT	GRGALGV	WGQGTTA TVSS	AGGG
177	N/A								
212	N/A								
229	N/A								
230	LLHAILFQETVIMKYL LPTAAAGLLLLAAQP AMA	QVQLVQSGGGLVQPGRSLR LSCAASGFTFD	DYAMH	WVRQAPGKGLEWVS	GISWNSGSIGYADSVK G	RFTISRDNAKNSLYLQMN SLRAEDTALYYCAR	GPVPRAFDI	WGQGTM VTVSS	GGGG

Table 4.2 Summary of sequence variation of heavy chain regions of monoclonal phage clones. AbYsis was used to align sequencing results with the variable loops and CDR regions of the heavy chain. Highlighted in green are the two clones used in further ScFv purification experiments. N/A indicates that sequencing results did not in a clear read.

The results of the light chain sequencing identified the regions for clones: 109, 110, 127, 139, 140, 156 and 230. The His-tag, identified by 6 Histidine (H) residues, was used to mark the end of the light chain region and identify the codon frame. Clone 212 contained an in-frame stop codon in the V_L region and therefore not selected for further purification. The results of the heavy chain identified the regions for clones: 110, 127, 140, 150, 151, 156, 166 and 230, although the reads for clones 110 and 151 were short and were not selected for further purification.

AbYsis analysis identified the class of light chain, kappa and lambda and their subgroups. It also classed the subgroup of the heavy chain, listed in Table 4.3. It also provided a score for 'humanness' of the region (Abhinandan and Martin, 2007), identifying residues that frequently appear in human antibodies assessed against those frequently found in mice.

Heavy and Light Chain Subgroup

Colony	Light Chain (V_L) Subgroup	Heavy Chain (V_H) Subgroup	Summary
24	N/A	N/A	Failed sequencing
109	Kappa Light chain subgroup I	N/A	Failed V_H read
110	Lambda Light chain subgroup I	Heavy chain subgroup III	Short V_H read
127	**Lambda Light chain subgroup I**	**Heavy chain subgroup III**	**Continue with purification**
139	Lambda Light chain subgroup I	N/A	Failed V_H read
140	**Lambda Light chain subgroup I**	**Heavy chain subgroup III**	**Continue with purification**
150	N/A	Heavy chain subgroup III	Noisy read - multiple peaks
151	N/A	Heavy chain subgroup III	Failed V_L read and short V_H read
156	Lambda Light chain subgroup IV	Heavy chain subgroup I	Mutated PAMA sequence in V_H read
166	N/A	Heavy chain subgroup III	Failed V_L read
177	N/A	N/A	Failed sequencing
212	N/A	N/A	Stop codon in V_L ; Failed V_H Read
229	N/A	N/A	Failed sequencing
230	Kappa Light chain subgroup II	Heavy chain subgroup III	Low Humanness score ; lower affinity than clones 127 and 140

Table 4.3. Heavy and Light chain subgroups of each monoclonal phage clone. The subgroups of the light and heavy chain regions of the ScFv. Highlighted in green are the two clones used in further ScFv purification experiments. N/A indicates that sequencing results did not in a clear read.

Due to time constraints and availability of reagents, only two clones were selected for further ScFv purification experiments. The only clones that resulted in suitable sequencing results in both the light and heavy chain reads i.e without stop codons or noisy reads, were clones 127, 140, 156 and 230. Clones 127 and 140 displayed the highest level of phage binding to GST-Rab19 in the ELISA test results, and were therefore selected for purification. Clones 156 and 230 had a lower readout in phage binding to GST-Rab19, as well as the fact that clone 230 had been given a low humanness score. Clone 156 has a mutated PAMA region in the V_H read, which can be used as a cleavage site and was therefore also not selected for further purification. Clone 127 and 140 consisted of a lambda light chain subgroup I and a heavy chain subgroup III.

4.5 Purification of ScFv clones 127 and 140

Clones 127 and 140 were selected for ScFv purification. Phage purification was done in TG1 cells. However, for the purification of the ScFv region, without the phage, HB2151 cells were used. HB2151 cells do not suppress the amber stop codon, resulting in amplification of the ScFv peptide only, as the phage region is encoded downstream of the ScFv region. Successful purification of the ScFv peptide was validated with a protein gel stain and western blot. The ScFv region also encoded for a His-tag and a Myc-tag. The His-tag was used for affinity chromatography protein purification of ScFv peptides using Ni-NTA beads, and the Myc-tag was used to detect the purified ScFv (Figure 4.6).

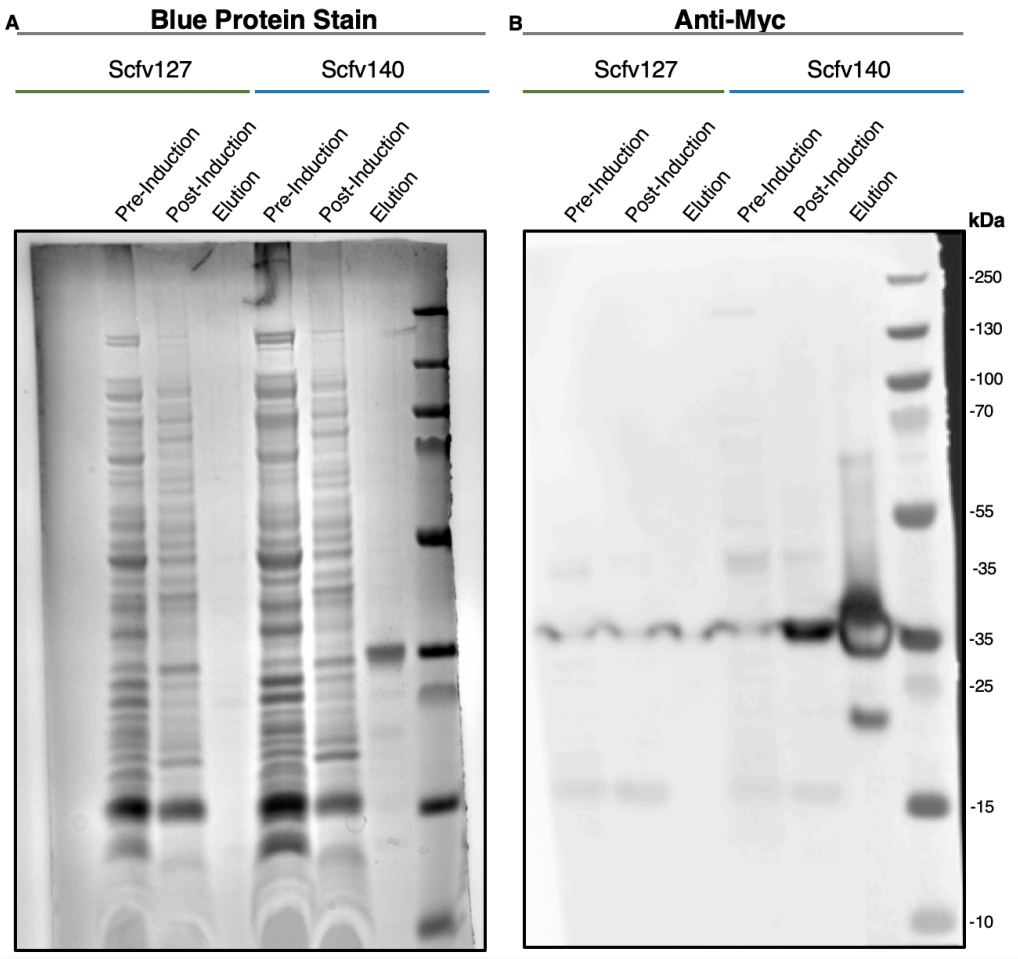

Figure 4.6 Purification of ScFv clones 127 and 140. (A) One-Step Blue protein stain and (B) Western blot of using an anti-myc antibody of pre-induction, post induction and elution samples for ScFv 127 and 140.

The pre and post-induction samples and the eluted ScFv samples are shown in the blue protein gel stain (Figure 4.6A). Purification of the ScFv clone 127 had failed, as no band was detected in the eluted sample. A band was detected at 35 kDa in the eluted sample of the ScFv clone 140. An anti-myc antibody was used to confirm the identity of this peptide by western blot. We confirmed that the band seen at 35 kDa contained the myc tag, and the ScFv 140 has been purified successfully (Figure 4.6B). A 35 kDa band in the post-induction lane also confirmed the enrichment of ScFv expression after IPTG induction.

Following the successful purification of ScFv clone 140, we attempted to validate its binding to Rab19. We tested 0.5 µg/ml, 2.5 µg/ml and 5 µg/ml of ScFv against the recombinant GST and GST-Rab19 proteins. We also tested untransfected and GFP-Rab19 overexpressing MG-63 cell lysates (Figure 4.7).

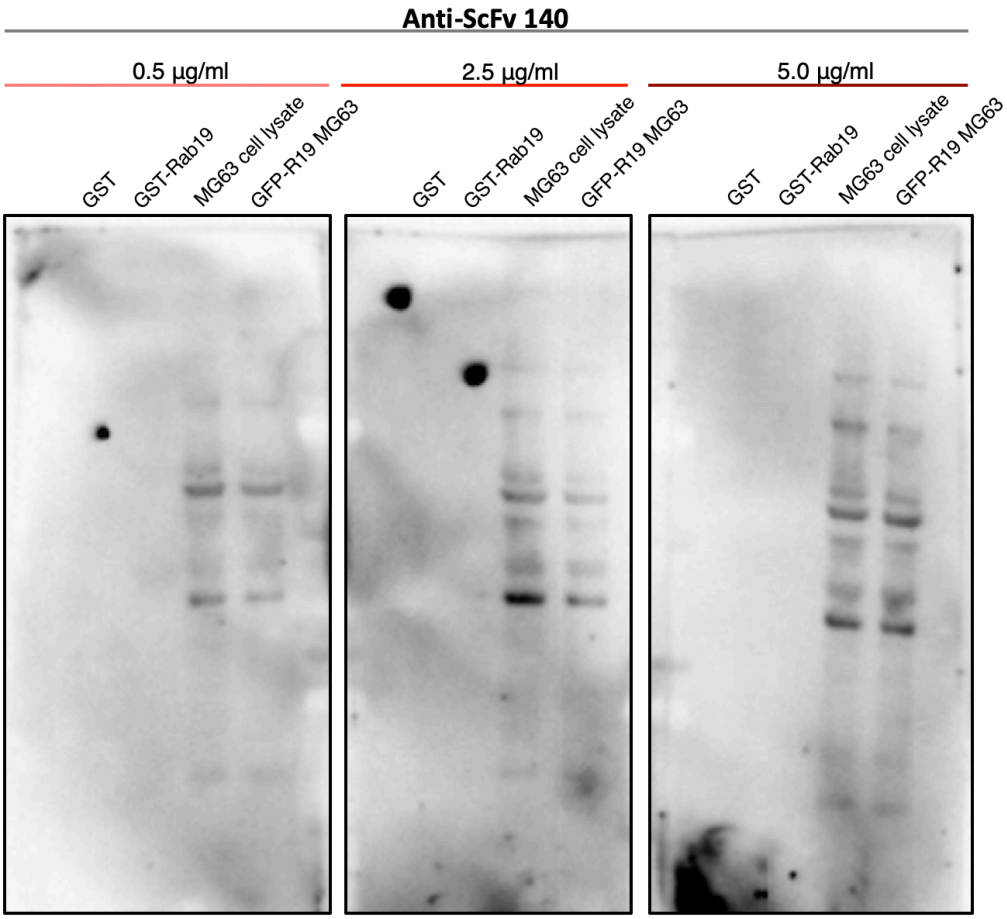

Figure 4.7 Affinity of ScFv 140 to Rab19. Western blot to show the binding of ScFv clone 140 against recombinant GST or GST-Rab19 proteins, or cell lysates of wild type or GFP-Rab19 transfected MG-63 cells. ScFv 140 was detected with a HRP-linked anti-myc antibody.

Even at the highest concentration of 5 µg/ml, ScFv 140 failed to bind GST-Rab19, with no bands detected. ScFv 140 showed multiple bands against MG-63 cell lysate, and no enrichment shown in the GFP-Rab19 overexpressing cells, suggesting non-specific binding. It is possible that as the protein purification was carried out using a native antigen, ScFv 140 only has affinity towards the folded antigen, rather than the denatured Rab19 used for the western blot. An ELISA test was also conducted using an anti-myc antibody, which also failed to bind to the native Rab19 antigen (not shown). This result shows that ScFv clone 140 fails to bind Rab19 (Figure 4.7).

4.6 Discussion

In this chapter, we attempted to find an ScFv that binds to Rab19. We successfully identified ScFv encoding phage clone 140 that bound to purified GST-Rab19, as detected by ELISA. However, upon purification of the ScFv peptide alone, it failed to bind the recombinant GST-Rab19 protein. Although ScFv 140 bound to proteins in the cell lysate, there was no enrichment in the condition with GFP-Rab19 overexpressing cells, indicating non-specific binding. It is possible that the GFP tag interferes with ScFv 140 binding to Rab19, however, multiple bands demonstrate that ScFv has high level of non-specific binding to cell lysates.

It is possible that removal of the phage from the ScFv peptide interferes with its binding to Rab19. Another possibility is that ScFv 140 does bind to Rab19, but only with low affinity. Detection of the ScFv encoded phage was carried out with an anti-M13 antibody that recognises pVIII on the phage coat. Around 2700 copies of pVIII is expressed on each M13 phage (Marvin et al., 1974), resulting in high sensitivity in the assay for the anti-M13 antibody recognition the phage. However, there is only a single myc tag encoded in the ScFv peptide, resulting in lower sensitivity in the western blot using the anti-myc antibody. If ScFv 140 binds to GST-Rab19 with low affinity, it is more likely that these bound ScFv peptides will be removed in the wash steps, and the assay is not sensitive enough to detect the low amounts of ScFv peptides present by western blot using an anti-myc antibody.

We conclude that ScFv 140 would not be suitable for use in further assays for the detection of Rab19. Characterisation of Rab19 function will have to be conducted using GFP-tagged Rab19 overexpression. Although endogenous levels of Rab19 cannot be studied using this method, transfection methods combined with microscopy-based assays can still be insightful to study intracellular localisation, mobilisation and interactions of GFP-Rab19.

Chapter 5: Investigating the Role of Rab19 at the Nucleus

5.1 Introduction

Rab19 emerged during metazoan evolution from its ancestor Rab1. In humans, Rab19 is a 27 kDa protein, encoded by a 217 amino acid sequence (Lütcke et al., 1995). Members of the Rab GTPase family are involved in the regulation of membrane trafficking. Results from Chapter 3 revealed that Rab19 regulates PE trafficking to the nucleus, implicating its role in the NAE Pathway.

Much of the characterisation of Rab19 comes from work in *Drosophila.* The first clues to the subcellular localisation of Rab19 was determined by microscopy experiments conducted by the Munro Lab, stating that GFP-Rab19 primarily localises to the Golgi in *Drosophila* S2 cells. The authors found that proteins with the GRIP domains, e.g. golgins, are effector proteins of Rab19 (Sinka et al., 2008). Follow up work identified the *Drosophila* protein Pollux, an adhesion molecule and ortholog of human Rab GAPs, TBC1D1 and TBC1D4/AS160, as effector proteins (Gillingham et al., 2014).

Other studies have shown that in *Drosophila,* Huntingtin (HTT) is trafficked in Rab19 vesicles, and the reduction of HTT perturbs bidirectional motility of Rab19 vesicles (White et al., 2015). They refer to Rab19 as a Rab associated with recycling endosomes, however other than its association with the adhesion molecule Pollux, there is little evidence that Rab19 is involved in recycling. Rab19 has also been shown to localise to Vacuole-Like Compartments (VLC) in *Drosophila*, which are involved in endocytic and secretion processes (Prince et al., 2019). Recently, Rab19 has also been implicated in cilliogenesis in *Zebrafish*, where Rab19 is likely to be involved in cortical clearing, providing further evidence that Rab19 vesicles localise to the

apical cell surface. The authors identified the RAB-GAP TBC1D4 and the HOPS vesicle-tethering complex as Rab19 effector proteins and claimed that it is required for the formation of primary cilia in zebrafish (Jewett et al., 2021).

A paralog of Rab19, Rab43, exists in vertebrates and reportedly localises to the Golgi. Studies have been conducted in mammalian cells to study Rab43 function, which suggests that it has a role in sorting of membrane proteins at the Golgi (Cox, Kansal and Whitt, 2016) and anterograde trafficking of proteins, including GPCRs, from the ER to Golgi (Leonard et al., 2008; Li et al., 2017). The TRAnsport Protein Particle (TRAPP) complexes act as GEFs for Rab GTPases, and TRAPPII was revealed as a GEF for Rab19 and Rab43 (Jenkins et al., 2020).

Membrane trafficking can be broken down into four essential steps: Vesicle formation/budding, translocation, docking and fusion. The Rab GTPases are involved in the regulation of each of these steps. The high-content screening results in Chapter 3 led to the identification of Rab19 as a player in the NAE pathway. The screen did not reveal at which step of the pathway Rab19 acts, nor whether it functions at the level of the nucleus (docking or fusion), or upstream (vesicle formation or translocation). The experiments detailed in Chapter 4 aimed to identify a ScFv against Rab19 using phage display technology. Due to the failure of ScFv 140 to bind recombinant GST-Rab19, we were unable to study the endogenous activity of Rab19. In this chapter live cell high-resolution confocal microscopy is used to visualize fluorescently tagged Rab19 and understand its intracellular localization and dynamics.

5.2 Novel Subcellular Localisation of Rab19

Studies in *Drosophila* have reported that Rab19 localises to the Golgi apparatus and to the apical membrane of polarised cells. However, neither localisation provides an explanation for its involvement in PE trafficking to the nucleus and in the NAE pathway. I therefore investigated the subcellular

localisation of Rab19 in human cells. Cells overexpressing GFP-Rab19 or the constitutively active (GFP-Rab19-QL) or dominant negative mutant (GFP-Rab19-TN) in MG-63 and Hela cells were visualised to determine the subcellular localisation of Rab19. High resolution microscopy revealed that Rab19 localises to various intracellular compartments, with vesicular, nuclear envelope, Golgi and cytoplasmic pools of Rab19 identified (Figure 5.1).

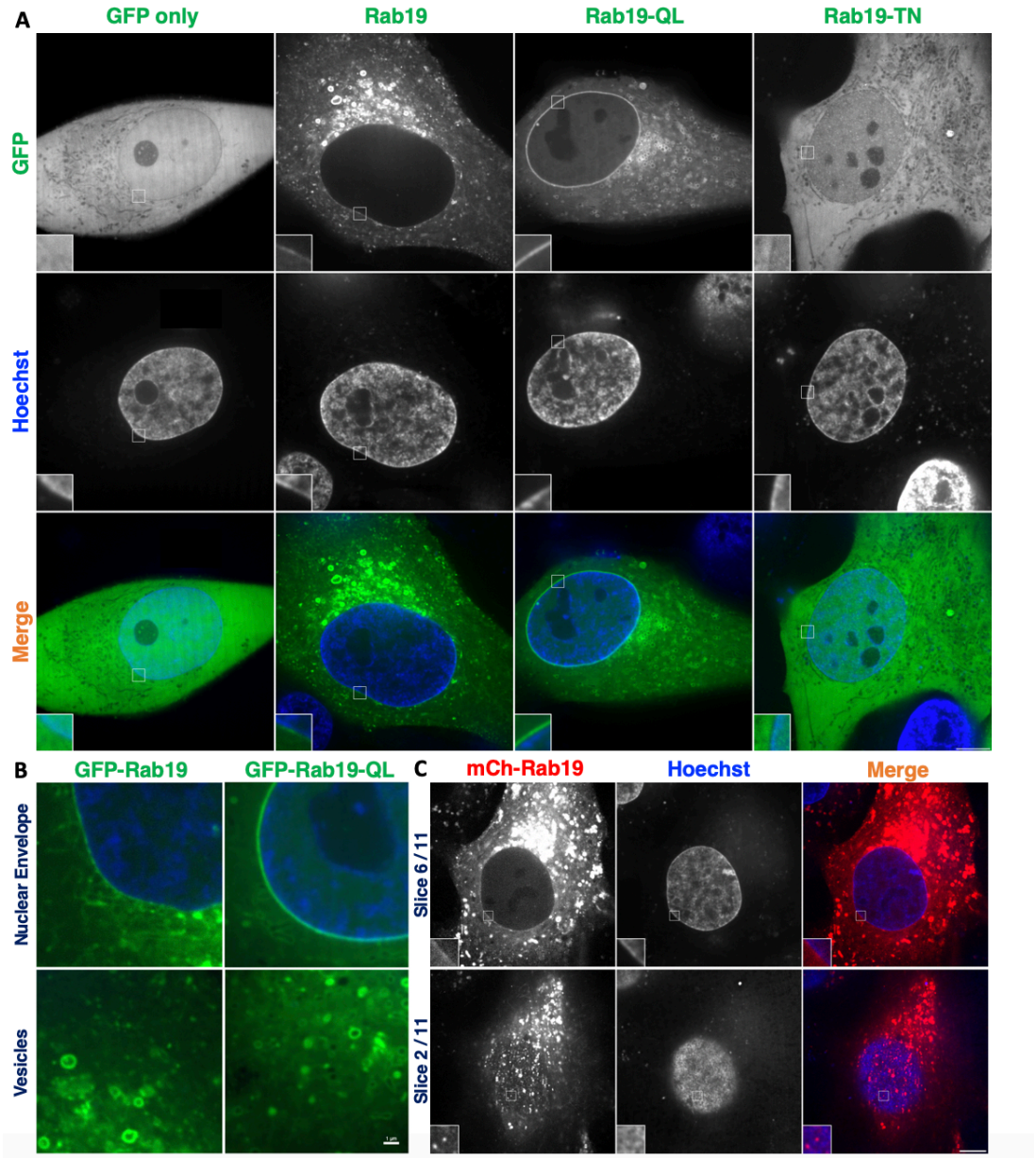

Figure 5.1 Rab19 Localises to the nuclear envelope and to intracellular vesicles (A) Typical confocal images of GFP, GFP-Rab19, GFP-Rab19-QL and GFP-Rab19-TN (shown in green) in live MG63 cells, nucleus stained with Hoechst (shown in blue). Scale bar 10 µm. 3X magnification zoom inset to show nuclear envelope and vesicular localisation. (B) 4X magnification zoom panels to show GFP-Rab19 and GFP-Rab19-QL vesicular and nuclear

envelope localisation in MG63 cells, nuclei were stained with Hoechst. Scale bar 1 µm. (C) mCherry-Rab19 (shown in red) z slices, displaying nuclear envelope inset panel in slice 6/11 and vesicles in slice 2/11. Scale bar 10 µm.

A vesicular localisation of GFP-Rab19 was observed. This observation was unsurprising, as many of the members of the Rab GTPase family have been known to localise to and function at vesicular membranes. Expression of the constitutively active mutant (GFP-Rab19-QL) displayed a similar vesicular localisation, whereas the dominant negative mutant (GFP-Rab19-TN) did not, having diffuse cytoplasmic and nucleoplasmic signal more similar to GFP alone (Figure 5.1A). This result indicates that, as described previously for other Rabs, it is the GTP-bound (active) form of Rab19 that localises to the correct target membrane.

Surprisingly, GFP-Rab19 was also localised to the periphery of the nucleus. A ring-like structure marked the nuclear periphery at the middle confocal slice of the cell, suggesting that Rab19 localises to the nuclear envelope. This ring-like structure was even more intense in the cells expressing GFP-Rab19-QL (Figure 5.1B). This localisation was not seen in the control cells expressing GFP or those expressing GFP-Rab19-TN. These observations suggest that the active Rab19 localises to the nuclear envelope. To our knowledge, this is the first study to report that a member of the Rab GTPase family localises to the nuclear envelope.

Since it is known that fusion of a fluorescent tag to a protein can affect its localisation, we wanted to test whether similar localisations of Rab19 could be observed with a secondary tag. We cannot change which terminus of the protein is fluorescently tagged, as the Rab GTPases have to be tagged at the N-terminus, due to the hypervariable domain on the C-terminus responsible for the membrane targeting and subcellular localisation of the Rab proteins (Li et al., 2014). However, the GFP tag can be swapped for another fluorescent protein, mCherry, to test whether this affects Rab19 localisation. We confirmed

that the mCherry tagged Rab19 also displayed a vesicular and nuclear envelope localisation. (Figure 5.1C).

5.3 Examining the Nuclear Envelope Localisation of Rab19

Confocal microscopy of cells overexpressing Rab19 revealed that GFP-Rab19 and GFP-Rab19-QL localise to the periphery of the nucleus, indicating a nuclear envelope localisation (Figure 5.1). To validate the presence of Rab19 at the nuclear envelope, co-immunostaining with nuclear envelope markers, SUN2 and Lamin A/C was performed (Figure 5.2).

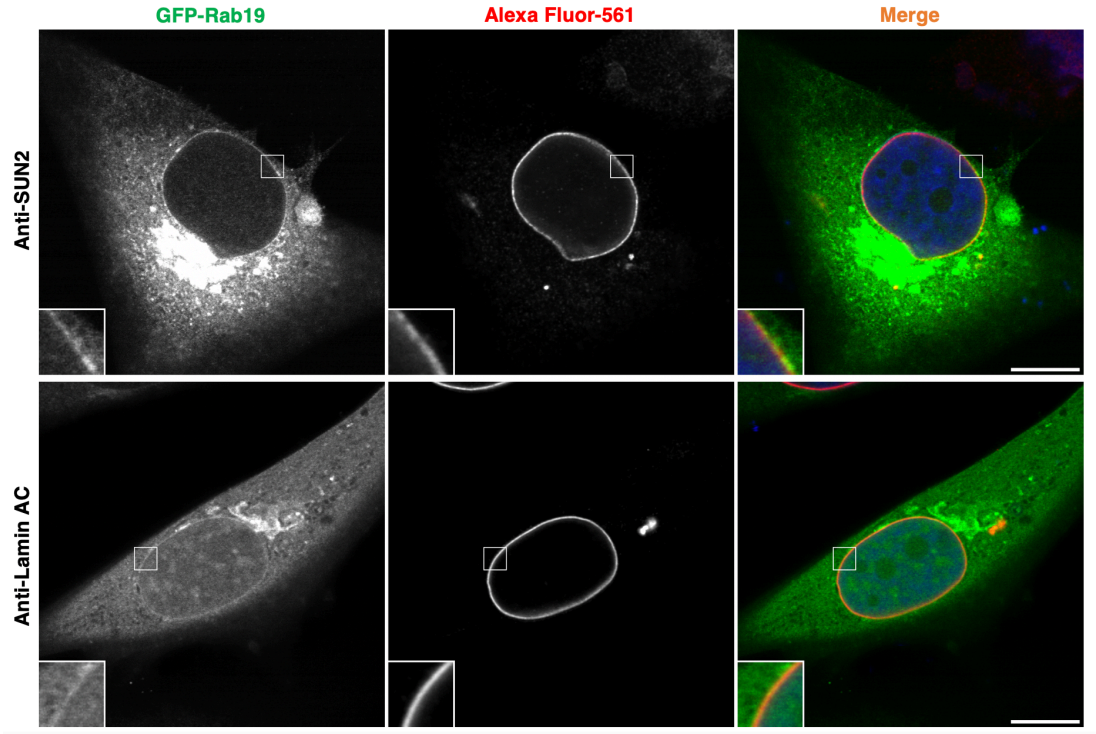

Figure 5.2 Non-uniform distribution of Rab19 at the nuclear envelope. MG63 cells were transfected with GFP-Rab19 (shown in green) followed by fixation and immunostaining with Anti-SUN2 and Anti-Lamin A/C antibodies (shown in red). Scale bar is 10 µm.

Rab19 displayed co-localisation with both of the nuclear envelope markers, SUN2 and Lamin A/C, establishing that Rab19 does localise to the nuclear membrane. The presence of Rab19 on the nuclear envelope suggests that it may have an active function here. To further investigate the nuclear envelope localisation of Rab19 and to show that this localisation is not an artefact of

fixation, we used live cell imaging to closely examine the nuclear envelope of cells expressing GFP-Rab19 or GFP-Rab19-QL (Figure 5.3).

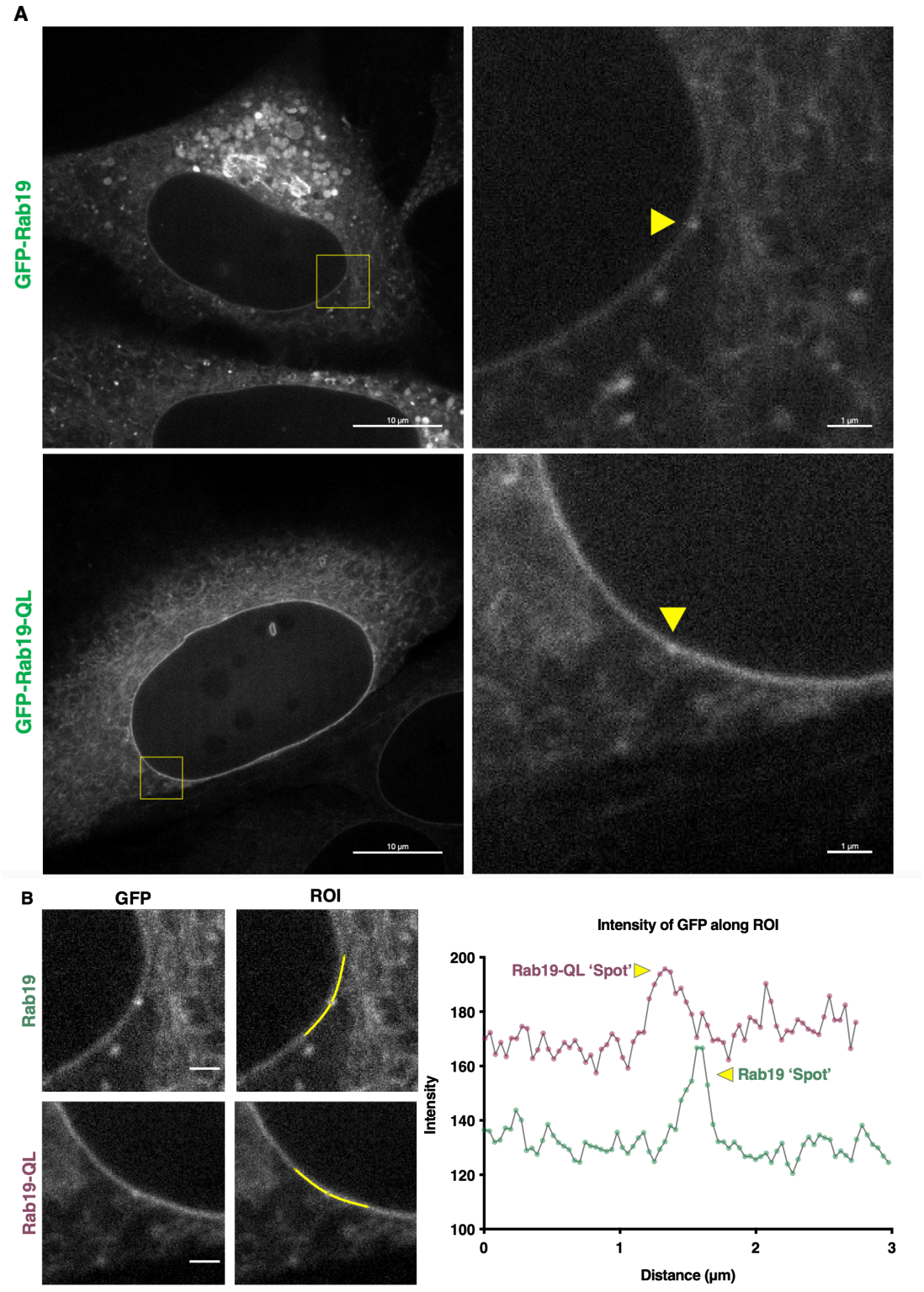

Figure 5.3 Non-uniform distribution of Rab19 at the nuclear envelope. (A) HeLa cells were transfected with GFP-Rab19 or GFP-Rab19-QL. 4X magnification zoom shown in right panel. Scale bar is 10 µm and 1 µm in left and right panels respectively. (B) Yellow line to

show ROI along Nuclear envelope of cells transfected with GFP-Rab19 or GFP-Rab19-QL. Scale bar is 1 µm. Graph shows quantification of GFP intensity along points of the ROI.

Upon close examination of the nuclear envelope localisation of GFP-Rab19 and GFP-Rab19-QL, we discovered that the nuclear ring of Rab19 had non-uniform intensity along the nuclear envelope, with punctate 'spot' structures seen along the ring (Figure 5.3). We quantified the intensity of GFP using an ROI along the nuclear envelope and found that there was a 26% and 15% increase in GFP intensity that corresponded with the spot structures seen for GFP-Rab19 and GFP-Rab19-QL.

The experiments above revealed that GFP-Rab19 localises to the nuclear envelope, but not whether it is present on the inner nuclear membrane (INM) or outer nuclear membrane (ONM). The resolution of the confocal microscope used in this study was not high enough to differentiate between the INM and the ONM, with just a 40 nm gap forming the lumen of the nuclear envelope (WATSON, 1955). To test whether Rab19 is present on the outer or inner nuclear membrane, a split GFP assay with nuclear envelope markers or a Nuclear Localisation Signal (NLS) / Nuclear Export Signal (NES) was conducted (Figure 5.4). Rab19, Rab19-QL or Rab19-TN were tagged with GFP-11. Emerin (an INM protein), an ONM localised KASH domain, an NLS and a NES were tagged with GFP-10. A fluorescent signal should only be detected where GFP11 and GFP1-10 come into close proximity with one another (Hu and Kerppola, 2003).

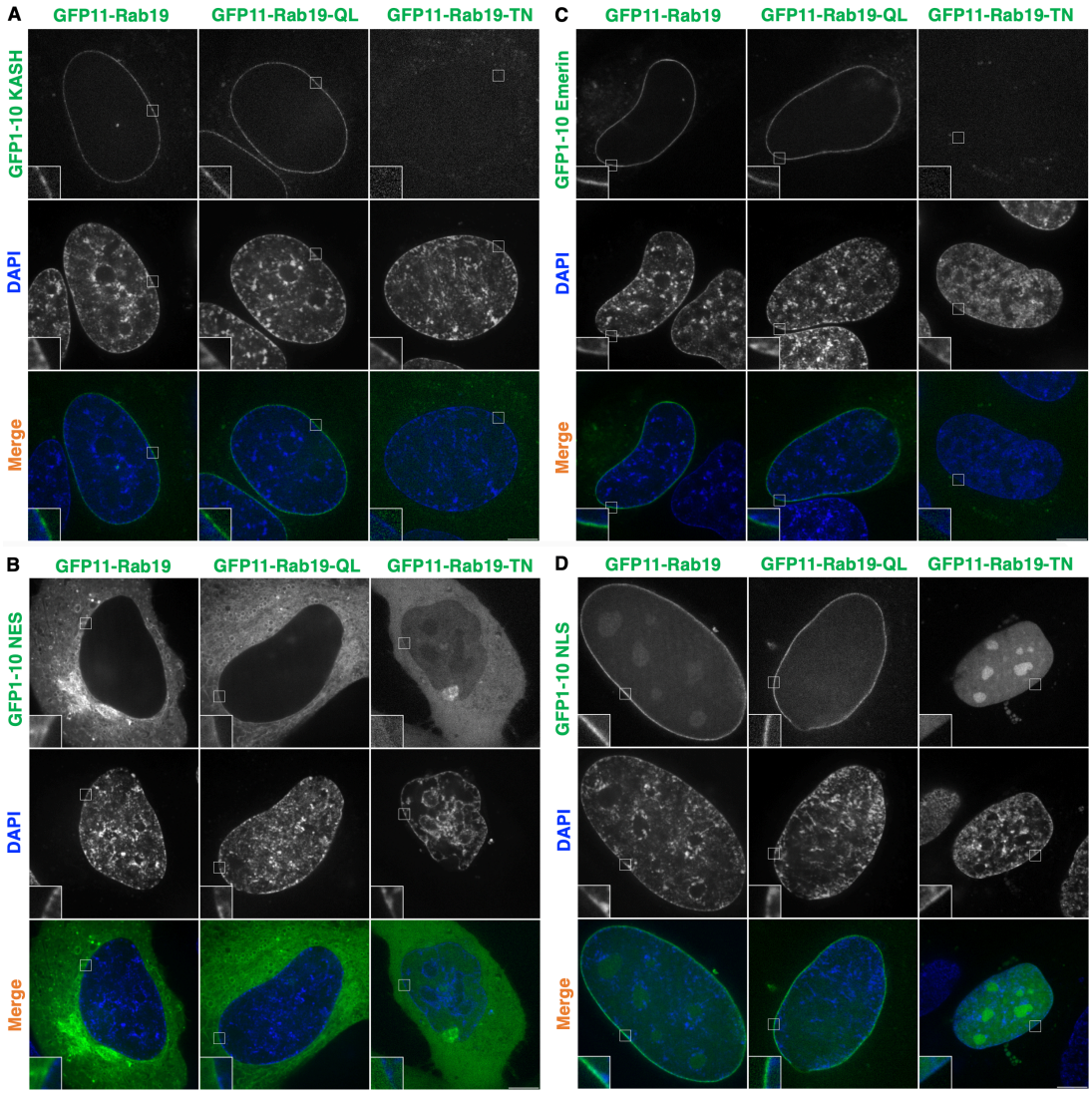

Figure 5.4 Rab19 is present on the outer and inner nuclear membranes Split GFP assay to determine Rab19 interactions. Rab19, Rab19-QL and Rab19-TN were tested for proximity to proteins tagged with GFP1-10. GFP11 tagged Rab19, Rab19-QL, and Rab19-TN were tested for interaction with (A) Inner nuclear membrane protein Emerin (B) Outer nuclear membrane localised KASH domain. (C) Nuclear Localisation Signal (D) Nuclear Export Signal. Scale bar 10 µm. 3X magnification zoom inset. Nuclei were stained with Hoechst.

We detected Rab19 and Rab19-QL signal with the KASH domain, suggesting that these proteins localise at the ONM. A faint signal at the ONM could also be detected for GFP11-Rab19 and GFP11-Rab19-QL co-transfected with the GFP1-10 NES, however the ONM signal is subdued due to the cytoplasmic signal observed, caused by the extra-nuclear localisations of Rab19 (Figure 5.4A, B).

Surprisingly, signal of Rab19 and Rab19-QL with Emerin was also detected, indicating that Rab19 is also present on the INM. GFP11-Rab19, GFP11-Rab19-QL and GFP11-Rab19-TN displayed nucleoplasmic signal upon co-transfection with GFP1-10 NLS, indicating that all three forms of Rab19 localise to the nucleoplasm. Rab19 and Rab19-QL however, also showed an enrichment in signal around the periphery of the nucleoplasm, indicating that the two active forms of Rab19 have an INM localisation (Figure 5.4C, D). No signal was detected upon co-transfection of Rab19-TN with either the KASH domain or Emerin, suggesting that the dominant negative mutant of Rab19 is not present at the nuclear envelope. Moreover, the GFP11-Rab19-TN mutant illustrates that expression of either the GFP1-10-Emerin or the GFP1-10-KASH constructs is not sufficient to cause an ectopic localisation of the GFP11 Rab19 tagged constructs.

Two plausible models describe how Rab19 might function in the NAE Pathway (Figure 5.5). Model A depicts the pathway in which Rab19 actively functions at the *nuclear envelope*. Rab19 'patches' on the outer nuclear membrane could act as 'Hot Spots' for recruitment of docking factors that facilitate NAE fusion to the nuclear envelope. Model B depicts the pathway in which Rab19 actively functions at the *vesicular* level, with Rab19-positive NAE fusing with the nuclear envelope, resulting in transfer of Rab19 to the outer nuclear membrane. We therefore set out to investigate whether Rab19 acts at the nucleus or upstream at the vesicular level.

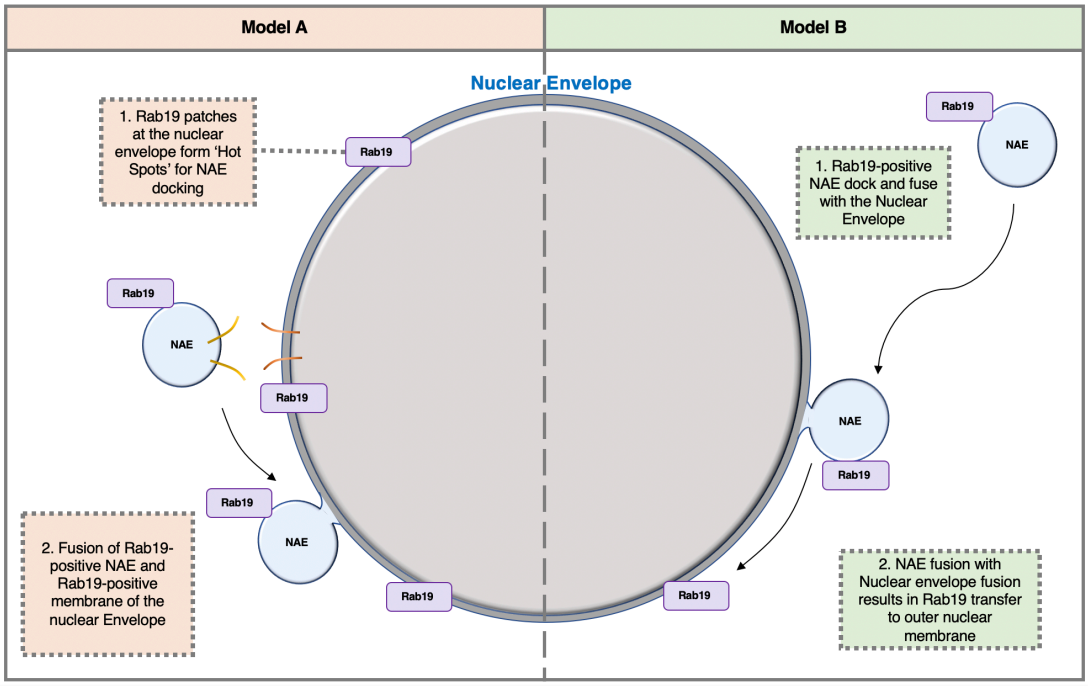

Figure 5.5 Illustration of two proposed models for the function of Rab19 in the NAE Pathway Model A: Rab19-postive NAE fuse with the nuclear envelope, resulting in transfer of Rab19 to the outer nuclear membrane. Model B: Rab19 'patches' on nuclear envelope act as 'Hot Spots' for docking of NAE.

5.4 Investigating the Role of Rab19 at the Nucleus

To test whether Rab19 is involved in vesicular docking at the nucleus (Model A), we wanted to assess whether the artificial re-localisation of Rab19 to other cellular organelles would result in an increase in vesicular docking at the ectopic compartment. The rapamycin based re-routing method has been used to study the effects of removal of the protein from its site of action (Robinson, Sahlender and Foster, 2010; Larocque et al., 2020). The protein of interest was tagged with an FK506-binding protein (FKBP) domain, which, upon the addition of rapamycin, rapidly dimerises with an FRB tagged 'anchor' protein. I tested whether GFP-FKBP-Rab19 would re-route to MitoTrap, a mitochondrial outer membrane protein fused to mCherry-FRB (Figure 5.6).

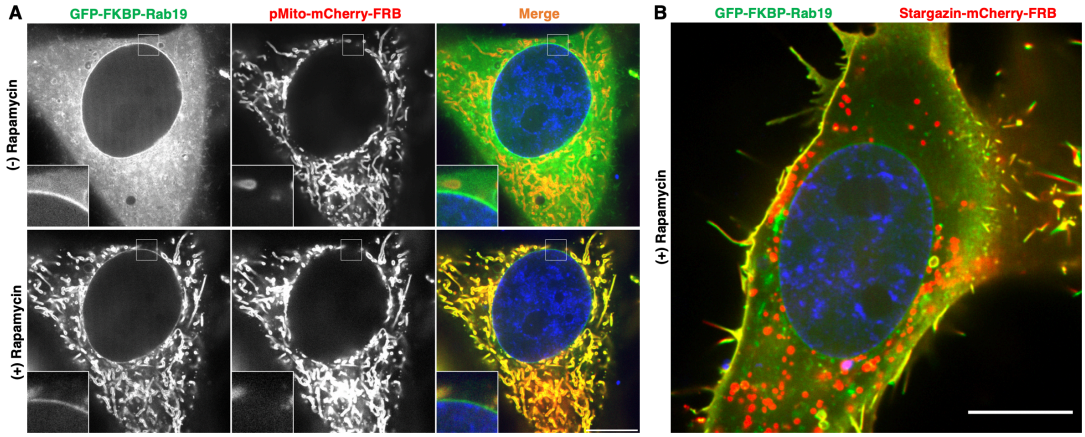

Figure 5.6 Re-routing Rab19 to the mitochondria and the plasma membrane. (A) HeLa cells were co-transfected with GFP-FKBP-Rab19 and pMito-mCherry-FRB. Lower panel shows stills from movie of cells after 15 s of supplementation with 200 nM rapamycin (B). Cells co-transfected with GFP-FKBP-Rab19 and Stargazin-mCherry-FRB. Nuclei were stained with Hoechst. Scale bar 10 µm. 3X magnification zoom inset.

Live cell imaging revealed that upon addition of rapamycin, GFP-FKBP-Rab19 was rapidly re-routed to the mitochondria, with the majority of the protein re-routed within the first 15 s upon addition of rapamycin. We observed that the nuclear envelope pool of Rab19 did not entirely re-route (Figure 5.6A). Whilst the re-localisation of GFP-FKBP-Rab19 to the MitoTrap was successful, it is still unclear how much of either the inactive and/or the active pool of Rab19 was re-routed, further discussed in Chapter 5.6.

The re-routing of GFP-FKBP-Rab19 to a second anchor was tested, using the construct Stargazin-mCherry-FRB as an anchor to the plasma membrane. As with the MitoTrap construct, a large fraction of GFP-FKBP-Rab19 successfully re-routed to the plasma membrane anchor upon addition of rapamycin. Once again, the majority of the nuclear envelope pool of Rab19 remained at the nuclear membrane, indicating that the nuclear pool of Rab19 may not be available for rapamycin-based re-routing. A fraction of the cytoplasmic pool of GFP-FKBP-Rab19 also did not re-route to the plasma membrane. Therefore, the MitroTrap construct will be used in further experiments to investigate the role of Rab19 in vesicular docking.

As the nuclear envelope pool of GFP-FKBP-Rab19 did not immediately re-route to the mitochondria, we wanted to determine whether incubation with rapamycin for a longer period of time would result in the removal of the nuclear envelope pool (Figure 5.7).

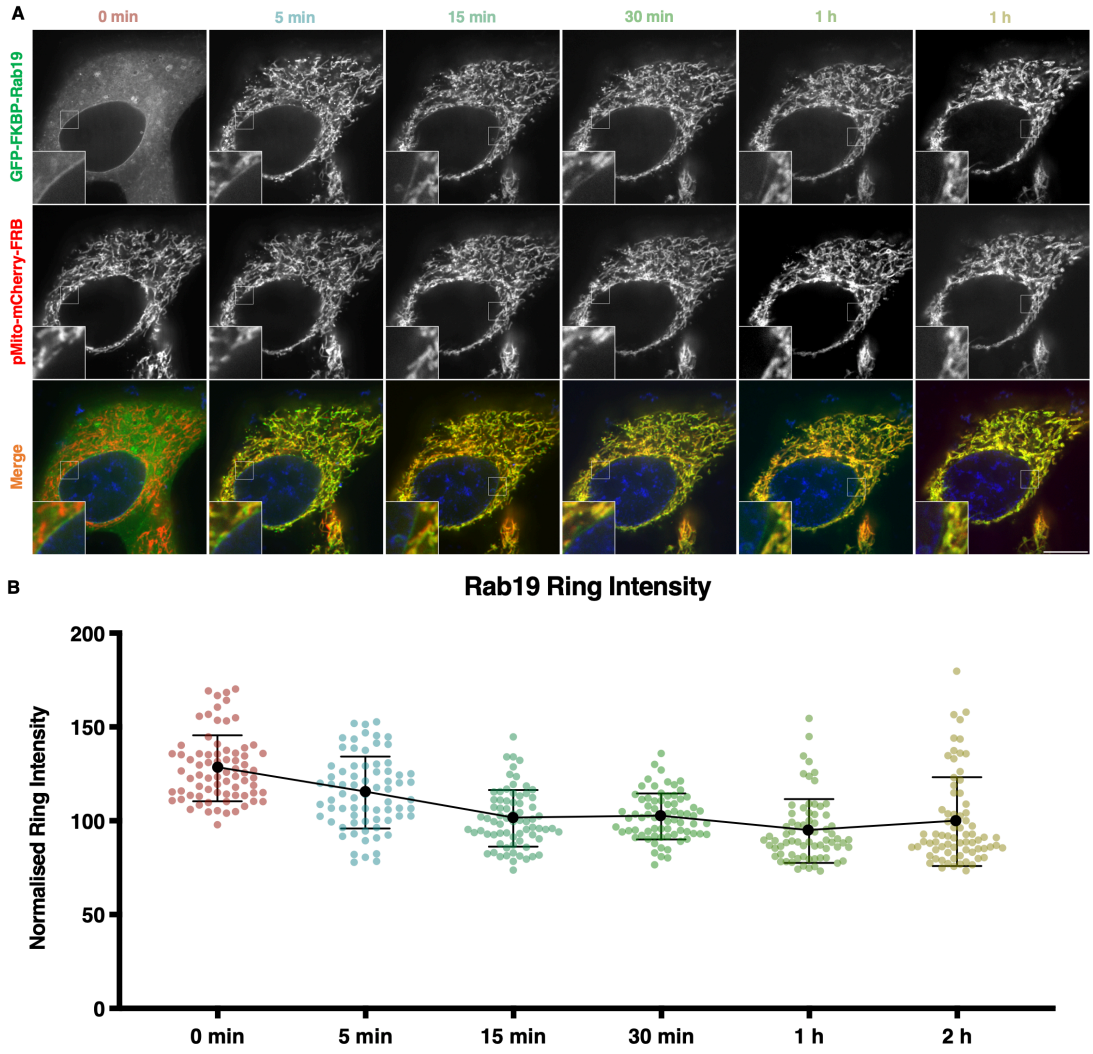

Figure 5.7 Nuclear envelope pool of GFP-FKBP-Rab19 fails to re-route to MitoTrap upon addition of rapamycin. (A) HeLa cells were co-transfected with GFP-FKBP-Rab19 and pMito-mCherry-FRB. Images were acquired at 0 min, 5 min, 15 min, 30 min, 1 h and 2 h after addition of 200 nM rapamycin. The nucleus was stained with Hoechst. Scale bar 10 µm. 3X magnification zoom inset. (B) Quantification of intensity of GFP-FKBP-Rab19 at multiple points along the nuclear envelope normalised to whole cell intensity of one HeLa cell. Error bars show standard deviation and black dots show mean.

Upon incubation with rapamycin for 2 h, there was a slight reduction in the nuclear envelope pool of GFP-FKBP-Rab19, with a 23% decrease in the

average ring intensity (Figure 5.7). Even with a 2 h incubation time, the majority of the nuclear envelope pool did not re-route. Longer incubation periods could not be assessed as incubation with rapamycin for longer periods led to cell toxicity and death. These results indicate that Rab19 is tightly associated with the nuclear membrane and that the nuclear envelope pool of Rab19 is not easily accessible for re-routing.

The re-routing of Rab19 to the mitochondria allowed us to test whether there would be an increase in vesicular docking to the ectopic location. We tested whether the re-routing of GFP-FKBP-Rab19 to MitoTrap would result in the re-localisation of EEA1 endosomes and cause an increase in EEA1 positive endosomal docking at the mitochondria (Figure 5.8).

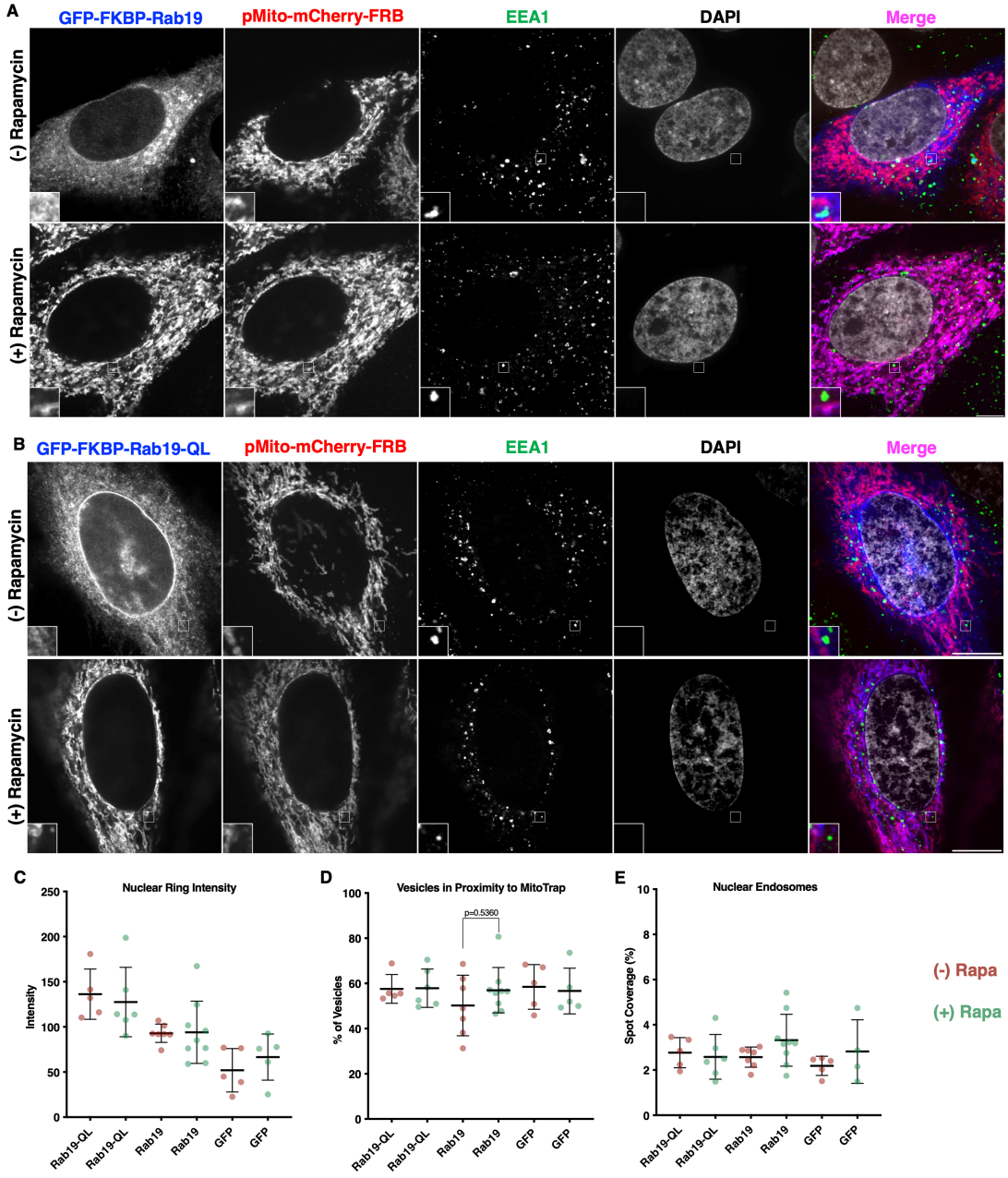

Figure 5.8 EEA1 endosomes do not re-localise to the mitochondria upon Rab19 re-routing. (A,B) HeLa cells were co-transfected with GFP-FKBP-Rab19 or GFP-FKBP-Rab19-QL or GFP-FKBP vector (shown in blue) and pMito-mCherry-FRB (shown in red). Cells were supplemented with of 200 nM rapamycin or control for 30 min before fixation and immunostaining with an anti-EEA1 antibody (shown in green). Nuclei were stained with Hoechst (shown in grey). Scale bar 10 µm. 3X magnification zoom inset. (C) Quantification of intensity of GFP-FKBP-Rab19 at multiple points along the nuclear envelope normalised to whole cell intensity. (D) Quantification of the percentage of EEA1 vesicles in proximity to the mitochondria. (E) Quantification of EEA1 vesicles at the nucleus as a nuclear spot coverage index. Error bars show mean and standard deviation.

A distance map from the MitoTrap was created to measure the proximity of each EEA1 vesicle to the mitochondria. The distance map assigned a grey

value ranging from 0-255 dependent on its proximity to the mitochondria. Endosomes that overlapped with the 0 grey value were assigned as 'proximal' to the mitochondria. 57% of EEA1 vesicles were proximal to the mitochondria in cells supplemented with rapamycin compared to 50% in control cells without rapamycin. However, this change was non-significant (p=0.5360), indicating that EEA1 vesicles do not re-localise to the MitoTrap after the re-routing of GFP-FKBP-Rab19 to the mitochondria. The number of EEA1 vesicles at the nucleus was also unaffected, however, this is likely to be due to the lack of complete removal of the nuclear pool of GFP-FKBP-Rab19 (Figure 5.8A, C).

It is possible that the lack of the re-localisation of EEA1 vesicles to the mitochondria upon re-routing of Rab19 could be due to the fact that the inactive GDP-bound Rab19 is the predominantly re-routed form of GFP-FKBP-Rab19, rendering it unable to recruit effector proteins involved in endosomal docking. We therefore tested the effects of re-routing the constitutively active pool of Rab19, GFP-FKBP-Rab19-QL, to the mitochondria. We confirmed that the active GFP-FKBP-Rab19-QL successfully re-routed to the mitochondria and that the nuclear envelope pool of Rab19 remained intact. Re-routing of the active form of Rab19 to the mitochondria also did not have any significant change on EEA1 endosomal capture at the mitochondria, with an average of 57% of EEA1 vesicles that were proximal to the mitochondria in both the test and negative control conditions (Figure 5.8B, C). These results suggest that Rab19 is not involved in EEA1 vesicle docking, however it does not rule out that Rab19 is involved in NAE docking to the nucleus, because PE-containing vesicles were not tested in these experiments. Interpretations of these results will be further explored in the discussion section of this chapter (Chapter 5.5).

5.5 Characterisation of Rab19 Vesicles

We next investigated the alternate hypothesis that Rab19 is involved at the vesicular level in the nuclear trafficking pathway. PE is a cargo molecule that translocates to the nucleus in NAE, and was used as a marker for NAE in

Chapter 3. Knockdown of Rab19 has been shown to cause a reduction in the number of PE vesicles at the nucleus (Chapter 3, Figure 3.6). PE has also been shown to be internalised into early endosomes (Chapter 3, Figure 3.2). To understand the relationship between EEA1 endosomes and Rab19 vesicular compartments, confocal microscopy was used to visualise cells co-expressing GFP-EEA1 and mCherry-Rab19 (Figure 5.9).

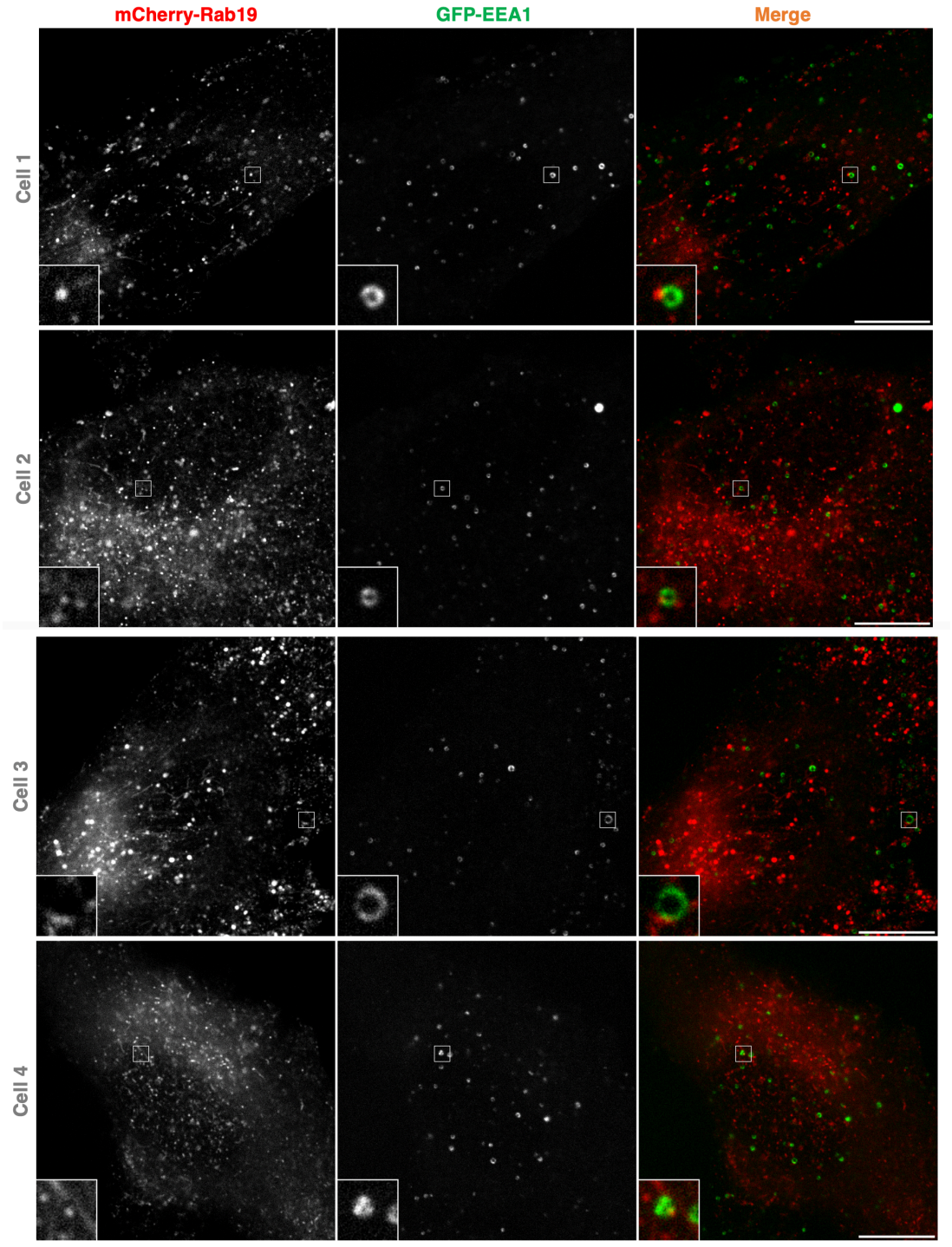

Figure 5.9 Rab19 vesicles are associated with EEA1-positive early endosomes. HeLa cells were co-transfected with mCherry-Rab19 (shown in red) and GFP-EEA1 (shown in green). Scale bar 10 µm. 3X magnification zoom inset.

We observed that some EEA1-positive early endosomes have Rab19-positive vesicles associated with them in close proximity. The Rab19 vesicles associated with EEA1 endosomes are much smaller in size than the large early endosomes. These results suggest that Rab19 vesicles are either docked at early endosomes or that Rab19 compartments bud off from Early endosomes.

Results from Chapter 3 showed that PE is internalised into early endosomes. Now, there is evidence that Rab19 vesicles are associated with early endosomes. To assess the relationship between Rab19 and PE, we expressed GFP-Rab19 in HeLa cells followed by incubation with PE (Figure 5.10).

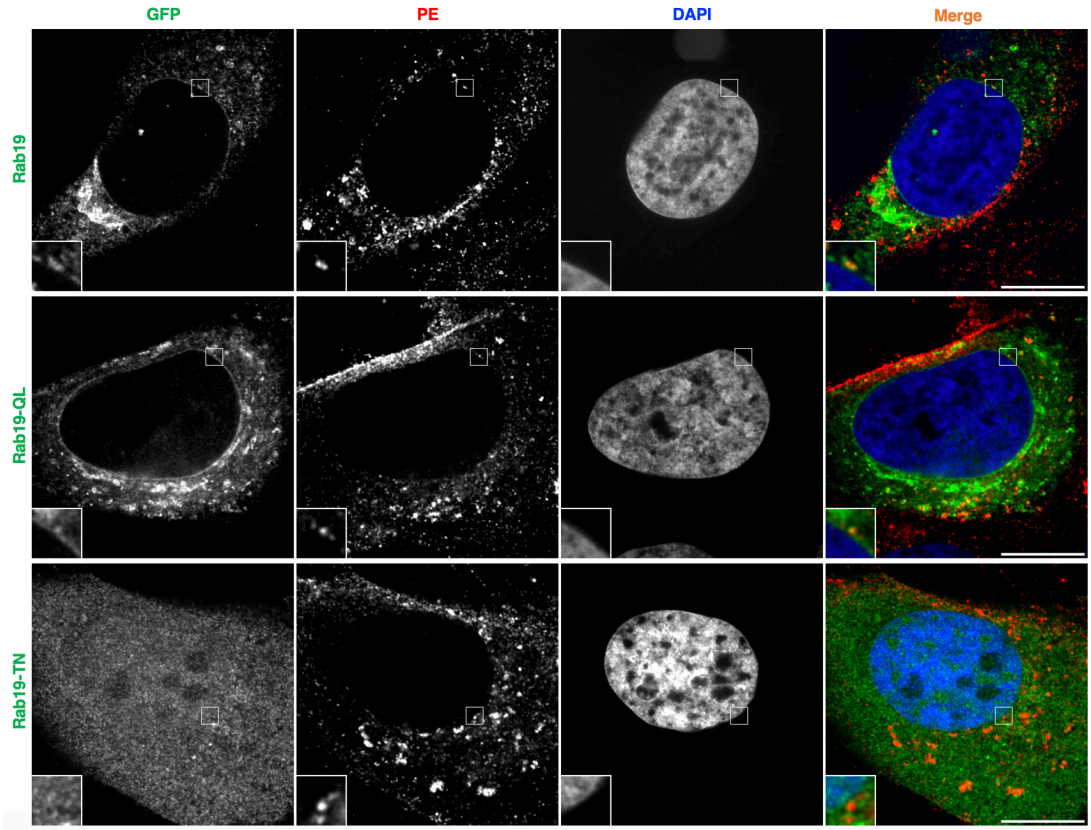

Figure 5.10 Rab19-positive structures at the nucleus are NAE that contain PE. HeLa cells were transfected with GFP-Rab19, GFP-Rab19-QL or GFP-Rab19-TN (shown in green). Cells were supplemented with 500 nM PE for 1 h, fixed and immunostained with an anti-PE

antibody (shown in red). Nuclei were stained with DAPI (shown in blue). Scale bar 10 µm. 3X magnification zoom inset.

Confocal microscopy confirmed that the GFP-Rab19 punctate 'spot' structures present at the nuclear envelope, which we first observed in Figure 5.3, co-localised with PE vesicles. PE vesicles also co-localised with GFP-Rab19-QL vesicular structures at the periphery of nucleus, but not with the dominant negative mutant GFP-Rab19-TN, indicating that these structures present at the nuclear envelope could be vesicles. These results suggest that the Rab19 marked vesicles containing PE at the nuclear envelope are NAE. However, not all PE vesicles at the nucleus co-localised with Rab19, and not all Rab19-structures at the nuclear envelope contained PE.

We wanted to understand the relationship between PE-laden vesicles, early endosomes and Rab19 vesicles. To characterise the Rab19 compartments that were associated with early endosomes, we quantified the vesicular size of Rab19-positive vesicles adjacent to early endosomes, PE vesicles at the nucleus, and the size of the EEA1 positive endosomes (Figure 5.11).

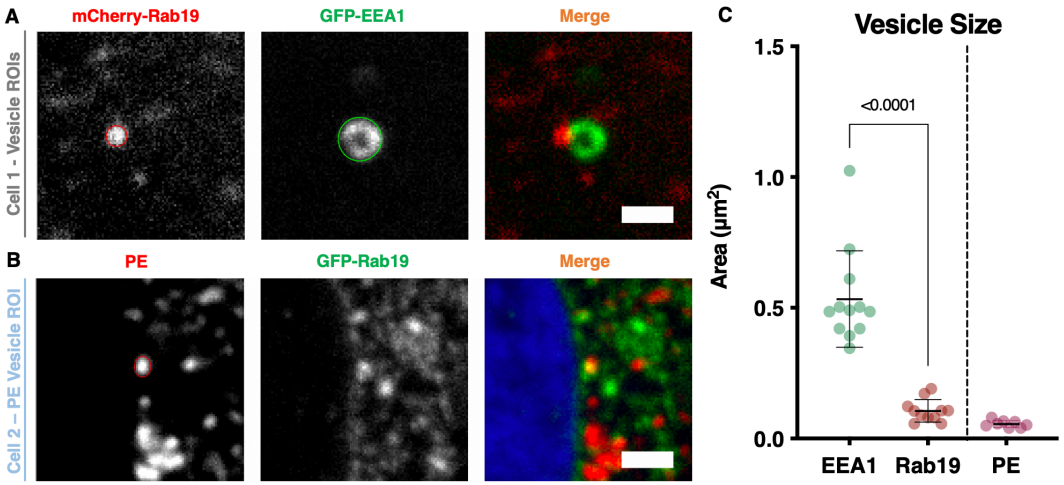

Figure 5.11 Size of Rab19 vesicles associated with EEA1-positive early endosomes. (A) HeLa cells were co-transfected with mCherry-Rab19 (shown in red) and GFP-EEA1 (shown in green). Vesicle ROI of the EEA1 early endosome and Rab19-vesicle are shown. (B) HeLa cells transfected with GFP-Rab19 (shown in green), fixed and and immunostained with anti-PE antibody (shown in red). Vesicle ROI of the PE vesicle is shown. Scale bar 1 µm. (C) Quantification of EEA1 and the adjacent Rab19 vesicle size in 4 cells, and of PE vesicles that co-localised with Rab19 at the nucleus. Error bars show mean and standard deviation. Scale bar 1 µm. P value <0.0001.

The EEA1 positive endosomes were much larger than the adjacent Rab19 vesicles, with an average vesicle size of 0.53 µm. The adjacent Rab19 vesicles were nearly 5 times smaller, with an average vesicle size of 0.11 µm. We confirmed that the PE vesicles that co-localised with GFP-Rab19 at the nucleus, were close in size to the Rab19 vesicles that were adjacent to EEA1 endosomes at 0.06 µm, hinting that the Rab19-positive PE vesicles at nucleus could originate from EEA1 positive early endosomes.

Although we have shown that Rab19 structures at the nuclear envelope co-localise with PE, this does not confirm that these structures are vesicles, as PE containing vesicles could be docked at the Rab19 'hot spots' at the nuclear envelope. We therefore wanted to observe the co-localisation of PE containing vesicles with Rab19 vesicles in the cytoplasm (Figure 5.12).

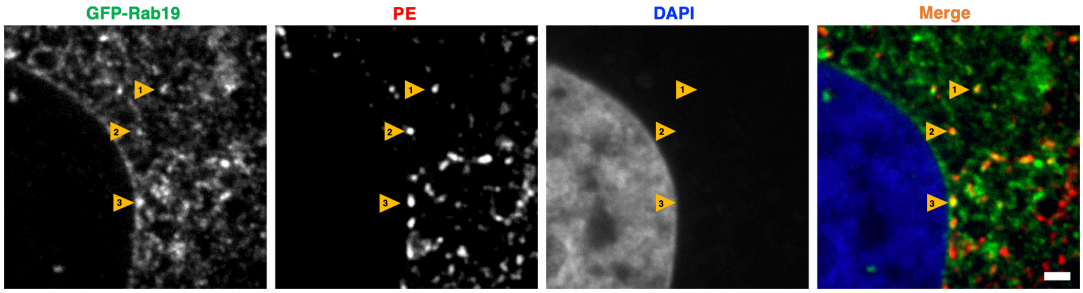

Figure 5.12 Rab19-positive NAE carry PE to the nucleus. HeLa cells were transfected with GFP-Rab19 (shown in green). Cells were supplemented with 500 nM PE for 1 h, fixed and immunostained with an anti-PE antibody (shown in red). Nuclei were stained with DAPI (shown in blue). Scale bar 1 µm.

We visualised that PE vesicles co-localise with Rab19 vesicles at variable distances from the nucleus. These results suggest that the Rab19-positive vesicles are NAE that carry PE to the nucleus, and that these Rab19 positive vesicles likely bud off from early endosomes.

5.6 Discussion

In this chapter we investigated Rab19, the primary hit obtained from the high-content screening results from Chapter 3, that identified regulators of the NAE

pathway. We identified that Rab19 localises to vesicular compartments as well as to the nuclear envelope. Rab19 may function at the vesicular level, for the formation or translocation of NAE, or at nuclear level for the recruitment of factors that facilitate the docking of NAE to the nuclear envelope. The data presented in this chapter indicate that the vesicular function is more likely.

We propose a model for Rab19 function in the NAE Pathway (Figure 5.13). Rab19 vesicles were shown to be associated with EEA1-positive early endosomes. We hypothesise that Rab19 vesicles bud off from early endosomes and carry cargo such as PE towards the nucleus. Once at the nucleus, the Rab19 NAE can undergo fusion with the nuclear envelope. This fusion event could result in the transfer of Rab19 to the nuclear envelope, providing an explanation for its localisation at the target membrane (Chapter 6, Figure 6.13).

The nuclear envelope localisation of Rab19 is novel. Some Rab GTPases, such as Rab24 and Rab28, have been reported to translocate to the nucleus (Maltese et al., 2002; Jiang et al., 2013). However, the Rab GTPases are active in their membrane bound state where they can recruit effector proteins, and Rab19 is the first reported Rab to localise to the nuclear membrane, indicating that it could actively function here.

The split GFP assay determined that Rab19 and the constitutively active mutant, Rab19-QL, localises to the outer nuclear membrane through its interactions with the KASH domain and NES at the ONM. The outer nuclear membrane localisation is concordant with both models for Rab19 function in the NAE Pathway. If Rab19 acts as a docking factor to facilitate NAE fusion to the nuclear envelope, then it would require an ONM localisation. If Rab19 functions at the vesicular level and is involved in translocation of NAE to the nucleus, then the transfer of Rab19 between NAE and the ONM during fusion could explain its ONM localisation. An inner nuclear membrane localisation of Rab19 was also determined by split GFP, through its enrichment at the INM

via its interactions with Emerin and NLS. We do not currently have an explanation for the INM localisation of Rab19, and whether it has a function at this membrane. It is possible that the INM localisation is an artefact of overexpression, due to the continuous membrane of the ONM and the INM, causing a leakage between the membranes. As Emerin must also transiently localise to the ONM to reach its destination at the INM, it is possible that its transient interaction resulted signal at the ONM, giving a false positive result. It is also possible that a nuclear localised GEF is responsible for Rab19 extraction from the inner nuclear envelope, as it has been reported that GEFs can determine the specificity of Rab membrane targeting (Blümer et al., 2013).

High-resolution microscopy allowed us to examine the nuclear envelope localisation of Rab19 in detail. The nuclear envelope localisation of Rab19 was non-uniform in intensity, with Rab19 vesicular structures observed at the envelope. The Rab19 vesicular structures at the nuclear envelope showed co-localisation with PE vesicles, suggesting that the Rab19 vesicles are PE containing NAE. Moreover, we confirmed that these Rab19 spots found at the nuclear envelope are a similar size to the Rab19 vesicles that are associated with EEA1 early endosomes, indicating that Rab19 vesicles could bud off from early endosomes to carry PE to the nucleus. We initially thought that PE-containing early endosomes (marked by EEA1) could mature into Rab19-positive NAE, however these results suggest that NAE could bud off from early endosomes, rather than a maturation step. It is also possible that the Rab19 vesicles seen adjacent to EEA1 endosomes are fusing with early endosomes, indicating that Rab19 is involved in PE internalisation and delivery to the early endosome, as the images were not able to distinguish between fusion or budding events. However, the presence of PE containing Rab19 structures at the nuclear level suggests that it is involved downstream of early endosomal trafficking.

Docked vesicles have typically been previously identified using Electron Microscopy or Total Internal Reflection Fluorescence (TIRF) Microscopy for

categorising vesicles close to membranes (Verhage and Sørensen, 2008). Confocal microscopy has also been used to visualise stages of homotypic vesicle tethering, docking and fusion for early endosomes based on the morphology of these structures (Shao et al., 2016). Chaumet et al. (2015) conducted live-cell imaging to determine the identification of docked vesicles, defining docked NAE as vesicular structures that are in proximity to the nucleus and which display low motility.

Another strategy for the identification of vesicular tethering factors, is based on the rapamycin induced re-routing of the putative tethering factors to the mitochondria by Wong and Munro (2014). The authors tested whether re-routing the tethering factor to the mitochondria would result in the re-direction of vesicles to the ectopic location. The authors were able to successfully capture endosome to Golgi and ER to Golgi carriers at the mitochondria upon re-routing of candidate Golgi tethering factors – the golgins. We used this strategy on this study to test whether re-routing of Rab19 to the mitochondria would result in the capture of NAE to this ectopic compartment.

Investigations into the involvement of Rab19 in NAE docking were challenging. We confirmed that rapamycin-induced re-routing of Rab19 to the mitochondria did not affect EEA1 endosomal docking at this site. At the time these experiments were conducted, we did not fully understand the relationship between EEA1 vesicles and NAE, believing that a maturation step would be involved in the transition of early endosomes to NAE, due to the evidence that PE colocalised with EEA1. However, we now suspect that NAE likely bud off from early endosomes, and therefore investigations of Rab19 docking experiments would have given more insight if conducted using PE as a marker for NAE, rather than EEA1. It could also not be concluded whether other factors would be required for the re-direction and transport of PE or EEA1 vesicles spatially to dock at the mitochondria. The nuclear pool of Rab19 was also not completely re-routed, and these levels of Rab19 at the nucleus could be sufficient to facilitate endosomal docking.

Another limitation of the docking experiment was that we did not fully discern how the different pools of GFP-FKBP-Rab19 pools were re-routed. The lack of cytoplasmic signal upon re-routing suggests that a large pool of the 'inactive' GDP-bound GFP-FKBP-Rab19 was re-routed to the mitochondria. However, it was unclear how the membranous pool 'active' of GFP-FKBP-Rab19 was re-routed. The first possibility is that the Rab19 positive vesicles could have been re-routed to the mitochondria, but whether the vesicles maintained structural integrity upon rapid re-localisation was difficult to determine. It was also possible that Rab19 was removed from the organelles, yet the lack of removal of nuclear envelope suggests that this is unlikely. However, Rab19 could still have been extracted from smaller vesicular membranes. The final possibility is that the active-GTP on Rab19 is hydrolysed and converted to the inactive GDP-bound Rab19, which is extracted from membranes and free in the cytoplasm for re-routing to the mitochondria.

The lack of evidence for the role of Rab19 in vesicular docking may indicate that it does not have a function in vesicular tethering or docking. Although the Rab GTPases have been implicated in vesicular tethering and docking, how they mediate this process remains unclear. Whilst tethering is reversible, docking and fusion is not (Mima, 2018). Some studies claim that Rabs are required for tethering and recruitment of docking factors, such as the Rab5 mediated recruitment of EEA1, which facilitates early endosomal tethering (Simonsen et al., 1998). However, other studies have suggested that the Rab proteins can be dispensable for tethering. Sato et al. (2015) investigated the role of the Rab GTPases in golgin-mediated tethering. The authors demonstrated that the golgin, GMAP-210, specifically binds Rab2 via two regions in its coiled-coil domain, however they reported that Rab2 binding was dispensable for vesicular tethering, suggesting that Rab function is secondary to the initial tethering event (Witkos and Lowe, 2016). These conflicting reports add ambiguity into the role of the Rab GTPases in vesicular tethering and docking. Furthermore, the studies that managed to successfully capture

vesicles that re-directed to ectopic locations were conducted by directly re-routing the tethering factor, rather than the Rab. The tethering factor that mediate NAE fusion to the nuclear envelope have not yet been identified, and therefore the effect of the tethering factor could not directly be tested, which could be another reason for why we were not able to capture endosomes at the mitochondria upon Rab19 re-routing.

Rab19 is present on both the vesicular membrane and the nuclear envelope. This is not the first report to claim that a Rab GTPase is present on the target and donor membrane. Studies have reported that Rab9 mediates the trafficking of cargo from late endosomes to the TGN, and that Rab9 localises to both compartments (Shapiro, Riederer and Pfeffer, 1993; Delgado Cruz and Kim, 2019). Barbero, Bittova and Pfeffer (2002) state that there was a loss of Rab9 signal at the Golgi just before or following Rab9 vesicular fusion to the Golgi. They claim that this loss of signal could be due to dilution of Rab9 signal in the target membrane bilayer, or the GDI-mediated removal of Rab9, indicating that this is a rapid event, however the details of the time stamps are not stated. This would contradict our hypothesis that Rab19 is present on the nuclear envelope due to transfer of Rab19 from NAE to the nuclear envelope upon fusion, as Rab19 remains at the nuclear envelope, suggesting that the removal of Rab19 from the nuclear envelope is not rapid. However, the removal of Rabs from the Golgi and the nuclear envelope could differ temporally. Yet, the evidence that Rab19 is not rapidly removed from the nuclear membrane could be an indication that it actively functions at the ONM, and it cannot be ruled out that Rab19 is required on both the NAE and ONM membranes to mediate docking and fusion.

Chapter 6: Discussion

6.1 The Role of Rab19 in NAE formation, Translocation or Docking

A high-content imaging assay was used for the identification of regulators in the NAE pathway, using PE, a cargo molecule that translocates to the nucleus as a marker for NAE. Rab19, a member of the Rab GTPase family, was identified as a key player in the NAE pathway, because the knockdown of Rab19 led to a reduction in NAE present at the nucleus. Confocal microscopy revealed that GFP-Rab19 localises to intracellular vesicles and the nuclear envelope. Intracellular Rab19 vesicles were seen closely associated with large EEA1-positive endosomes, leading to the hypothesis that Rab19 vesicles could bud from early endosomes, however further validation using live cell imaging is required to validate this hypothesis. Rab19 vesicles at the nuclear envelope were observed, and a fraction these co-localise with PE, suggesting that these spots are NAE. We proposed a model for the function of Rab19 in the NAE Pathway: Rab19 vesicles bud from early endosomes and carry cargo, such as PE, from the early endosome to the nucleus in NAE. The Rab19-positive vesicles then dock and ultimately fuse with the nuclear envelope, causing it to become enriched with Rab19 (Figure 6.13).

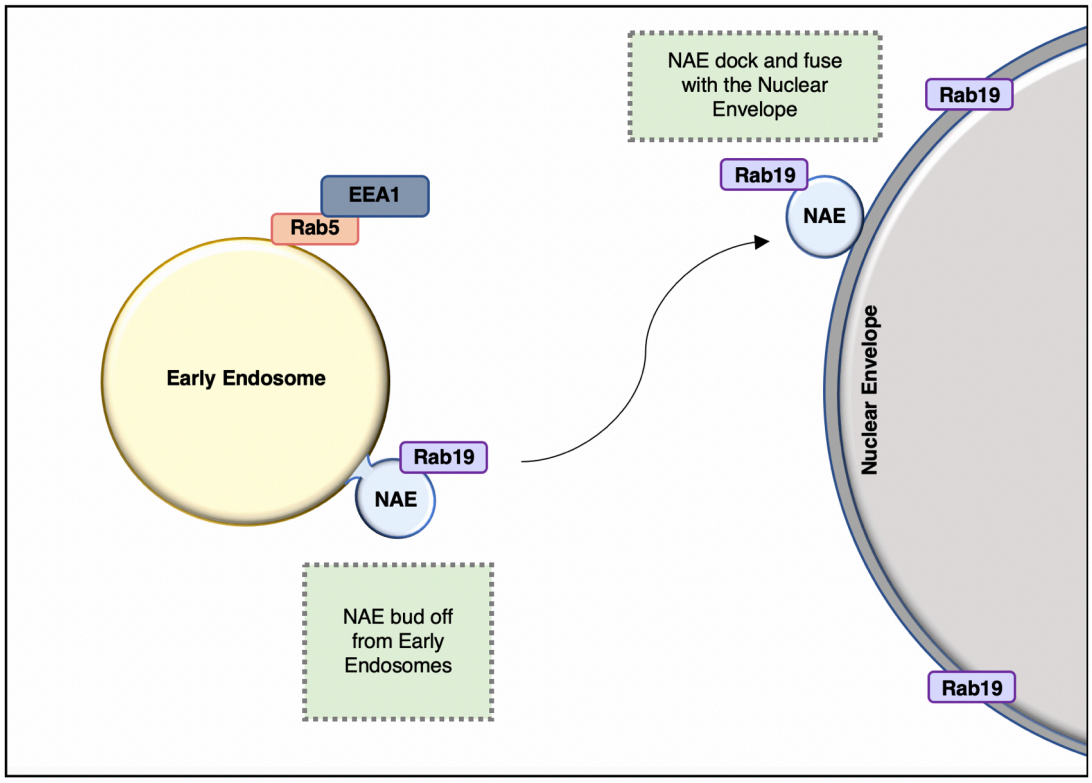

Figure 6.13 Illustration of proposed pathway to show Rab19 function in NAE Pathway. Rab19-positive NAE bud off from early endosome and dock and fuse with the nuclear envelope.

Interpretations of the findings and the limitations of the experiments has been described in the discussion section of each chapter (Chapter 3.4, Chapter 4.6 and Chapter 5.6). Here we discuss the evidence on whether Rab19 could be involved in: (1) NAE cargo internalisation at the plasma membrane, (2) NAE translocation to the nucleus, (3) NAE docking or fusion at the nuclear envelope.

High-content imaging, revealed that the knockdown of Rab19 led to a significant decrease in the number of PE vesicles at the nucleus (Figure 3.7). Although this indicated that Rab19 functions in the NAE pathway, it did not reveal which step of the pathway it acts upon. As there is evidence that there are fewer nuclear PE vesicles upon knockdown of Rab19 and the realisation that Rab19 localises to the nuclear envelope, we hypothesised that Rab19 likely functions at the level of the nucleus. However, this would not rule out the role of Rab19 in the early stages of endocytosis and membrane trafficking.

Other members of the Rab GTPase family, such as Rab5, have been implicated in the initial stages of endocytosis. For example, Rab5 is involved in sequestering ligands into clathrin coated pits (McLauchlan et al., 1998). Rab19 could be involved in the internalisation of PE, leading to the downstream effects in the reduction of NAE at the nucleus. It is unlikely that Rab19 is required for the endocytosis of all internalised PE, as the changes in cytoplasmic PE vesicles upon knockdown of Rab19 were minor, whereas knockdown of LRP1 led to a drastic reduction in the internalisation of PE (Figure 3.11). However, it cannot be ruled out that Rab19 is specifically involved in the internalisation of nuclear-targeted LRP1/PE or PE-containing NAE formation. Data from subcellular fractionation experiments back up this hypothesis, as knockdown of Rab19 led to a reduction of PE levels in the total lysate, implicating its potential role in the internalisation of PE (Figure 3.14).

The reduction in cytoplasmic PE vesicles and PE levels in the total lysate could be explained by the possibility that perturbation of the nuclear pathway would lead to the re-direction of PE by the cell machinery to other pathways. Re-direction of trafficking towards lysosomal degradation of GPCR PAR upon the inhibition of recycling pathways has been previously reported by Grimsey et al. (2016). Therefore, blocking the nuclear entry of PE could result in the re-direction of PE towards degradation or recycling pathways, leading to the observations seen in the screening results. The possibilities stated above, together with the evidence that PE co-localises with Rab19 structures at the nuclear envelope, suggests that it is likely that Rab19 functions downstream in the NAE pathway rather than for the internalisation of nuclear-targeted cargo.

Recently a study by Marco et al. (2021) states that EphA2 translocates to the nucleus in via endosomal trafficking upon stimulation with hepatocyte growth factor (HGF). The authors claim that the EphA2 receptor ‘captures’ nuclear endosomes (NAE) to the nucleus, providing evidence that the putative NLS in the cytoplasmic tail of the EphA2 receptors interacts with nuclear import

machinery, and that the mutation of the NLS domains impairs nuclear capture. They also provide evidence that the internalisation of EphA2 is Rab17 dependent, by demonstrating that the depletion of Rab17 leads to a slight reduction in the nuclear and total internalised EphA2 levels. EphA2 was shown to localise to Rab17 vesicles in proximity to the nucleus. These findings mirror the results of this study, with PE and Rab19. We did not observe any co-localisation of Rab17 with PE vesicles in Chapter 3 (Table 3.1). This suggests EphA2 and PE/LRP1 internalisation are dependent on different Rabs. Rab17 was not identified as a hit in the NAE quantification screen. This could due to a dissimilarity in the assay, which uses PE as a marker for NAE, as opposed to EphA2 used in the study by Marco et al. (2021). One interpretation is that NAE are heterogenous subset of vesicles, and that various cargo can be trafficked to the nucleus in NAE marked by different Rab proteins. Another interpretation is that Rab17 and Rab19 are both involved at different stages of the NAE pathway.

High-resolution microscopy determined that GFP-Rab19 localises to both intracellular vesicles and at the nuclear envelope, leaving the possibility open for Rab19 to function in vesicular translocation to the nucleus or for NAE docking and fusion at the nuclear envelope (Figure 5.1). We therefore designed experiments to determine whether Rab19 functions at the vesicular level (NAE translocation) or at the level of the nuclear envelope (NAE tethering, docking or fusion).

Rapamycin-induced dimerization methods were used to re-route Rab19 to an alternative compartment. We tested whether endosomes would re-localise and dock at the mitochondria upon Rab19 re-routing. We confirmed that EEA1 positive endosomes were not captured at the mitochondria upon re-routing of Rab19 (Figure 5.8). The lack of the removal of the nuclear envelope pool of Rab19 prevented us from testing NAE motility at the nucleus (Figure 5.6, Figure 5.7). However, this experiment warrants further investigation, using a

nuclear targeted cargo molecule, such as PE, to assess the role of Rab19 in NAE docking.

Rab19 localises to nuclear envelope localisation with a non-uniform distribution along the membrane and vesicular structures observed at the envelope (Figure 5.3). These Rab19 vesicles were shown to be NAE, as they co-localised with nuclear targeted cargo, PE, at the nuclear envelope. A fraction of Rab19 vesicles were seen associated with large EEA1-positive endosomes (Figure 5.9). It is possible that Rab19 vesicles could be docked at or fusing to large early endosomes. However, it is more likely that Rab19 vesicles are budding from early endosomes given the evidence that PE was shown to be internalised into early endosomes and also co-localises with Rab19 vesicles in proximity to the nuclear envelope (Figure 3.2, Figure 5.10, 5.12). This suggests that a fraction of PE-containing vesicles bud from early endosomes and is carried to the nucleus in Rab19 compartments. Rab19 function in NAE formation or budding from early endosomes explains the phenotype observed in the experiments that demonstrated that there are fewer PE-containing NAE present upon knockdown of Rab19 (Figure 3.11). Knockdown of Rab19 could result in the retention of PE in early endosomes, explaining why larger PE vesicles were observed, and therefore implicates a role for Rab19 in cargo translocation to the nucleus (Figure 3.12D).

There is substantial evidence that Rab19 is involved in vesicular translocation to the nucleus. It can be argued that if Rab19 was only required for NAE docking at the nuclear envelope, then why does it localise to intracellular vesicles? However, these two functions are not mutually exclusive. Rab19 could be essential for vesicular translocation to the nucleus and be required to be present on both the vesicular and nuclear envelope membranes. Studies have shown that two membranes containing the same Rab protein caused fusion of artificial liposomal membranes for Rab1a, Rab3a, Rab4a, Rab5a, Rab6a, Rab7a, Rab9a, Rab11a, and Rab33b but not Rab27a. Whereas fusion of membranes with heterotypic assembly of the Rab proteins on the

membranes required selective Rab combinations (Segawa, Tamura and Mima, 2019). Homotypic assembly of Rab19 could be required to recruit factors that facilitate membrane tethering and docking of NAE to the nuclear envelope.

6.2 Future Work and Significance

Whilst we were able to identify the role of Rab19 in vesicular trafficking to the nucleus, investigations that determine whether Rab19 is also required at the nucleus to facilitate NAE docking to the nucleus would be insightful. For example, knockdown of Rab19 with live cell imaging to determine whether docking of NAE is affected upon depletion of Rab19 at the nucleus would validate its role at the nuclear envelope. Identification of Rab19 GEFS or effector proteins, such as docking factors or SNAREs would also help in understanding its function. Live imaging of EEA1, Rab19 and PE would also confirm that PE can be transferred between large early endosomes to the putative Rab19 positive NAE, this would indicate that NAE do originate from large early endosomal structures.

General characterisation of the NAE pathway would help us understand its physiological significance. High-throughput screens to identify which cargo is translocated to the nucleus, and whether there is a sorting signal that targets proteins for NAE trafficking could be conducted. Are nuclear-associated vesicles always derived from early endosomes, or can post-Golgi vesicles or vesicles from other compartments also translocate to the nucleus? And if those post-Golgi vesicles do translocate to the nucleus, are the post-golgi NAE also marked by Rab19, or can a variety of Rab-marked intermediate vesicles fuse with the nucleus? This would address whether Rab19 vesicles are markers of NAE, or whether NAE encompass a variety of subtypes of vesicles that fuse with the nucleus.

Bibliography

ABHINANDAN, K.R. and MARTIN, A.C.R. (2007) Analyzing the “Degree of Humanness” of Antibody Sequences. *Journal of Molecular Biology*, 369(3), [Online] Available from: doi.org/10.1016/j.jmb.2007.02.100.

AGRAWAL, P. et al. (2016) CPPsite 2.0: A repository of experimentally validated cell-penetrating peptides. *Nucleic Acids Research*, 44(D1), [Online] Available from: doi.org/10.1093/nar/gkv1266.

AHMAD, Z.A. et al. (2012). ScFv antibody: Principles and clinical application. *Clinical and Developmental Immunology* (Vol. 2012). [Online] Available from: https://doi.org/10.1155/2012/980250

ALAMI, M. et al. (1998) Involvement of ATP-dependent Pseudomonas exotoxin translocation from a late recycling compartment in lymphocyte intoxication procedure. *Molecular Biology of the Cell*, 9(2), [Online] Available from: doi.org/10.1091/mbc.9.2.387.

ALBERTS (2019) *Molecular Biology of the Cell 6th edition*. 6th ed.

ALVARCZ-DOMINGUEZ, C. and STAHL, P.D. (1998) Interferon-γ/selectively induces Rab5a synthesis and processing in mononuclear cells. *Journal of Biological Chemistry*, 273(51), [Online] Available from: doi.org/10.1074/jbc.273.51.33901.

AMAYA, M.J. et al. (2014) The insulin receptor translocates to the nucleus to regulate cell proliferation in liver. *Hepatology*, 59(1), [Online] Available from: doi.org/10.1002/hep.26609.

DE ANGELIS CAMPOS, A.C. et al. (2011) Epidermal growth factor receptors destined for the nucleus are internalized via a clathrin-dependent pathway. *Biochemical and Biophysical Research Communications*, 412(2), [Online] Available from: doi.org/10.1016/j.bbrc.2011.07.100.

ATMARAMANI, R., PANCRAZIO, J.J. and BLACK, B.J. (2020) Adaptation of robust Z’ factor for assay quality assessment in microelectrode array based screening using adult dorsal root ganglion neurons. *Journal of Neuroscience Methods*, 339, [Online] Available from: doi.org/10.1016/j.jneumeth.2020.108699.

BAIBAKOV, B. et al. (2010) Shiga toxin is transported into the nucleoli of intestinal epithelial cells via a carrier-dependent process. *Toxins*, 2(6), [Online] Available from: doi.org/10.3390/toxins2061318.

BARBAS, C.F. et al. (1991) Assembly of combinatorial antibody libraries on phage surfaces: The gene III site. *Proceedings of the National Academy of Sciences of the United States of America*, 88(18), [Online] Available from: doi.org/10.1073/pnas.88.18.7978.

BARBERO, P., BITTOVA, L. and PFEFFER, S.R. (2002) Visualization of Rab9-mediated vesicle transport from endosomes to the trans-Golgi in living cells. *Journal of Cell Biology*, 156(3), [Online] Available from: doi.org/10.1083/jcb.200109030.

BARDERAS, R. and BENITO-PEÑA, E. (2019) The 2018 Nobel Prize in Chemistry: phage display of peptides and antibodies. *Analytical and*

Bioanalytical Chemistry, 411(12), [Online] Available from: doi.org/10.1007/s00216-019-01714-4.

BARR, F.A. (2013). Rab GTPases and membrane identity: Causal or inconsequential? *Journal of Cell Biology* (Vol. 202, Issue 2). [Online] Available from: https://doi.org/10.1083/jcb.201306010

BETHANI, I. et al. (2009) Endosomal fusion upon SNARE knockdown is maintained by residual snare activity and enhanced docking. *Traffic*, 10(10), [Online] Available from: doi.org/10.1111/j.1600-0854.2009.00959.x.

BHOSLE, V.K., RIVERA, J.C. and CHEMTOB, S. (2019).

BLÜMER, J. et al. (2013) RabGEFs are a major determinant for specific Rab membrane targeting. *Journal of Cell Biology*, 200(3), [Online] Available from: doi.org/10.1083/jcb.201209113.

BOIVIN, B. et al. (2008). G protein-coupled receptors in and on the cell nucleus: A new signaling paradigm? *Journal of Receptors and Signal Transduction* (Vol. 28, Issues 1–2). [Online] Available from: https://doi.org/10.1080/10799890801941889

BONIFACINO, J.S. and HURLEY, J.H. (2008). Retromer. *Current Opinion in Cell Biology* (Vol. 20, Issue 4). [Online] Available from: https://doi.org/10.1016/j.ceb.2008.03.009

BOROWIEC, M. et al. (2016) Towards engineering novel PE-based immunotoxins by targeting them to the nucleus. *Toxins*, 8(11), [Online] Available from: doi.org/10.3390/toxins8110321.

BRAHAM, K. et al. (1988) Kinetic Analysis of Choriocarcinoma Cell Intoxication Induced by Ricin and Ricin A Chain Immunotoxin. *Cancer Research*, 48(4).

BRAND, T.M. et al. (2013). Nuclear EGFR as a molecular target in cancer. *Radiotherapy and Oncology* (Vol. 108, Issue 3). [Online] Available from: https://doi.org/10.1016/j.radonc.2013.06.010

BRIGOTTI, M. et al. (2002) Damage to nuclear DNA induced by Shiga toxin 1 and ricin in human endothelial cells 1 . *The FASEB Journal*, 16(3), [Online] Available from: doi.org/10.1096/fj.01-0521com.

BRODSKY, F.M. et al. (2001) Biological basket weaving: Formation and function of clathrin-coated vesicles. In: *Annual Review of Cell and Developmental Biology*.

BUCCI, C. et al. (1995) Co-operative regulation of endocytosis by three RAB5 isoforms. *FEBS Letters*, 366(1), [Online] Available from: doi.org/10.1016/0014-5793(95)00477-Q.

BUCCI, C. et al. (1992) The small GTPase rab5 functions as a regulatory factor in the early endocytic pathway. *Cell*, 70(5), [Online] Available from: doi.org/10.1016/0092-8674(92)90306-W.

CARPENTER, G. and LIAO, H.J. (2013). Receptor tyrosine kinases in the nucleus. *Cold Spring Harbor Perspectives in Biology* (Vol. 5, Issue 10). [Online] Available from: https://doi.org/10.1101/cshperspect.a008979

CHAUMET, A. et al. (2015) Nuclear envelope-associated endosomes deliver surface proteins to the nucleus. *Nature Communications*, 6, [Online] Available from: doi.org/10.1038/ncomms9218.

CHAVRIER, P. et al. (1991) Hypervariable C-termmal domain of rab proteins acts as a targeting signal. *Nature*, 353(6346), [Online] Available from: doi.org/10.1038/353769a0.
CHAVRIER, P. et al. (1990) Localization of low molecular weight GTP binding proteins to exocytic and endocytic compartments. *Cell*, 62(2), [Online] Available from: doi.org/10.1016/0092-8674(90)90369-P.
CHEN, D.J. and NIRODI, C.S. (2007). The epidermal growth factor receptor: A role in repair of radiation-induced DNA damage. *Clinical Cancer Research* (Vol. 13, Issue 22). [Online] Available from: https://doi.org/10.1158/1078-0432.CCR-07-1610
CHEN, P.I. et al. (2009) Rab5 isoforms differentially regulate the trafficking and degradation of epidermal growth factor receptors. *Journal of Biological Chemistry*, 284(44), [Online] Available from: doi.org/10.1074/jbc.M109.034546.
CHEN, P.I. et al. (2014) Rab5 isoforms orchestrate a “division of labor” in the endocytic network; Rab5c modulates rac-mediated cell motility. *PLoS ONE*, 9(2), [Online] Available from: doi.org/10.1371/journal.pone.0090384.
CHEN, Q.Q. et al. (2005) Identification of novel nuclear localization signal within the ErbB-2 protein. *Cell Research*, 15(7), [Online] Available from: doi.org/10.1038/sj.cr.7290320.
CHEN, W.J., GOLDSTEIN, J.L. and BROWN, M.S. (1990) NPXY, a sequence often found in cytoplasmic tails, is required for coated pit-mediated internalization of the low density lipoprotein receptor. *Journal of Biological Chemistry*, 265(6), [Online] Available from: doi.org/10.1016/s0021-9258(19)39742-x.
CHIARIELLO, M., BRUNI, C.B. and BUCCI, C. (1999) The small GTPases Rab5a, Rab5b and Rab5c are differentially phosphorylated in vitro. *FEBS Letters*, 453(1–2), [Online] Available from: doi.org/10.1016/S0014-5793(99)00686-9.
CHRISTOFORIDIS, S. et al. (1999) The rab5 effector EEA1 is a core component of endosome docking. *Nature*, 397(6720), [Online] Available from: doi.org/10.1038/17618.
CORDO RUSSO, R.I. et al. (2015) Targeting ErbB-2 nuclear localization and function inhibits breast cancer growth and overcomes trastuzumab resistance. *Oncogene*, 34(26), [Online] Available from: doi.org/10.1038/onc.2014.272.
COX, J. V., KANSAL, R. and WHITT, M.A. (2016) Rab43 regulates the sorting of a subset of membrane protein cargo through the medial Golgi. *Molecular Biology of the Cell*, 27(11), [Online] Available from: doi.org/10.1091/mbc.E15-03-0123.
DAI, J. et al. (2004) ACAP1 promotes endocytic recycling by recognizing recycling sorting signals. *Developmental Cell*, 7(5), [Online] Available from: doi.org/10.1016/j.devcel.2004.10.002.
DELGADO CRUZ, M. and KIM, K. (2019). The inner workings of intracellular heterotypic and homotypic membrane fusion mechanisms. *Journal of Biosciences* (Vol. 44, Issue 4). [Online] Available from: https://doi.org/10.1007/s12038-019-9913-3

DITTMANN, K. et al. (2005) Radiation-induced epidermal growth factor receptor nuclear import is linked to activation of DNA-dependent protein kinase. *Journal of Biological Chemistry*, 280(35), [Online] Available from: doi.org/10.1074/jbc.M506591200.
DJAKBAROVA, U. et al. (2021). Dynamic interplay between cell membrane tension and clathrin-mediated endocytosis. *Biology of the Cell* (Vol. 113, Issue 8). [Online] Available from: https://doi.org/10.1111/boc.202000110
DOMINGUES, I. et al. (2011) VEGFR2 translocates to the nucleus to regulate its own transcription. *PLoS ONE*, 6(9), [Online] Available from: doi.org/10.1371/journal.pone.0025668.
DORFMUELLER, S. et al. (2016) Isolation of a recombinant antibody specific for a surface marker of the corneal endothelium by phage display. *Scientific Reports*, 6, [Online] Available from: doi.org/10.1038/srep21661.
EDELMAN, G.M. and GALLY, J.A. (1962) The nature of Bence-Jones proteins. Chemical similarities to polypetide chains of myeloma globulins and normal gamma-globulins. *The Journal of experimental medicine*, 116, [Online] Available from: doi.org/10.1084/jem.116.2.207.
FARIA, J.A.Q.A. et al. (2016) Effects of different ligands on epidermal growth factor receptor (EGFR) nuclear translocation. *Biochemical and Biophysical Research Communications*, 478(1), [Online] Available from: doi.org/10.1016/j.bbrc.2016.07.097.
FAWELL, S. et al. (1994) Tat-mediated delivery of heterologous proteins into cells. *Proceedings of the National Academy of Sciences of the United States of America*, 91(2), [Online] Available from: doi.org/10.1073/pnas.91.2.664.
FERGUSON, S.M. and DE CAMILLI, P. (2012).
FIELDING, A.B. et al. (2012) Clathrin-mediated endocytosis is inhibited during mitosis. *Proceedings of the National Academy of Sciences of the United States of America*, 109(17), [Online] Available from: doi.org/10.1073/pnas.1117401109.
FOTI, M. et al. (2007) The neck of caveolae is a distinct plasma membrane subdomain that concentrates insulin receptors in 3T3-L1 adipocytes. *Proceedings of the National Academy of Sciences of the United States of America*, 104(4), [Online] Available from: doi.org/10.1073/pnas.0610523104.
FRANKEL, A.D. and PABO, C.O. (1988) Cellular uptake of the tat protein from human immunodeficiency virus. *Cell*, 55(6), [Online] Available from: doi.org/10.1016/0092-8674(88)90263-2.
GABE LEE, M.T., MISHRA, A. and LAMBRIGHT, D.G. (2009).
GAVRILJUK, K. et al. (2013) Membrane extraction of Rab proteins by GDP dissociation inhibitor characterized using attenuated total reflection infrared spectroscopy. *Proceedings of the National Academy of Sciences of the United States of America*, 110(33), [Online] Available from: doi.org/10.1073/pnas.1307655110.
GEUMANN, U. et al. (2008) SNARE function is not involved in early endosome docking. *Molecular Biology of the Cell*, 19(12), [Online] Available from: doi.org/10.1091/mbc.E08-05-0457.

GILLINGHAM, A.K. et al. (2014) Toward a Comprehensive Map of the Effectors of Rab GTPases. *Developmental Cell*, 31(3), [Online] Available from: doi.org/10.1016/j.devcel.2014.10.007.
GILLINGHAM, A.K. and MUNRO, S. (2003).
GIRARD, E. et al. (2014) Rab7 is functionally required for selective cargo sorting at the early endosome. *Traffic*, 15(3), [Online] Available from: doi.org/10.1111/tra.12143.
GIRI, D.K. et al. (2005) Endosomal Transport of ErbB-2: Mechanism for Nuclear Entry of the Cell Surface Receptor. *Molecular and Cellular Biology*, 25(24), [Online] Available from: doi.org/10.1128/mcb.25.24.11005-11018.2005.
GOH, L.K. and SORKIN, A. (2013) Endocytosis of receptor tyrosine kinases. *Cold Spring Harbor Perspectives in Biology*, 5(5), [Online] Available from: doi.org/10.1101/cshperspect.a017459.
GORVEL, J.P. et al. (1991) rab5 controls early endosome fusion in vitro. *Cell*, 64(5), [Online] Available from: doi.org/10.1016/0092-8674(91)90316-Q.
GRANT, B.D. and DONALDSON, J.G. (2009). Pathways and mechanisms of endocytic recycling. *Nature Reviews Molecular Cell Biology* (Vol. 10, Issue 9).), [Online] Available from: https://doi.org/10.1038/nrm2755
GRIMSEY, N.J. et al. (2016) Recycling and endosomal sorting of protease-activated receptor-1 is distinctly regulated by Rab11A and Rab11B proteins. *Journal of Biological Chemistry*, 291(5), [Online] Available from: doi.org/10.1074/jbc.M115.702993.
GRUENBERG, J. (2001). The endocytic pathway: A mosaic of domains. *Nature Reviews Molecular Cell Biology* (Vol. 2, Issue 10). [Online] Available from: https://doi.org/10.1038/35096054
HANADA, N. et al. (2006) Co-regulation of B-Myb expression by E2F1 and EGF receptor. *Molecular Carcinogenesis*, 45(1), [Online] Available from: doi.org/10.1002/mc.20147.
HANCOCK, M.L. et al. (2019) Insulin Receptor Associates with Promoters Genome-wide and Regulates Gene Expression. *Cell*, 177(3), [Online] Available from: doi.org/10.1016/j.cell.2019.02.030.
HAUGSTEN, E.M. et al. (2014) Photoactivation Approaches Reveal a Role for Rab11 in FGFR4 Recycling and Signalling. *Traffic*, 15(6), [Online] Available from: doi.org/10.1111/tra.12168.
HELENIUS, A. et al. (1980) On the entry of semliki forest virus into BHK-21 cells. *Journal of Cell Biology*, 84(2), [Online] Available from: doi.org/10.1083/jcb.84.2.404.
HICKE, L. (1999). Gettin' down with ubiquitin: Turning off cell-surface receptors, transporters and channels. *Trends in Cell Biology* (Vol. 9, Issue 3). [Online] Available from: https://doi.org/10.1016/S0962-8924(98)01491-3
HINRICHSEN, L. et al. (2006) Bending a membrane: How clathrin affects budding. *Proceedings of the National Academy of Sciences of the United States of America*, 103(23), [Online] Available from: doi.org/10.1073/pnas.0600312103.

HOEPFNER, S. et al. (2005) Modulation of receptor recycling and degradation by the endosomal kinesin KIF16B. *Cell*, 121(3), [Online] Available from: doi.org/10.1016/j.cell.2005.02.017.
HOWE, E.N. et al. (2020) Rab11b-mediated integrin recycling promotes brain metastatic adaptation and outgrowth. *Nature Communications*, 11(1), [Online] Available from: doi.org/10.1038/s41467-020-16832-2.
HSU, C.Y. et al. (1990) Generation of recombinant cytoplasmic domain of epidermal growth factor receptor with intrinsic protein tyrosine kinase activity. *Cell growth & differentiation : the molecular biology journal of the American Association for Cancer Research*, 1(4).
HSU, J.L. and HUNG, M.C. (2016) The role of HER2, EGFR, and other receptor tyrosine kinases in breast cancer. *Cancer and Metastasis Reviews*, 35(4), [Online] Available from: doi.org/10.1007/s10555-016-9649-6.
HU, C.D. and KERPPOLA, T.K. (2003) Simultaneous visualization of multiple protein interactions in living cells using multicolor fluorescence complementation analysis. *Nature Biotechnology*, 21(5), [Online] Available from: doi.org/10.1038/nbt816.
HUANG, W.C. et al. (2011) Nuclear translocation of epidermal growth factor receptor by Akt-dependent phosphorylation enhances breast cancer-resistant protein expression in gefitinib-resistant cells. *Journal of Biological Chemistry*, 286(23), [Online] Available from: doi.org/10.1074/jbc.M111.240796.
HUNG, L.Y. et al. (2008) Nuclear epidermal growth factor receptor (EGFR) interacts with signal transducer and activator of transcription 5 (STAT5) in activating Aurora-A gene expression. *Nucleic Acids Research*, 36(13), [Online] Available from: doi.org/10.1093/nar/gkn417.
HUTAGALUNG, A.H. and NOVICK, P.J. (2011). Role of Rab GTPases in membrane traffic and cell physiology. *Physiological Reviews* (Vol. 91, Issue 1). [Online] Available from: https://doi.org/10.1152/physrev.00059.2009
IGLEWSKI, B.H. and KABAT, D. (1975) NAD dependent inhibition of protein synthesis by Pseudomonas aeruginosa toxin. *Proceedings of the National Academy of Sciences of the United States of America*, 72(6), [Online] Available from: doi.org/10.1073/pnas.72.6.2284.
IGNATEV, A. et al. (2008) A structural model of the GDP dissociation inhibitor Rab membrane extraction mechanism. *Journal of Biological Chemistry*, 283(26), [Online] Available from: doi.org/10.1074/jbc.M709718200.
JACKSON, A.L. et al. (2003) Expression profiling reveals off-target gene regulation by RNAi. *Nature Biotechnology*, 21(6), [Online] Available from: doi.org/10.1038/nbt831.
JANISZEWSKA, M. et al. (2010) Transportin regulates nuclear import of CD44. *Journal of Biological Chemistry*, 285(40), [Online] Available from: doi.org/10.1074/jbc.M109.075838.
JENKINS, M.L. et al. (2020) The substrate specificity of the human TRAPPII complex's Rab-guanine nucleotide exchange factor activity. *Communications Biology*, 3(1), [Online] Available from: doi.org/10.1038/s42003-020-01459-2.

JEWETT, C.E. et al. (2021) RAB19 Directs Cortical Remodeling and Membrane Growth for Primary Ciliogenesis. *Developmental Cell*, 56(3), [Online] Available from: doi.org/10.1016/j.devcel.2020.12.003.
JIANG, J. et al. (2013) Involvement of Rab28 in NF-κB Nuclear Transport in Endothelial Cells. *PLoS ONE*, 8(2), [Online] Available from: doi.org/10.1371/journal.pone.0056076.
JOHANNES, L. and RÖMER, W. (2010). Shiga toxins from cell biology to biomedical applications. *Nature Reviews Microbiology* (Vol. 8, Issue 2). [Online] Available from: https://doi.org/10.1038/nrmicro2279
JONG, Y.J.I., HARMON, S.K. and O'MALLEY, K.L. (2018). GPCR signalling from within the cell. *British Journal of Pharmacology* (Vol. 175, Issue 21). [Online] Available from: https://doi.org/10.1111/bph.14023
JOVIC, M. et al. (2010). The early endosome: A busy sorting station for proteins at the crossroads. *Histology and Histopathology* (Vol. 25, Issue 1). [Online] Available from: https://doi.org/10.14670/HH-25.99
KAMIO, T. et al. (1990) Immunohistochemical expression of epidermal growth factor receptors in human adrenocortical carcinoma. *Human Pathology*, 21(3), [Online] Available from: doi.org/10.1016/0046-8177(90)90227-V.
KAUR, S. et al. (2014) An unmet actin requirement explains the mitotic inhibition of clathrin-mediated endocytosis. *eLife*, 2014(3), [Online] Available from: doi.org/10.7554/eLife.00829.001.
KELLY, B.T. et al. (2008) A structural explanation for the binding of endocytic dileucine motifs by the AP2 complex. *Nature*, 456(7224), [Online] Available from: doi.org/10.1038/nature07422.
VAN KERKHOF, P. et al. (2005) Sorting nexin 17 facilitates LRP recycling in the early endosome. *EMBO Journal*, 24(16), [Online] Available from: doi.org/10.1038/sj.emboj.7600756.
KETEMA, M. et al. (2007) Requirements for the localization of nesprin-3 at the nuclear envelope and its interaction with plectin. *Journal of Cell Science*, 120(19), [Online] Available from: doi.org/10.1242/jcs.014191.
KIM, G.H.E. et al. (2014) PIKfyve inhibition interferes with phagosome and endosome maturation in macrophages. *Traffic*, 15(10), [Online] Available from: doi.org/10.1111/tra.12199.
KIM, S.J. and BASSHAM, D.C. (2013) Functional redundancy between trans-Golgi network SNARE family members in Arabidopsis thaliana. *BMC Biochemistry*, 14(1), [Online] Available from: doi.org/10.1186/1471-2091-14-22.
KIRCHHAUSEN, T. and HARRISON, S.C. (1981) Protein organization in clathrin trimers. *Cell*, 23(3), [Online] Available from: doi.org/10.1016/0092-8674(81)90439-6.
KNITTLE, A.M. et al. (2017) SUMOylation regulates nuclear accumulation and signaling activity of the soluble intracellular domain of the ErbB4 receptor tyrosine kinase. *Journal of Biological Chemistry*, 292(48), [Online] Available from: doi.org/10.1074/jbc.M117.794271.
KORNFELD, S. and MELLMAN, I. (1989).
KOZIK, P. et al. (2010) A Screen for Endocytic Motifs. *Traffic*, 11(6), [Online] Available from: doi.org/10.1111/j.1600-0854.2010.01056.x.

KUROKAWA, K., OKAMOTO, M. and NAKANO, A. (2014) Contact of cis-Golgi with ER exit sites executes cargo capture and delivery from the ER. *Nature Communications*, 5, [Online] Available from: doi.org/10.1038/ncomms4653.

LAATSCH, A. et al. (2012) Low density lipoprotein receptor-related protein 1 dependent endosomal trapping and recycling of apolipoprotein E. *PLoS ONE*, 7(1), [Online] Available from: doi.org/10.1371/journal.pone.0029385.

LAN, H. et al. (2018) Porcine growth hormone induces the nuclear localization of porcine growth hormone receptor in vivo. *Asian-Australasian Journal of Animal Sciences*, 31(4), [Online] Available from: doi.org/10.5713/ajas.17.0585.

LAROCQUE, G. et al. (2020) Tumor protein D54 defines a new class of intracellular transport vesicles. *Journal of Cell Biology*, 219(1), [Online] Available from: doi.org/10.1083/jcb.201812044.

LECHER, J.C., NOWAK, S.J. and MCMURRY, J.L. (2017). Breaking in and busting out: Cell-penetrating peptides and the endosomal escape problem. *Biomolecular Concepts* (Vol. 8, Issues 3–4).), [Online] Available from: https://doi.org/10.1515/bmc-2017-0023

LEE, D.K. et al. (2004) Agonist-independent Nuclear Localization of the Apelin, Angiotensin AT 1, and Bradykinin B2 Receptors. *Journal of Biological Chemistry*, 279(9), [Online] Available from: doi.org/10.1074/jbc.M306377200.

LEONARD, D. et al. (2008) Sorting of EGF and transferrin at the plasma membrane and by cargo-specific signaling to EEA1-enriched endosomes. *Journal of Cell Science*, 121(20), [Online] Available from: doi.org/10.1242/jcs.031484.

LI, C. et al. (2009) Nuclear EGFR contributes to acquired resistance to cetuximab. *Oncogene*, 28(43), [Online] Available from: doi.org/10.1038/onc.2009.234.

LI, C. et al. (2017) The GTPase Rab43 Controls the Anterograde ER-Golgi Trafficking and Sorting of GPCRs. *Cell Reports*, 21(4), [Online] Available from: doi.org/10.1016/j.celrep.2017.10.011.

LI, F. et al. (2014) The role of the hypervariable C-terminal domain in Rab GTPases membrane targeting. *Proceedings of the National Academy of Sciences of the United States of America*, 111(7), [Online] Available from: doi.org/10.1073/pnas.1313655111.

LIAO, H.J. and CARPENTER, G. (2007) Role of the Sec61 translocon in EGF receptor trafficking to the nucleus and gene expression. *Molecular Biology of the Cell*, 18(3), [Online] Available from: doi.org/10.1091/mbc.E06-09-0802.

LIN, S.Y. et al. (2001) Nuclear localization of EGF receptor and its potential new role as a transcription factor. *Nature Cell Biology*, 3(9), [Online] Available from: doi.org/10.1038/ncb0901-802.

LIN, X. et al. (2005) siRNA-mediated off-target gene silencing triggered by a 7 nt complementation. *Nucleic Acids Research*, 33(14), [Online] Available from: doi.org/10.1093/nar/gki762.

LIU, X. and ERIKSON, R.L. (2003) Polo-like kinase (Plk)1 depletion induces apoptosis in cancer cells. *Proceedings of the National Academy of Sciences of the United States of America*, 100(10), [Online] Available from: doi.org/10.1073/pnas.1031523100.

LIU, Y. and BARLOWE, C. (2002) Analysis of Sec22p in endoplasmic reticulum/golgi transport reveals cellular redundancy in SNARE protein function. *Molecular Biology of the Cell*, 13(9), [Online] Available from: doi.org/10.1091/mbc.E02-04-0204.

LO, H.W., XIA, W., et al. (2005) Novel prognostic value of nuclear epidermal growth factor receptor in breast cancer. *Cancer Research*, 65(1).

LO, H.W., HSU, S.C., et al. (2005) Nuclear interaction of EGFR and STAT3 in the activation of the iNOS/NO pathway. *Cancer Cell*, 7(6), [Online] Available from: doi.org/10.1016/j.ccr.2005.05.007.

LOERKE, D. et al. (2009) Cargo and dynamin regulate clathrin-coated pit maturation. *PLoS Biology*, 7(3), [Online] Available from: doi.org/10.1371/journal.pbio.1000057.

LÜTCKE, A. et al. (1995) Isolation of a murine cDNA clone encoding Rab 19, a novel tissue-specific small GTPase. *Gene*, 155(2), [Online] Available from: doi.org/10.1016/0378-1119(94)00931-H.

MAKURVET, F.D. (2021) Biologics vs. small molecules: Drug costs and patient access. *Medicine in Drug Discovery*, 9, [Online] Available from: doi.org/10.1016/j.medidd.2020.100075.

MALTESE, W.A. et al. (2002) Mutant Rab24 GTPase is targeted to nuclear inclusions. *BMC Cell Biology*, 3, [Online] Available from: doi.org/10.1186/1471-2121-3-25.

MAO, H., XIE, L. and PI, X. (2017). Low-Density Lipoprotein Receptor-Related Protein-1 Signaling in Angiogenesis. *Frontiers in Cardiovascular Medicine* (Vol. 4). [Online] Available from: https://doi.org/10.3389/fcvm.2017.00034

MARCO, S. et al. (2021) Nuclear-capture of endosomes depletes nuclear G-actin to promote SRF/MRTF activation and cancer cell invasion. *Nature Communications*, 12(1), [Online] Available from: doi.org/10.1038/s41467-021-26839-y.

MARTI, U. et al. (1991) Localization of epidermal growth factor receptor in hepatocyte nuclei. *Hepatology*, 13(1), [Online] Available from: doi.org/10.1002/hep.1840130104.

MARVIN, D.A. et al. (1974) Filamentous bacterial viruses. XII. Molecular architecture of the class I (fd, If1, IKe) virion. *Journal of Molecular Biology*, 88(3), [Online] Available from: doi.org/10.1016/0022-2836(74)90409-4.

MATLIN, K.S. et al. (1982) Pathway of vesicular stomatitis virus entry leading to infection. *Journal of Molecular Biology*, 156(3), [Online] Available from: doi.org/10.1016/0022-2836(82)90269-8.

MAYOR, S., PRESLEY, J.F. and MAXFIELD, F.R. (1993) Sorting of membrane components from endosomes and subsequent recycling to the cell surface occurs by a bulk flow process. *Journal of Cell Biology*, 121(6), [Online] Available from: doi.org/10.1083/jcb.121.6.1257.

McBride, H.M. et al. (1999) Oligomeric complexes link Rab5 effectors with NSF and drive membrane fusion via interactions between EEA1 and syntaxin 13. *Cell*, 98(3), [Online] Available from: doi.org/10.1016/S0092-8674(00)81966-2.
McCafferty, J. et al. (1990) Phage antibodies: filamentous phage displaying antibody variable domains. *Nature*, 348(6301), [Online] Available from: doi.org/10.1038/348552a0.
McLauchlan, H. et al. (1998) A novel role for Rab5-GDI in ligand sequestration into clathrin-coated pits. *Current Biology*, 8(1), [Online] Available from: doi.org/10.1016/S0960-9822(98)70018-1.
McNally, K.E. et al. (2017) Retriever is a multiprotein complex for retromer-independent endosomal cargo recycling. *Nature Cell Biology*, 19(10), [Online] Available from: doi.org/10.1038/ncb3610.
Mercer, J., Schelhaas, M. and Helenius, A. (2010).
Méré, J. et al. (2005) Acid-triggered membrane insertion of Pseudomonas exotoxin A involves an original mechanism based on pH-regulated tryptophan exposure. *Journal of Biological Chemistry*, 280(22), [Online] Available from: doi.org/10.1074/jbc.M412656200.
Miaczynska, M. et al. (2004) APPL proteins link Rab5 to nuclear signal transduction via an endosomal compartment. *Cell*, 116(3), [Online] Available from: doi.org/10.1016/S0092-8674(04)00117-5.
Michalska, M. and Wolf, P. (2015).
Mima, J. (2018). Reconstitution of membrane tethering mediated by Rab-family small GTPases. *Biophysical Reviews* (Vol. 10, Issue 2). [Online] Available from: https://doi.org/10.1007/s12551-017-0358-3
Minna, J.D., Peyton, M.J. and Gazdar, A.F. (2005).
Moja, L. et al. (2012). Trastuzumab containing regimens for early breast cancer. *Cochrane Database of Systematic Reviews* (Vol. 2021, Issue 2). [Online] Available from: https://doi.org/10.1002/14651858.CD006243.pub2
Moreau, D. et al. (2011) Genome-Wide RNAi Screens Identify Genes Required for Ricin and PE Intoxications. *Developmental Cell*, 21(2), [Online] Available from: doi.org/10.1016/j.devcel.2011.06.014.
Morlon-Guyot, J. et al. (2009) Processing of Pseudomonas aeruginosa exotoxin A is dispensable for cell intoxication. *Infection and Immunity*, 77(7), [Online] Available from: doi.org/10.1128/IAI.01390-08.
Muratoglu, S.C. et al. (2010) Low density lipoprotein receptor-related protein 1 (LRP1) forms a signaling complex with platelet-derived growth factor receptor-β in endosomes and regulates activation of the MAPK pathway. *Journal of Biological Chemistry*, 285(19), [Online] Available from: doi.org/10.1074/jbc.M109.046672.
Murphy, J.E. et al. (2009). Endosomes: A legitimate platform for the signaling train. *Proceedings of the National Academy of Sciences of the United States of America* (Vol. 106, Issue 42). [Online] Available from: https://doi.org/10.1073/pnas.0906541106
Murphy, J.R. (2011). Mechanism of diphtheria toxin catalytic domain delivery to the eukaryotic cell cytosol and the cellular factors that directly

participate in the process. *Toxins* (Vol. 3, Issue 3).). [Online] Available from: https://doi.org/10.3390/toxins3030294

MURRAY, D.H. et al. (2016) An endosomal tether undergoes an entropic collapse to bring vesicles together. *Nature*, 537(7618), [Online] Available from: doi.org/10.1038/nature19326.

NAKAMURA, K. et al. (1999) Role of the rate of internalization of the agonist-receptor complex on the agonist-induced down-regulation of the lutropin/choriogonadotropin receptor. *Molecular Endocrinology*, 13(8), [Online] Available from: doi.org/10.1210/mend.13.8.0331.

NASLAVSKY, N. and CAPLAN, S. (2018). The enigmatic endosome - Sorting the ins and outs of endocytic trafficking. *Journal of Cell Science* (Vol. 131, Issue 13). [Online] Available from: https://doi.org/10.1242/jcs.216499

NICOLAS, A. et al. (2014) The spectrin family of proteins: A unique coiled-coil fold for various molecular surface properties. *Journal of Structural Biology*, 186(3), [Online] Available from: doi.org/10.1016/j.jsb.2014.03.011.

NIELSEN, E. et al. (1999) Rab5 regulates motility of early endosomes on microtubules. *Nature Cell Biology*, 1(6), [Online] Available from: doi.org/10.1038/14075.

OGATA, M. et al. (1992) Cell-mediated cleavage of Pseudomonas exotoxin between Arg279 and Gly280 generates the enzymatically active fragment which translocates to the cytosol. *Journal of Biological Chemistry*, 267(35), [Online] Available from: doi.org/10.1016/s0021-9258(19)74054-x.

OHNO, H. et al. (1995) Interaction of tyrosine-based sorting signals with clathrin-associated proteins. *Science*, 269(5232), [Online] Available from: doi.org/10.1126/science.7569928.

OLSNES, S. et al. (1991). Bacterial protein toxins acting on intracellular targets. *Seminars in cell biology* (Vol. 2, Issue 1).

PADMAKUMAR, V.C. et al. (2005) The inner nuclear membrane protein Sun1 mediates the anchorage of Nesprin-2 to the nuclear envelope. *Journal of Cell Science*, 118(15), [Online] Available from: doi.org/10.1242/jcs.02471.

PANDEY, K.N. (2010). Small peptide recognition sequence for intracellular sorting. *Current Opinion in Biotechnology* (Vol. 21, Issue 5).), [Online] Available from: https://doi.org/10.1016/j.copbio.2010.08.007

PAOLO, P., FIORE, D. and DE CAMILLI, P. (2001) Endocytosis and Signaling: Minireview An Inseparable Partnership. *Cell*, 106.

PAPADOPOULOS, N., LENNARTSSON, J. and HELDIN, C.H. (2018) PDG FRβ translocates to the nucleus and regulates chromatin remodeling via TATA element-modifying factor 1. *Journal of Cell Biology*, 217(5), [Online] Available from: doi.org/10.1083/jcb.201706118.

PEREIRA-LEAL, J.B. and SEABRA, M.C. (2000) The mammalian Rab family of small GTPases: Definition of family and subfamily sequence motifs suggests a mechanism for functional specificity in the Ras superfamily. *Journal of Molecular Biology*, 301(4), [Online] Available from: doi.org/10.1006/jmbi.2000.4010.

PIPER, R.C. and KATZMANN, D.J. (2007). Biogenesis and function of multivesicular bodies. *Annual Review of Cell and Developmental Biology* (Vol. 23). [Online] Available from: https://doi.org/10.1146/annurev.cellbio.23.090506.123319

PLANQUE, N. (2006). Nuclear trafficking of secreted factors and cell-surface receptors: New pathways to regulate cell proliferation and differentiation, and involvement in cancers. *Cell Communication and Signaling* (Vol. 4). [Online] Available from: https://doi.org/10.1186/1478-811X-4-7

PODLECKI, D.A. et al. (1987) Nuclear translocation of the insulin receptor. A possible mediator of insulin's long term effects. *Journal of Biological Chemistry*, 262(7), [Online] Available from: doi.org/10.1016/s0021-9258(18)61511-x.

PRINCE, E. et al. (2019) Rab-mediated trafficking in the secondary cells of Drosophila male accessory glands and its role in fecundity. *Traffic*, 20(2), [Online] Available from: doi.org/10.1111/tra.12622.

PYLYPENKO, O. et al. (2006) Structure of doubly prenylated Ypt1:GDI complex and the mechanism of GDI-mediated Rab recycling. *EMBO Journal*, 25(1), [Online] Available from: doi.org/10.1038/sj.emboj.7600921.

PYLYPENKO, O. and GOUD, B. (2012). Posttranslational modifications of Rab GTPases help their insertion into membranes. *Proceedings of the National Academy of Sciences of the United States of America* (Vol. 109, Issue 15). [Online] Available from: https://doi.org/10.1073/pnas.1202494109

RAIBORG, C. and STENMARK, H. (2009). The ESCRT machinery in endosomal sorting of ubiquitylated membrane proteins. *Nature* (Vol. 458, Issue 7237). [Online] Available from: https://doi.org/10.1038/nature0796

RAJGOR, D. and SHANAHAN, C.M. (2013). Nesprins: from the nuclear envelope and beyond. *Expert reviews in molecular medicine* (Vol. 15). [Online] Available from: https://doi.org/10.1017/erm.2013.6

RAKOWICZ-SZULCZYNSKA, E.M. et al. (1986) Chromatin binding of epidermal growth factor, nerve growth factor and platelet-derived growth factor in cells bearing the appropriate surface receptor. *Proceedings of the National Academy of Sciences of the United States of America*, 83(11), [Online] Available from: doi.org/10.1073/pnas.83.11.3728.

RAO, M.S. et al. (2019) Novel Computational Approach to Predict Off-Target Interactions for Small Molecules. *Frontiers in Big Data*, 2, [Online] Available from: doi.org/10.3389/fdata.2019.00025.

RAPER, S.E. et al. (1987) Translocation of Epidermal Growth Factor to the Hepatocyte Nucleus During Rat Liver Regeneration. *Gastroenterology*, 92(5), [Online] Available from: doi.org/10.1016/S0016-5085(87)91084-5.

RAUCHER, D. and SHEETZ, M.P. (1999) Membrane expansion increases endocytosis rate during mitosis. *Journal of Cell Biology*, 144(3), [Online] Available from: doi.org/10.1083/jcb.144.3.497.

REILLY, J.F. and MAHER, P.A. (2001) Importin β-mediated nuclear import of fibroblast growth factor receptor: Role in cell proliferation. *Journal of Cell Biology*, 152(6), [Online] Available from: doi.org/10.1083/jcb.152.6.1307.

DE RENZIS, S., SÖNNICHSEN, B. and ZERIAL, M. (2002) Divalent Rab effectors regulate the sub-compartmental organization and sorting of early endosomes. *Nature Cell Biology*, 4(2), [Online] Available from: doi.org/10.1038/ncb744.

RICHARD, J.P. et al. (2003) Cell-penetrating peptides: A reevaluation of the mechanism of cellular uptake. *Journal of Biological Chemistry*, 278(1), [Online] Available from: doi.org/10.1074/jbc.M209548200.

RINK, J. et al. (2005) Rab conversion as a mechanism of progression from early to late endosomes. *Cell*, 122(5), [Online] Available from: doi.org/10.1016/j.cell.2005.06.043.

RIVERA-MOLINA, F.E. and NOVICK, P.J. (2009) A Rab GAP cascade defines the boundary between two Rab GTPases on the secretory pathway. *Proceedings of the National Academy of Sciences of the United States of America*, 106(34), [Online] Available from: doi.org/10.1073/pnas.0906536106.

ROBINSON, M.S., SAHLENDER, D.A. and FOSTER, S.D. (2010) Rapid Inactivation of Proteins by Rapamycin-Induced Rerouting to Mitochondria. *Developmental Cell*, 18(2), [Online] Available from: doi.org/10.1016/j.devcel.2009.12.015.

ROTH, T.F. and PORTER, K.R. (1964) YOLK PROTEIN UPTAKE IN THE OOCYTE OF THE MOSQUITO AEDES AEGYPTI. L. *The Journal of cell biology*, 20, [Online] Available from: doi.org/10.1083/jcb.20.2.313.

ROYLE, S.J. (2006). The cellular functions of clathrin. *Cellular and Molecular Life Sciences* (Vol. 63, Issue 16). [Online] Available from: https://doi.org/10.1007/s00018-005-5587-0

RUBINO, M. et al. (2000) Selective membrane recruitment of EEA1 suggests a role in directional transport of clathrin-coated vesicles to early endosomes. *Journal of Biological Chemistry*, 275(6), [Online] Available from: doi.org/10.1074/jbc.275.6.3745.

RUDEL, T., KEPP, O. and KOZJAK-PAVLOVIC, V. (2010). Interactions between bacterial pathogens and mitochondrial cell death pathways. *Nature Reviews Microbiology* (Vol. 8, Issue 10). [Online] Available from: https://doi.org/10.1038/nrmicro2421

SANDVIG, K. et al. (2010). Protein toxins from plants and bacteria: Probes for intracellular transport and tools in medicine. *FEBS Letters* (Vol. 584, Issue 12). [Online] Available from: https://doi.org/10.1016/j.febslet.2010.04.008

SATO, K. et al. (2015) Coupling of vesicle tethering and Rab binding is required for in vivo functionality of the golgin GMAP-210. *Molecular Biology of the Cell*, 26(3), [Online] Available from: doi.org/10.1091/mbc.E14-10-1450.

SCHEIBER, J. et al. (2009) Gaining insight into off-target mediated effects of drug candidates with a comprehensive systems chemical biology analysis. *Journal of Chemical Information and Modeling*, 49(2), [Online] Available from: doi.org/10.1021/ci800344p.

SCHILLACI, R. et al. (2012) Clinical relevance of ErbB-2/HER2 nuclear expression in breast cancer. *BMC Cancer*, 12, [Online] Available from: doi.org/10.1186/1471-2407-12-74.

SCHIRMER, E.C. and GERACE, L. (2005). The nuclear membrane proteome: Extending the envelope. *Trends in Biochemical Sciences* (Vol. 30, Issue 10). [Online] Available from: https://doi.org/10.1016/j.tibs.2005.08.003

SCHMID, S.L. et al. (1988) Two distinct subpopulations of endosomes involved in membrane recycling and transport to lysosomes. *Cell*, 52(1), [Online] Available from: doi.org/10.1016/0092-8674(88)90532-6.

SCOTT, C.C., VACCA, F. and GRUENBERG, J. (2014). Endosome maturation, transport and functions. *Seminars in Cell and Developmental Biology* (Vol. 31). [Online] Available from: https://doi.org/10.1016/j.semcdb.2014.03.034

SEDRAK, P., HSU, K. and MOHAN, C. (2003) Molecular signatures of anti-nuclear antibodies - Contribution of heavy chain framework residues. *Molecular Immunology*, 40(8), [Online] Available from: doi.org/10.1016/S0161-5890(03)00223-2.

SEGAWA, K., TAMURA, N. and MIMA, J. (2019) Homotypic and heterotypic trans-assembly of human Rab-family small GTPases in reconstituted membrane tethering. *Homotypic and heterotypic trans-assembly of human Rabfamily small GTPases in reconstituted membrane tethering*, [Online] Available from: doi.org/10.1101/544379.

SEGEV, N. (2001). Ypt and Rab GTPases: Insight into functions through novel interactions. *Current Opinion in Cell Biology* (Vol. 13, Issue 4). [Online] Available from: https://doi.org/10.1016/S0955-0674(00)00242-8

SELA-CULANG, I., KUNIK, V. and OFRAN, Y. (2013) The structural basis of antibody-antigen recognition. *Frontiers in Immunology*, 4(OCT), [Online] Available from: doi.org/10.3389/fimmu.2013.00302.

Semerdjieva, S., Shortt, B., Maxwell, E., Singh, S., Fonarev, P., Hansen, J., Schiavo, G., Grant, B. D., & Smythe, E. (2008). Coordinated regulation of AP2 uncoating from clathrin-coated vesicles by rab5 and hRME-6. *Journal of Cell Biology*, *183*(3). https://doi.org/10.1083/jcb.200806016

SHAH, P. et al. (2019) The NAE Pathway: Autobahn to the Nucleus for Cell Surface Receptors. *Cells*, 8(8), p. 915.

SHAO, X. et al. (2016) Numb regulates vesicular docking for homotypic fusion of early endosomes via membrane recruitment of Mon1b. *Cell Research*, 26(5), [Online] Available from: doi.org/10.1038/cr.2016.34.

SHAPIRO, A.D., RIEDERER, M.A. and PFEFFER, S.R. (1993) Biochemical analysis of rab9, a ras-like GTPase involved in protein transport from late endosomes to the trans Golgi network. *Journal of Biological Chemistry*, 268(10), [Online] Available from: doi.org/10.1016/s0021-9258(18)53128-8.

SIECZKARSKI, S.B. and WHITTAKER, G.R. (2002) Influenza Virus Can Enter and Infect Cells in the Absence of Clathrin-Mediated Endocytosis. *Journal of Virology*, 76(20), [Online] Available from: doi.org/10.1128/jvi.76.20.10455-10464.2002.

SIGISMUND, S. et al. (2013) Threshold-controlled ubiquitination of the EGFR directs receptor fate. *EMBO Journal*, 32(15), [Online] Available from: doi.org/10.1038/emboj.2013.149.

SIMONSEN, A. et al. (1998) EEA1 links PI(3)K function to Rab5 regulation of endosome fusion. *Nature*, 394(6692), [Online] Available from: doi.org/10.1038/28879.
SIMONSEN, A. et al. (1999) The Rab5 effector EEA1 interacts directly with syntaxin-6. *Journal of Biological Chemistry*, 274(41), [Online] Available from: doi.org/10.1074/jbc.274.41.28857.
SINKA, R. et al. (2008) Golgi coiled-coil proteins contain multiple binding sites for rab family G proteins. *Journal of Cell Biology*, 183(4), [Online] Available from: doi.org/10.1083/jcb.200808018.
SLASTNIKOVA, T.A. et al. (2018) Targeted intracellular delivery of antibodies: The state of the art. *Frontiers in Pharmacology*, 9(OCT), [Online] Available from: doi.org/10.3389/fphar.2018.01208.
SÖNNICHSEN, B. et al. (2000) Distinct membrane domains on endosomes in the recycling pathway visualized by multicolor imaging of Rab4, Rab5, and Rab11. *Journal of Cell Biology*, 149(4), [Online] Available from: doi.org/10.1083/jcb.149.4.901.
SOSA, B.A. et al. (2012) LINC complexes form by binding of three KASH peptides to domain interfaces of trimeric SUN proteins. *Cell*, 149(5), [Online] Available from: doi.org/10.1016/j.cell.2012.03.046.
SPÄNKUCH-SCHMITT, B. et al. (2002) Downregulation of human polo-like kinase activity by antisense oligonucleotides induces growth inhibition in cancer cells. *Oncogene*, 21(20), [Online] Available from: doi.org/10.1038/sj.onc.1205412.
STACHOWIAK, M.K., MAHER, P.A. and STACHOWIAK, E.K. (2007). Integrative nuclear signaling in cell development - A role for FGF receptor-1. *DNA and Cell Biology* (Vol. 26, Issue 12). [Online] Available from: https://doi.org/10.1089/dna.2007.0664
STENMARK, H. (2009). Rab GTPases as coordinators of vesicle traffic. *Nature Reviews Molecular Cell Biology* (Vol. 10, Issue 8). [Online] Available from: https://doi.org/10.1038/nrm2728
STENMARK, H. et al. (1995) Rabaptin-5 is a direct effector of the small GTPase Rab5 in endocytic membrane fusion. *Cell*, 83(3), [Online] Available from: doi.org/10.1016/0092-8674(95)90120-5.
STEVENS, C.F. and WILLIAMS, J.H. (2000) "Kiss and run" exocytosis at hippocampal synapses. *Proceedings of the National Academy of Sciences of the United States of America*, 97(23), [Online] Available from: doi.org/10.1073/pnas.230438697.
SWINDELLS, M.B. et al. (2017) abYsis: Integrated Antibody Sequence and Structure—Management, Analysis, and Prediction. *Journal of Molecular Biology*, 429(3), [Online] Available from: doi.org/10.1016/j.jmb.2016.08.019.
TAMURA, N. and MIMA, J. (2014) Membrane-anchored human Rab GTPases directly mediate membrane tethering in vitro. *Biology Open*, 3(11), [Online] Available from: doi.org/10.1242/bio.20149340.
TING, T.A., CHAUMET, A. and BARD, F.A. (2020) Targeting c-Myc with a novel Peptide Nuclear Delivery Device. *Scientific Reports*, 10(1), [Online] Available from: doi.org/10.1038/s41598-020-73998-x.

TRAHEY, M. and HAY, J.C. (2010). Transport vesicle uncoating: It's later than you think. *F1000 Biology Reports* (Vol. 2, Issue 1).), [Online] Available from: https://doi.org/10.3410/B2-47

TRAUB, L.M. and BONIFACINO, J.S. (2013) Cargo recognition in clathrin-mediated endocytosis. *Cold Spring Harbor Perspectives in Biology*, 5(11), [Online] Available from: doi.org/10.1101/cshperspect.a016790.

TRAYNOR, A.M. et al. (2013) Nuclear EGFR protein expression predicts poor survival in early stage non-small cell lung cancer. *Lung Cancer*, 81(1), [Online] Available from: doi.org/10.1016/j.lungcan.2013.03.020.

Tu, Y., Zhao, L., Billadeau, D. D., & Jia, D. (2020). Endosome-to-TGN Trafficking: Organelle-Vesicle and Organelle-Organelle Interactions. In *Frontiers in Cell and Developmental Biology* (Vol. 8). https://doi.org/10.3389/fcell.2020.00163

TURGAY, Y. et al. (2010) A classical NLS and the SUN domain contribute to the targeting of SUN2 to the inner nuclear membrane. *EMBO Journal*, 29(14), [Online] Available from: doi.org/10.1038/emboj.2010.119.

ULLRICH, O. et al. (1996) Rab11 regulates recycling through the pericentriolar recycling endosome. *Journal of Cell Biology*, 135(4), [Online] Available from: doi.org/10.1083/jcb.135.4.913.

UNGERMANN, C., SATO, K. and WICKNER, W. (1998) Defining the functions of trans-SNARE pairs. *Nature*, 396(6711), [Online] Available from: doi.org/10.1038/25069.

UNGEWICKELL, E. and BRANTON, D. (1981) Assembly units of clathrin coats. *Nature*, 289(5796), [Online] Available from: doi.org/10.1038/289420a0.

VANLANDINGHAM, P.A. and CERESA, B.P. (2009) Rab7 regulates late endocytic trafficking downstream of multivesicular body biogenesis and cargo sequestration. *Journal of Biological Chemistry*, 284(18), [Online] Available from: doi.org/10.1074/jbc.M809277200.

Vembar, S. S., & Brodsky, J. L. (2008). One step at a time: Endoplasmic reticulum-associated degradation. In *Nature Reviews Molecular Cell Biology* (Vol. 9, Issue 12). https://doi.org/10.1038/nrm2546

VERHAGE, M. and SØRENSEN, J.B. (2008). Vesicle docking in regulated exocytosis. *Traffic* (Vol. 9, Issue 9). [Online] Available from: https://doi.org/10.1111/j.1600-0854.2008.00759.x

VOGEL, C.L. et al. (2002) Efficacy and safety of trastuzumab as a single agent in first-line treatment of HER2-overexpressing metastatic breast cancer. *Journal of Clinical Oncology*, 20(3), [Online] Available from: doi.org/10.1200/JCO.20.3.719.

WAINSZELBAUM, M.J. et al. (2006) IL4/PGE2 induction of an enlarged early endosomal compartment in mouse macrophages is Rab5-dependent. *Experimental Cell Research*, 312(12), [Online] Available from: doi.org/10.1016/j.yexcr.2006.03.025.

WANDINGER-NESS, A. and ZERIAL, M. (2014). Rab proteins and the compartmentalization of the endosomal system. *Cold Spring Harbor perspectives in biology* (Vol. 6, Issue 11). [Online] Available from: https://doi.org/10.1101/cshperspect.a022616

WANG, J.L. et al. (2018) Prognostic value of localization of epidermal growth factor receptor in lung adenocarcinoma. *Journal of Biomedical Science*, 25(1), [Online] Available from: doi.org/10.1186/s12929-018-0451-3.
WANG, S.C. et al. (2006) Tyrosine phosphorylation controls PCNA function through protein stability. *Nature Cell Biology*, 8(12), [Online] Available from: doi.org/10.1038/ncb1501.
WANG, YING NAI, WANG, H., et al. (2010) COPI-mediated retrograde trafficking from the Golgi to the ER regulates EGFR nuclear transport. *Biochemical and Biophysical Research Communications*, 399(4), [Online] Available from: doi.org/10.1016/j.bbrc.2010.07.096.
WANG, Y. N. et al. (2010). Nuclear trafficking of the epidermal growth factor receptor family membrane proteins. *Oncogene* (Vol. 29, Issue 28). [Online] Available from: https://doi.org/10.1038/onc.2010.157
WANG, YING NAI, YAMAGUCHI, H., et al. (2010) The translocon Sec61β localized in the inner nuclear membrane transports membrane-embedded EGF receptor to the nucleus. *Journal of Biological Chemistry*, 285(49), [Online] Available from: doi.org/10.1074/jbc.M110.158659.
WANG, Y.N. and HUNG, M.C. (2012). Nuclear functions and subcellular trafficking mechanisms of the epidermal growth factor receptor family. *Cell and Bioscience* (Vol. 2, Issue 1). [Online] Available from: https://doi.org/10.1186/2045-3701-2-13
WARREN H LEWIS (1931) Pinocytosis. *Johns Hopkins Hosp. Bull.* , 49, pp. 17–26.
WATSON, M.L. (1955) The nuclear envelope; its structure and relation to cytoplasmic membranes. *The Journal of biophysical and biochemical cytology*, 1(3), [Online] Available from: doi.org/10.1083/jcb.1.3.257.
WELLS, A. and MARTI, U. (2002). Signalling shortcuts: Cell-surface receptors in the nucleus? *Nature Reviews Molecular Cell Biology* (Vol. 3, Issue 9). [Online] Available from: https://doi.org/10.1038/nrm905
WHITE, J.A. et al. (2015) Huntingtin differentially regulates the axonal transport of a sub-set of Rab-containing vesicles in vivo. *Human Molecular Genetics*, 24(25), [Online] Available from: doi.org/10.1093/hmg/ddv415.
WHITE, J.H. et al. (2000) The GABA(B) receptor interacts directly with the related transcription factors CREB2 and ATFx. *Proceedings of the National Academy of Sciences of the United States of America*, 97(25), [Online] Available from: doi.org/10.1073/pnas.240452197.
WILEY, H.S. et al. (1991) The role of tyrosine kinase activity in endocytosis, compartmentation, and down-regulation of the epidermal growth factor receptor. *Journal of Biological Chemistry*, 266(17), [Online] Available from: doi.org/10.1016/s0021-9258(18)99131-3.
WITKOS, T.M. and LOWE, M. (2016). The golgin family of coiled-coil tethering proteins. *Frontiers in Cell and Developmental Biology* (Vol. 3, Issue JAN). [Online] Available from: https://doi.org/10.3389/fcell.2015.00086
WONG, M. and MUNRO, S. (2014) The specificity of vesicle traffic to the Golgi is encoded in the golgin coiled-coil proteins. *Science*, 346(6209), [Online] Available from: doi.org/10.1126/science.1256898.

XIA, W. et al. (2009) Nuclear expression of epidermal growth factor receptor is a novel prognostic value in patients with ovarian cancer. *Molecular Carcinogenesis*, 48(7), [Online] Available from: doi.org/10.1002/mc.20504.

XIE, J. et al. (2020). Cell-Penetrating Peptides in Diagnosis and Treatment of Human Diseases: From Preclinical Research to Clinical Application. *Frontiers in Pharmacology* (Vol. 11). [Online] Available from: https://doi.org/10.3389/fphar.2020.00697

XU, Y. et al. (2009) Ultraviolet irradiation-induces epidermal growth factor receptor (EGFR) nuclear translocation in human keratinocytes. *Journal of Cellular Biochemistry*, 107(5), [Online] Available from: doi.org/10.1002/jcb.22195.

ZEIGERER, A. et al. (2012) Rab5 is necessary for the biogenesis of the endolysosomal system in vivo. *Nature*, 485(7399), [Online] Available from: doi.org/10.1038/nature11133.

ZENO, W.F. et al. (2021) Clathrin senses membrane curvature. *Biophysical Journal*, 120(5), [Online] Available from: doi.org/10.1016/j.bpj.2020.12.035.

ZHANG, J.H., CHUNG, T.D.Y. and OLDENBURG, K.R. (1999) A simple statistical parameter for use in evaluation and validation of high throughput screening assays. *Journal of Biomolecular Screening*, 4(2), [Online] Available from: doi.org/10.1177/108705719900400206.

ZHEN, Y. and STENMARK, H. (2015) Cellular functions of Rab GTPases at a glance. *Journal of Cell Science*, 128(17), [Online] Available from: doi.org/10.1242/jcs.166074.

ZULEGER, N., KORFALI, N. and SCHIRMER, E.C. (2008) Inner nuclear membrane protein transport is mediated by multiple mechanisms. In: *Biochemical Society Transactions*.

Appendix